SATTELITE REMOTE SENSING OF HARMFUL ALGAL BLOOMS IN THE SOUTHCENTRAL UNITED STATES OF AMERICA (USA)

By

ABUBAKARR SIDIQUE MANSARAY

Bachelor of Science in Environmental Chemistry
Njala University College, University of Sierra Leone
Freetown, Sierra Leone
2002

Master of Science in Environmental Chemistry
Njala University College, University of Sierra Leone
Freetown, Sierra Leone
2004

Master of Science in Environmental Science
University of Idaho
Mosco, Idaho
2010

Submitted to the Faculty of the
Graduate College of the
Oklahoma State University
in partial fulfillment of
the requirements for
the Degree of
DOCTOR OF PHILOSOPHY
July, 2018

SATELLITE REMOTE SENSING OF HARMFUL ALGAL BLOOMS IN THE SOUTHCENTRAL UNITED STATES OF AMERICA (USA)

Dissertation Approved:

Dr. Scott Stoodley

Dissertation Adviser

Dr. Andrew Dzialowski

Dr. Nathan Torbick

Dr. Kevin Wagner

ACKNOWLEDGEMENTS

The Grand River Dam Authority (GRDA) in Northeastern Oklahoma funded this PhD study. The GRDA also provided materials and equipment to enhance *in situ* sampling and collection of samples for laboratory analysis. The GRDA staff in the water quality laboratory were very supportive in data gathering and also in providing historical data. A special acknowledgement goes to Dr. Darrel Townsend, Steve Nikolai, and Dr. Richard Zamor.

I am indebted to the GRDA for providing the opportunity that made it possible for me to pursue and complete my PhD study. I hope the outcome of our research will add value to their water quality monitoring program.

I acknowledge the Oklahoma Water Resources Board for providing me with data for my fourth chapter. Julie Chambers helped coordinate the monitoring staff to put the data together. Thank you Julie. Curt Dikes my former classmate was key in putting the data together and making them available. Thank you Curt, for your help.

I acknowledge my Graduate Adviser and mentor Dr. Stoodley for his invaluable support towards my progress in academia and in life generally. Dr. Stoodley has been one of the greatest academic mentors I have ever worked with. His aggressive mentality did put me on my toes to work hard and complete my PhD in three years. Dr. Stoodley has also been supportive to my wife and my daughter. Our passion and love for each other has transcended into being family friends. I hope I will have the opportunity to reciprocate his kindness in due course.

Dr. Andrew Dzialowski was the closest of my committee members. In addition to accompanying me during field monitoring, he spared one day in every week to meet with me and discuss progress of my work. This helped keep me on track and develop the ideas in my dissertation. He was very nice to me and was always available to discuss anything at any time. We ended up becoming close friends and I intend to keep our friendship active. Thank you, Andy. I am truly grateful. I also acknowledge Dr. Dzialowski's student, Bill Mausbach for helping me collect field data.

Dr. Nathan Torbick, whom I have never met physically, was an incredible source of support especially in figuring out the technical aspect of my work. Dr. Torbick is very knowledgeable in remote sensing and its applications, and he is always happy to help in any way he can. I doubt if I would have completed this PhD dissertation without his help. I was a novice in remote sensing and GIS when I started my PhD program but, with Dr. Torbick, I am relatively comfortable in the subject area today. Dr. Torbick and I also had

fruitful discussions in other areas including my career trajectory, future collaborations, and general life encounters. We ended up becoming great friends and colleagues, something I intend to continue. Thank you, Dr. Torbick. I am grateful.

Dr. Daniel Storm was previously in my committee and had to leave due to retirement. Nonetheless, his support with the statistics aspect of my PhD research was invaluable. His office was always open for discussions on the statistical options in my research. Dr. Storm is man of humor always in a happy mood. His was the place to go in trying times because his sense of humor can be a healing to the soul. I thank him and I wish him all the best in his retirement.

Dr. Kevin Wagner agreed to replace Dr. Storm in my committee. He later became my boss in the Oklahoma Water Resource Center. Since then, we have become colleagues working together on a variety of issues affecting water resources in Oklahoma. Because of this, I have been able to discuss my research extensively with him. He is always excited to listen to the stories about my PhD study. Dr. Wagner is very knowledgeable in water resource issues and his reviews are very helpful. I like his idea of follow-up meetings to discuss his reviews further. Dr. Wagner is a very nice and simple man with a great personality. I am thankful that we have become colleagues and friends. Thank you, Dr. Wagner. I am grateful.

I was fortunate to have worked with three program coordinators in the Environmental Science Graduate Program, Debbie Inselman, Chandler Fann, and Dr. Kerri Farnsworth-Hoback. Debbie was about to leave when I started. She was very supportive and very friendly. I am grateful for her support. Chandler took over and was equally as supportive; I am grateful. Kerri has been by far the most supportive program coordinator. Her constant reminders, passion for my progress, pieces of advice, and editing of my work have been incredibly helpful to me. Thank you Kerri; Environmental Science graduate students are very proud of you. I hear the stories all the time.

I have met and worked with great professors, colleagues, and friends. Dr. Jason Vogel has a special interest in Sierra Leoneans and has been very supportive to us. Jeri Fleming and the Blue Thumb family have been a great pillar to my progress. Colleagues at the Oklahoma Clean Lakes and Watersheds Association (OCLWA) have been incredibly supportive. Jason Aamodt is a great friend and mentor. Dr. Amy Frazier and Dr. Dave Lampert were very helpful with my research ideas and write-up; their critically edits benefited the outcome of my dissertation. All my professors of the various courses have influenced the positive outcome of this work. My friends in SES, Fulbright, and ASO have been phenomenal.

My people of the Salone Crew: Josephus Borsuah, Alimamy Fornah, Keima Kamara, Isha Fofanah, and Haja Fornah have been incredibly supportive to me financially and morally. I am grateful to you all. I acknowledge my colleagues at Njala University especially Mrs. Elizabeth Kattah, Dr. Bashiru M Koroma, Alfred Bockarie, Mohamed Dumbuya, Sellu Mawundu, John Kaisam, I.K Foday, Dr. G.M.T Robert, Dr. A.B Gogra, Mr. K.J Ganda, and Dr. Sharman Kamara for all the support and confidence. The BWMA family have always loved and believed in me; I am grateful for all the support. My NUMY friends have always expressed love and support for my work; thank you my friends. I am grateful to the late Alhaji YD Kamara for his support and mentoring; may God bless his soul. My HIDO family and our founder and leader have kept me close to heart and in prayer. I am truly grateful. My close friends who supported me in this PhD were Alfred Bockarie, Alimamy Fornah, Josephus Borsuah, Keima Kamara, Edwin Kamara, Papa and mama Kamara, Moses Kanneh, Ibrahim Bngura, Dauda Bangura, Sima Bangura, Abdulai Barrie, Tejan Bah, Rashida Kamara, Aunty Hawa Kandeh, Aunty Nafi and Husband, David Aloysius Koroma, Mohamed Bobor Deen, Idrissa Kamara (specialist), Morison Saidu, Brima Amadu and wife, Brima Amara and kids, Abu-Bakarr Massaquoi, Grace Kargobai, Mariatu Barrie, Hawanatu Sam, Nadia Williams, Badrudeen Barrie and family, Kalfala Fofanah, Haja Mariatu Thomas, Saudatu Tejan Bah, Mohamed Alhaji Bangura and wife, Musa Kabbah, Aunty Jebbeh, Brad Rogers, Mitch Sawttelle, Kim Don Song, Caitlin Barnes, Solmatz Rasoulzadeh, Aniko Konya, Betty Kallon, Patricia Moriba, Esther and Bill Clair, Lahai Koroma and his family, Lawrence Koroma, Joesphine Banister, Abubakarr Swarray, and Sidie Sisay.

Most importantly, I acknowledge my family. I dedicate this work to my daughter and my unborn child. I love them very much. I endure all the struggles in life because they inspire me in many ways. I thank them for their love, support, and patience. My wife whom I love very much has been a great listener to my PhD stories. Sometimes the stories are very depressing, and because of that she strongly considered not to go for PhD. I hope she does because it is a great experience. I dedicate this PhD to my late biological and foster parents. They are no here today to see the end of this journey but I believe they will be celebrating in heaven.

I dedicate this PhD to my brothers and sisters. They are my treasure, especially Ali, sister Kaday, late Mohamed, and Yayah. They have shown unconditional love and support for me. I can't thank them enough. My DMV family Ishmael, his wife, his daughter (Nenneh), and Aminu are my sources of inspiration and hope. They are always there for me. Thank you guys. I dedicate this PhD to all my nieces and nephews who root for me and are inspired by this story. I hope you will all grow up and make us proud. The same goes for my aunties and uncles as well as my cousins.

My mother-in-law is a mother figure to me. I have enjoyed talking to her and learning from her numerous pieces of advice. She is very caring and supportive. My brother Musa Kabba and his wife have always rooted for me. I am grateful for their confidence and support that they give me. The same goes for the other siblings of my wife. I hope our PhD will inspire you all to do great things.

Over and above all, I am thankful to God Almighty. My God has been so good to me. He answers my prayers in many ways and He has guided me towards the right path.

Name: ABUBAKARR S MANSARAY

Date of Degree: JULY, 2018

Title of Study: SATELLITE REMOTE SENSING OF HARMFUL ALGAL BLOOMS IN THE SUTHCENTRAL UNITED STATES OF AMERICA (USA)

Major Field: ENVIRONMENTAL SCIENCE

Abstract

The goal of water quality monitoring is to detect pollutants such as harmful algal blooms (HABs) and guide management decisions. A major challenge to this is the uncertainty in detecting pollutants in space and time. In Grand Lake O' The Cherokees, HABs became a public health concern in July 2011 when an advisory for no body contact included the Fourth of July holiday. This created the need to develop new strategies for timely detection of HABs. Satellite remote sensing provided the opportunity to achieve this goal. The Grand River Dam Authority (GRDA) funded this research, which integrated *in situ* water quality data, Landsat 8 data, and machine learning to build a tool for automated detection of HABs in the Grand Lake Watershed. We collected *in situ* samples from four reservoirs in the watershed and developed indices for algae and turbidity for input in the HABs monitoring tool. The tool utilizes Python programming language and extracts Landsat data from the United States Geological Survey (USGS) website for an interpretation protocol (High, Medium, and Low). This research also studied lake water quality by ecoregion and hydrologic unit Levels 4 and 6 in Oklahoma to guide ground based sampling. The goal is to utilize this information for regional application of the HABs monitoring tool. Further studies will delineate the spatial extent of sample points within a pixel, fusion of different satellite platforms, empirical data to calibrate and validate the monitoring tool, and the social/economic benefits of this new HABs detection strategy.

TABLE OF CONTENTS

Chapter Page

LIST OF TABLES

Table Page

LIST OF FIGURES

Figure Page

CHAPTER 1

INTRODUCTION AND LITERATURE REVIEW

1.0 Introduction

The goal of water quality management is to restore and maintain the chemical, physical, and biological integrity of impaired waters in the nation (Downing, 2011). This need comes from problems caused by point and nonpoint sources of pollution. These sources introduce pollutants such as sediment, nutrients, and microorganisms that can impair water quality in water bodies and pose health threats to humans and aquatic organisms (Brooks, et al., 2016). Minimizing these sources of water quality impairment will ensure better water quality in lakes and reservoirs and sustainably support recreation, fishing, tourism, and transportation. Achieving this goal has been a major challenge over the years (Sharpley, 2016).

The goal of water quality monitoring is to detect the presence, magnitude, and spatial extent of pollutants from those sources and guide management decisions (USEPA, 2010). A major challenge to this goal has been the increasing uncertainties in detecting pollutants at the right time and place.

This is the case for harmful algal blooms (HABs), which result from erratic incidents of high nutrient concentrations. The nutrients may come from upstream land use practices such as agriculture or oxidation/reduction processes that release them from the sediments into the water column (Findlay, Pace, Lints, & Howe, 1992). Nitrogen and phosphorus are the two main nutrients that nourish algae and lead to their exponential growth (Bormans, Maršálek, & Jančula, 2016).

In this study, we conducted 2.5 years of *in situ* water quality monitoring in spatial and temporal coincidence with Landsat 8 Operational Land Imager (OLI). The goal is to overcome monitoring challenges by combining these two sets of data and use machine learning to run an automated monitoring tool that detects and characterizes HABs. The study was done in four lakes in the Grand Lake Watershed including Grand Lake O' The Cherokees in Oklahoma, John Redmond Lake in Kansas, Council Grove Lake in Kansas, and Marion Lake in Kansas.

The Grand Lake Watershed is contained within four states: Kansas, Missouri, Oklahoma, and Arkansas (Figure 1). The major river systems in the watershed are the Neosho, Spring, and Elk Rivers. They all converge in Oklahoma in the upper portion of Grand Lake. Land cover in the Grand Lake Watershed mainly includes planted pasture, natural grassland, cropland, forest, developed areas, and open water and wetlands (Holt, et al., 2008).

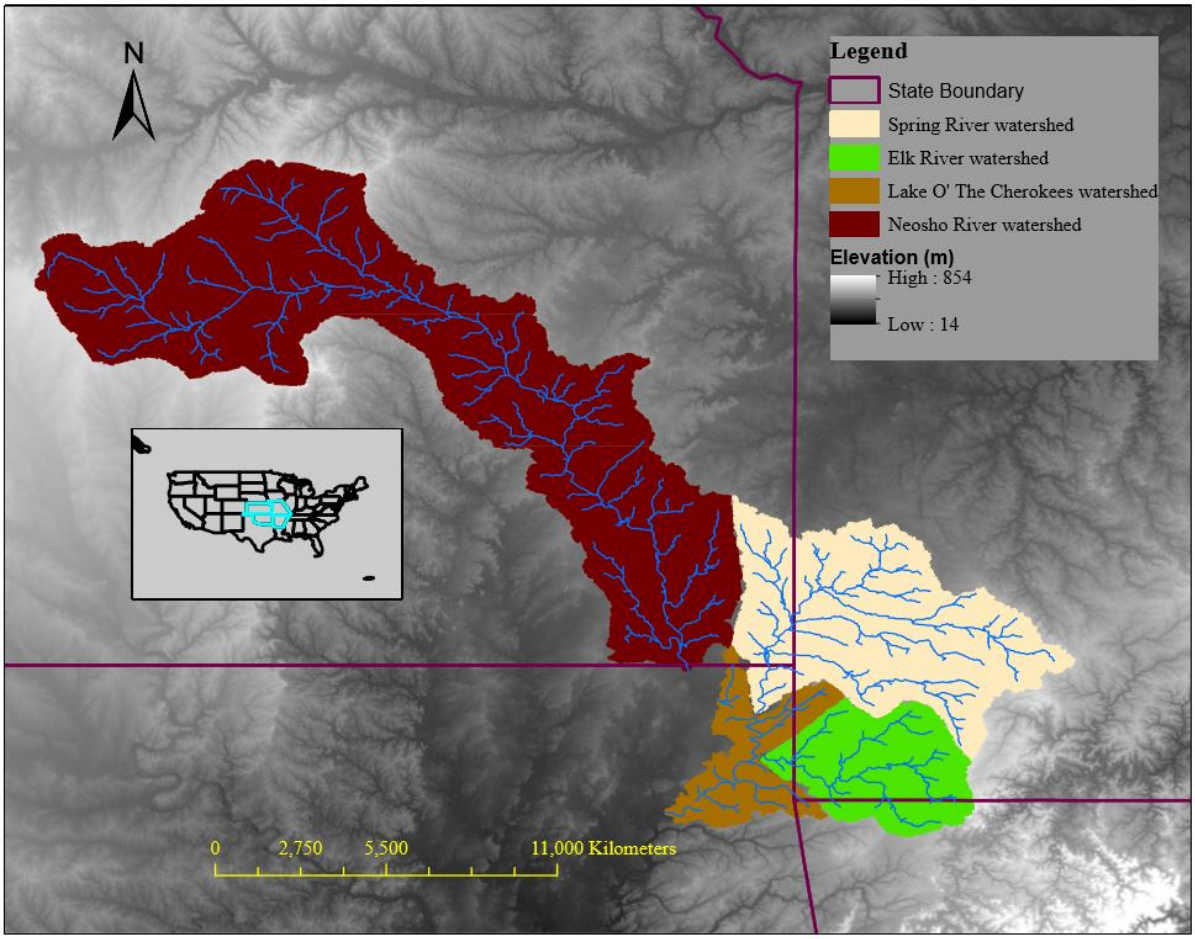

Figure 1. Map showing the Grand Lake Watershed located in Kansas, Missouri, Arkansas, and Oklahoma.

According to the Oklahoma Conservation Commission (OCC), nonpoint sources of pollution in this watershed are agriculture, construction, in-place contaminants, urban runoff, wastewater, resource extraction/exploration, mill, and mine tailings (OCC, 2014). These sources were determined through multiple assessment activities from 1990 to 2000 including pre-implementation monitoring, clean lakes identification studies, and monitoring by the United States Geological Survey (USGS). In 2001, a watershed advisory group was formed; watershed based plans were developed in 2005 and 2009. Total maximum daily loads (TMDLs) for bacteria were created in 2008 and nutrients in 2013. The OCC created the

United States Clean Water Act's Section 319(h) work plans through 2001-2012 to address those nonpoint sources of pollution. In 2006-2012, the United States Environmental Protection Agency (USEPA) approved the Honey Creek watershed based plan, which led to implementation of practices and post-implementation monitoring. The OCC also collaborated with their Kansas counterpart to draft a regional conservation partnership program in 2014 (OCC, 2014).

In Grand Lake O' the Cherokees, nonpoint sources have posed spatial and temporal challenges to the Grand River Dam Authority (GRDA) when monitoring and detecting HABs. Land use practices such as agriculture, small communities, and forestry activities supply nutrients that cause algal growth. They also serve as sources of organic carbon that aid microbial metabolism and subsequently anoxic conditions (Machmuller, et al., 2015), which release bioavailable phosphorus from sediments into the water column (Findlay, Pace, Lints, & Howe, 1992). Nitrogen also comes in through cyanobacterial fixation from the atmosphere (Howarth, Marino, Lane, & Cole, 1988), groundwater supply (USGS, 2016), and surface runoff (Filstrup & Downing, 2017).

In July 2011, there was a public health concern when an unprecedented algal bloom led to an advisory for cessation in recreational activities in Grand Lake, which included the Fourth of July holiday. The need to develop new monitoring strategies for timely detection of HABs became a priority. Advances in moderate resolution satellite datasets and associated applications provided the opportunity to integrate satellite spectral data, ground based *in situ* water quality data, and machine learning into an automated HABs detection tool for inland water bodies in the Grand Lake Watershed. Ultimately, this monitoring capability will be extended to HABs detection in the entire southcentral USA.

Utilizing satellite data for HABs detection is an active area of scientific research with many unexplored opportunities. Lake managers in the Grand Lake watershed will benefit from one such opportunity through this Grand River Dam Authority (GRDA) funded research. The dissertation has five chapters. Chapter 1 introduces the problem, its context, and reviews literature in the subject area. The three chapters that follow are in the form of journal articles. Chapter II presents a novel index for photosynthetic algae in the study area. There is also a mineral turbidity index to account for interference from other optically active objects. The indices developed in Chapter II are key components in the automated monitoring tool described in Chapter III. Chapter IV compares lakes by ecoregion and hydrologic unit in Oklahoma in terms of water quality and the potential for regional application of the monitoring tool. Chapter V is a conclusions chapter that ties all the chapters together into conclusions, recommendations, and limitations of the study.

1.1 Literature Review

1.1.1 Basic concepts

The primary steps in satellite remote sensing include delineating useful components of the electromagnetic radiation, image acquisition and processing, field data collection (Campbell & Wynne, 2011), and integration into management tools such as artificial intelligence (Jensen, 2015). Data from electromagnetic radiation combined with field data explains relationships between predictors and response variables (Pettorelli, et al., 2014). These relationships validate simulation through computer programming languages (such as Python) that synthesize information into algorithms, a set of instructions that guide development of a decision support tool (Theologou, Patelaki, & Karantzalos, 2015). The computer algorithm accomplishes this by deploying those variables with reference to

empirical data or experience, which result in the ability to estimate parameters of interest (Pettorelli, et al., 2014).

1.1.1.1 Electromagnetic radiation

The sun's thermonuclear fusion process leads to continuous emission of radiation that fluctuates between electrical and magnetic fields as it travels to earth (Campbell & Wynne, 2011). These interactive electrical and magnetic forces give the sinusoidal particle-wave nature of incident radiation on the surface of the earth. The application of remote sensing in natural resource research derives from different objects having unique properties that allow unique interactions with this radiation as it becomes incident on the earth's surface and reradiates back from it (Campbell & Wynne, 2011). Unique spectral characteristics give objects a spectral signature. Different substances have unique spectral signatures that make it possible to study their characteristics using remotely sensed, multispectral data. This creates the opportunity to overcome a number of monitoring challenges including accessibility issues, financial burdens, conflicting interests, and uncertainty in imminent pollution spikes (Pettorelli, et al., 2014).

Studies have characterized electromagnetic energy into component parts based on the wavelength of radiation in order to understand these spectral signatures. These arrangements in the number and dimensions of specific wavelengths of energy form the Electromagnetic Spectrum (EMS) (Campbell & Wynne, 2014). When substances interact with electromagnetic energy, they undergo one or more of the following:

- The substance may absorb some or all of the radiation and become excited to a higher energy level;
- The substance may reradiate the absorbed energy into different wavelengths;

- The substance may reflect back some or all of the radiation; or
- The substance may scatter the radiant energy.

The type of interaction depends on the inherent chemical properties of the substance as well as the environmental conditions affecting its physical state (Campbell & Wynne, 2014).

The observation and recording of these interactions in concert with the inherent properties of the substance in question form the basis of multispectral satellite remote sensing in natural resource research (Pettorelli et al., 2014). According to Campbell and Wynne (2014), these interactions are rooted in the following underlying characteristics of the electromagnetic energy:

- Wavelength: the distance between two crests of the sinusoidal wave of energy. It is affected by electric and magnetic fields;
- Frequency: the number of crests passing a fixed point in a given time period, usually measured in hertz (cycles per second). The frequency has an inverse relationship with the wavelength;
- Amplitude: the maximum height of the crests (the peak of displacement); and
- The speed of electromagnetic energy (c), a product of the frequency (ν) and the wavelength ($\boldsymbol{\lambda}$).

In remote sensing, the unit of electromagnetic energy is usually in wavelengths. It is common to cite wavelength in nanometers (10^{-9} meters, nm) or micrometers (10^{-6} meters, μm) in these applications. The EMS has regions of electromagnetic energy between extremes of long and short wavelengths. Each region has bands of different wavelengths with shorter wavelengths corresponding to higher energy. These regions range from Gamma Rays the highest energy region to Radio Waves the lowest energy region. Since different substances interact

differently with solar energy, spectral signatures are useful in building computer algorithms to explain changes in environmental conditions (Pettorelli et al., 2014). The two most important spectral bands to remote sensing of the environment are visible and infrared (IR) spectra (Campbell & Wynne, 2014); Table 1 shows the characteristics of the different bands as they apply to Landsat platforms.

1.1.1.2 The visible spectrum

This visible spectrum ranges between wavelengths of 400 and 700 nm. This portion of the sun's electromagnetic energy makes the sense of vision possible in humans and other animals. The visible spectrum divides into three primary regions of importance to remote sensing of the environment: 400-500 nm (Blue light), 500-600 nm (Green light), and 600-700 nm (Red light). One of these colors (Blue, Green, or Red) reflects and appears to the human eye when an object absorbs the other two. When an object reflects all three primary colors, we see white light. Absorption of all primary colors appears black (Jensen, 2015).

1.1.1.3 The infrared (IR) spectrum

The Infrared (IR) Spectrum spans from 700-2500 nm of the EMS (Jensen, 2015). Because of its broad range of wavelengths, IR has multiple applications in remote sensing of the environment. It divides into three sub regions: Near Infrared (NIR), Mid Infrared (MIR), and Far Infrared (FIR). Radiation in the NIR region has optical properties significant to natural resource studies. For example, a combination of Visible Green and NIR spectra have been useful in vegetation studies (Thenkabail, et al., 2013). Infrared is also useful in studying soils, heavy metals, and minerals (Shi, Chen, Liu, & Wu, 2014). The delineation of riparian areas around water bodies (Thenkabail, et al., 2013) utilizes the NIR region of radiation. The FIR, also known as Thermal IR, has been useful in understanding the thermal properties of

substances (Campbell & Wynne, 2014). In general, IR radiation is useful in delineating water bodies in the study area because clear water absorbs all of it (Jensen, 2015).

In Landsat sensors prior to Landsat 8 (Table 1), thermal IR is Band 6, lying between shortwave IR 1 (SWIR 1) and shortwave IR 2 (SWIR2). In Landsat 8 (Table 1), the SWIRs appear as Bands 6 and 7; thermal IR bands are Bands 10 and 11. The SWIRs are two useful bands in natural resource studies. They reflect high when incident on solid minerals, making them useful for delineating mineral turbidity in lakes and reservoirs (Jensen, 2015). The panchromatic band is a grey scale image that spans across the Red, Green, and Blue (RGB) portions of the electromagnetic spectrum. It has a higher spatial resolution (15 m) compared to the other bands (30 m). Landsat 8 has higher spectral resolution (i.e. the number of bands a sensor can detect) compared to the previous sensors because it has additional bands for detecting coastal aerosols (Band 2), cirrus clouds (Band 9), and an additional thermal IR band.

1.1.1.4 Landsat sensors

In the 1960s, the United States Department of the Interior (DOI), the National Aeronautics and Space Administration (NASA), and the United States Department of Agriculture (USDA) embarked on an ambitious effort to develop and launch the first civilian Earth observation sensors on satellite platforms (USGS, 2015). By July 1972, there was a successful launching of the Earth Resources Technology Satellite (ERTS-1), which was later renamed Landsat 1. The launches of Landsat 2, Landsat 3, and Landsat 4 followed in 1975, 1978, and 1982, respectively. They all carried multispectral scanners (MSS). The successful lunching of Landsat 5 Thematic Mapper (TM) in 1984 ensured continued delivery of high quality images of the surface of the Earth for 28 years and 10 months.

In 1993, Landsat 6 failed to achieve orbit leading to the launch of Landsat 7 Enhanced Thematic Mapper (ETM+) in 1999. On May 31, 2003, the Scan Line Corrector (SLC), which compensates for the forward motion of the Landsat platform, failed and has not recovered despite subsequent efforts. As a result, the ETM+ sensor returns images with duplicated areas and widths that increase toward the scene edge (USGS, 2015). The latest Landsat sensor is the operational land imager (OLI) launched on Landsat 8 in 2013. It collects images of the surface of the Earth every 16 days. The United States Geological Survey (USGS) archives and provides all the Landsat data to the public at no cost. Table 1 shows the Landsat types and their detailed information.

Table 1. Spectral details for the various Landsat platforms (USGS, 2015)

Multispectral Scanner (MSS)	Landsat 1-3	Landsat 4-5	Spectral Res (µm)	Spatial Res (m)
	Band 4	Band 1	0.5-0.6	60
	Band 5	Band 2	0.6-0.7	60
	Band 6	Band 3	0.7-0.8	60
	Band 7	Band 4	0.8-1.1	60
	Landsat 7		Spectral Res (µm)	Spatial Res (m)
Enhanced Thematic Mapper Plus (ETM+)	Band 1		0.45-0.52	30
	Band 2		0.52-0.60	30
	Band 3		0.63-0.69	30
	Band 4		0.77-0.90	30
	Band 5		1.55-1.75	30
	Band 6		10.40-12.50	30
	Band 7		2.09-2.35	30
	Band 8 - Panchromatic		0.52-0.90	15
	Landsat 8		Spectral Res (µm)	Spatial Res (m)
Landsat 8 Operational Land Imager (OLI) and Thermal Infrared Sensor (TIRS)	Band 1 - Coastal aerosol		0.43 - 0.45	30
	Band 2 – Blue		0.45 - 0.51	30
	Band 3 – Green		0.53 - 0.59	30
	Band 4 – Red		0.64 - 0.67	30
	Band 5 - Near Infrared (NIR)		0.85 - 0.88	30
	Band 6 - SWIR 1		1.57 - 1.65	30
	Band 7 - SWIR 2		2.11 - 2.29	30
	Band 8 – Panchromatic		0.50 - 0.68	15
	Band 9 – Cirrus		1.36 - 1.38	30

	Band 10 - (TIRS) 1		10.60 - 11.19	30
	Band 11 - (TIRS) 2		11.50- 12.51	30

1.1.1.5 Spectral signatures

Clear water reflects low amounts of visible light. When the water becomes turbid, this reflectance increases up to 10%, especially in the visible bands. Green vegetation reflects high in the Green band compared to the other visible bands and in the NIR region; it absorbs Blue and Red radiation. Due to these spectral properties, studies can discern different types of vegetation by examining their absorption/reflectance spectra in the visible and IR regions (Jensen, 2015). Figure 2 shows the spectral signatures of substances of interest in this research.

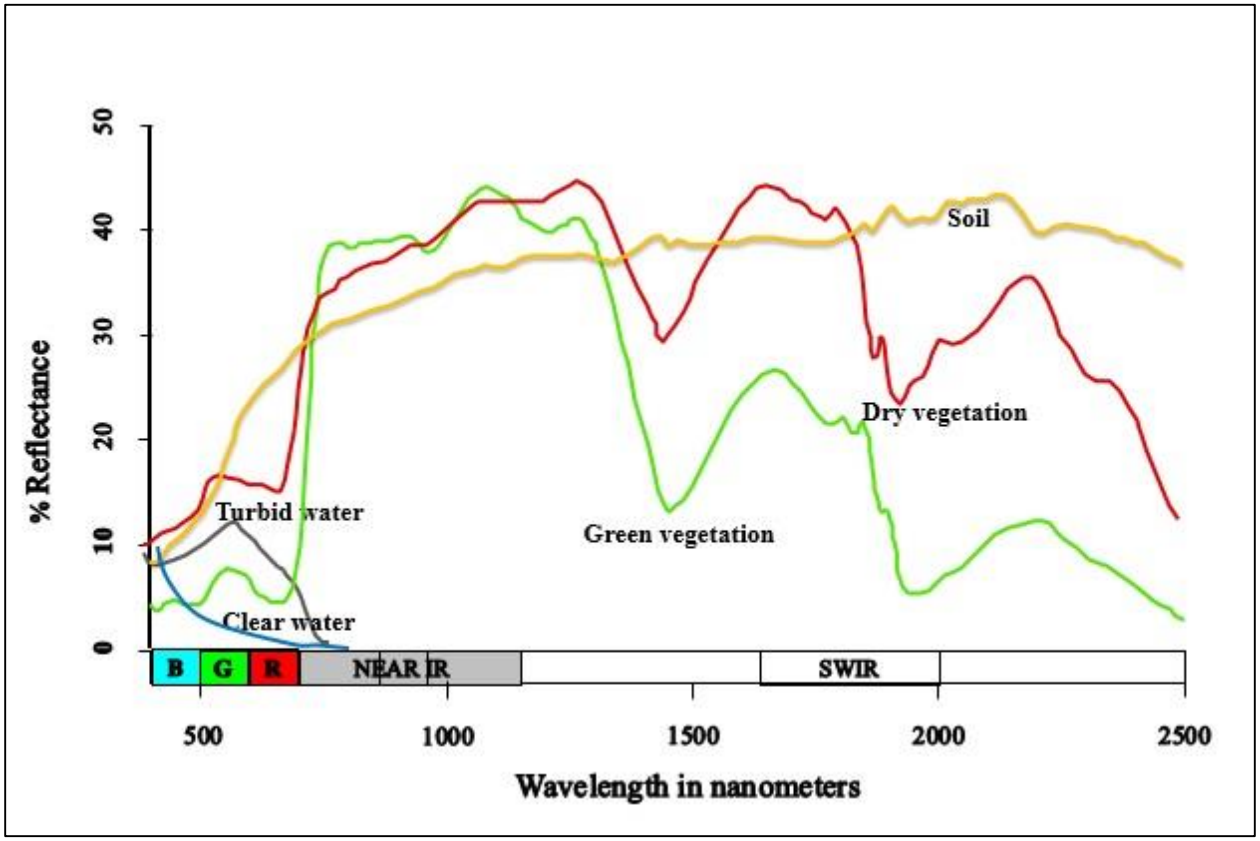

Figure 2. Spectral signatures of substances of interest *(Zorogastúa C, Quiroz, Potts, & Schulz, 2014)*

The spectral signature representing green vegetation is due to pigments that interact with visible light; they are present in all photosynthetic organisms including green plants and phytoplankton (microscopic plants and algae) in aquatic ecosystems (Kirk, 2011). The presence of photosynthetic pigments in diversity of organisms makes it difficult to provide unique spectral information for algal biomass. One way to address this problem is utilizing the differences in spectral signatures between green plants and algal biomass. In the leaves of green plants, the spongy mesophyll layer has the ability to reflect NIR radiation (Jensen, 2015). This spongy mesophyll layer is absent in algae. This serves as useful information in accounting for contribution from green plants in the development of a differential index for algal biomass.

Chlorophylls are the pigments that enhance reflection of Green light in photosynthetic organisms. Their porphyrin ring provides the required oxidation/reduction potential that allows for transfer of electrons in their excited states and energized by solar radiation. This transfer of energized electrons is made possible by chlorophyll-a (CHLa), which passes the electrons to sugar forming molecules. All photosynthetic organisms contain CHLa. Other forms of chlorophyll exist including chlorophyll b (CHLb), which occurs only in green algae and in plants, and many types of chlorophyll c (Kirk, 2011).

Carotenoids are the pigments responsible for reflectance of Red, Orange, and Yellow bands in plants and algae. The carbon rings of carotene connected by carbon chains do not transfer solar energized electrons through the photosynthetic pathway. They lose their absorbed energy to chlorophyll (Kirk, 2011). These exchanges between reflectance and absorbance through oxidation/reduction chains are useful in developing indices for algal biomass in the study area.

Delineating the spectral signature of water clarity in lakes and reservoirs also helps in development of an automated satellite-based monitoring tool. This is possible by accounting for Secchi disc depth (SDZ), turbidity, and colored dissolved organic matter. Soil reflects high in the NIR and SWIR regions (Jensen, 2015). This gives useful spectral signatures in developing a differential index for mineral and algal turbidity. Colored dissolved organic matter (CDOM) is the light absorbing component of dissolved organic matter (Harvey, Kratzer, & Anderson, 2015). There is difficulty in differentiating spectral signatures between CDOM and algal content using low spatial resolution Landsat (900-m^2 pixel size). Therefore, a differential algal index would require ground-based sampling of algal concentrations in the water column.

1.1.1.6 Image resolution

The four types of resolution used in remote sensing of natural resources are spatial, temporal, radiometric, and spectral (Jensen, 2015). Each type of resolution has unique information that defines the properties of pixels as well as the margin of error. All four resolutions give the overall properties of an image (Jensen, 2015).

Spatial resolution gives the minimum angle or distance separating two objects that can be resolved by a sensor. The spatial resolution represents the size of a pixel, which is the smallest unit of an image on computer screens or hard copy images. Landsat has a spatial resolution of 30 m x 30 m. Some sensors have higher spatial resolution, making them useful in detailed discrimination of objects on the surface of the Earth. Digital Globe's WorldView-2 has a spatial resolution of 0.46 cm x 0.46 cm for its panchromatic band and 1.85 m x 1.85 m for its four multispectral bands (Jensen, 2015).

Temporal resolution is the time a satellite takes to return to the same spot to collect an image. This enhances multiple records of the same spot on Earth over time, and this helps in developing models that relate spectral data and temporally related water quality parameters of interest. The temporal resolution of Landsat is 16 days (Jensen, 2015). This makes Landsat a useful tool for monitoring water quality parameters like algal pigments and water clarity. If the study area falls in more than one path/row combination, it is possible to conduct weekly monitoring using Landsat. A path/row combination is the area covered by the Landsat sensor as it takes pictures of the surface of the Earth during Landsat orbit from north to south and Earth orbit from east to west (USGS, 2016).

Radiometric resolution refers to the sensitivity of a remote sensing detector to differences in signal strength as it records the radiant flux reflected, emitted, or back scattered from the terrain (Jensen, 2015). The unit of radiometric resolution is bits, which gives a measure of the number of brightness values (BV). These are a range of colors between black and white contained within an image. The number of BV is calculated as the number 2 raised to the number of bits ($BV = 2^{bits}$) of the image (Jensen, 2015). The Landsat 1 MSS had 6-bits, giving 2^6 BV (0-63). The Landsat TM and ETM+ sensors had 8-bits, giving them higher radiometric resolution (0-255 BV) than the MSS platforms. Landsat 8 OLI has 16-bits giving its images 2^{16} BV (0-65,535 BV).

Spectral resolution refers to the number and dimensions of wavelength intervals or bands in the EMS to which a sensor is sensitive. The more bands a sensor can detect, the higher its spectral resolution. When the sensor detects multiples of bands, the phenomenon is called multispectral remote sensing. All Landsat sensors are multispectral as they have between 4 and 11 spectral bands. Hyperspectral remote sensing involves the detection of

hundreds of bands. In ultraspectral remote sensing, the sensor detects several hundreds of bands. (Jensen, 2015).

1.1.1.7 Image acquisition and processing

The USGS has made all of the Landsat data available for free download from one or more of the following websites: Earth Explorer (http://earthexplorer.usgs.gov), Global Visualization Viewer (GloVis) (http://glovis.usgs.gov), and Landsat Look Viewer (http://landsatlook.usgs.gov). Image processing begins with pre-processing by correcting errors sourced from the sensor, atmosphere, and topography (Jensen, 2015). Post-processing includes accuracy assessment, information extraction, and utilization of data from the image (Jensen, 2015). There are statistical and physical models that correct for errors in digital numbers and compute radiance values representing pixels (Campbell & Wynne, 2014). Statistical models (example, Dark Object Subtraction and apparent reflectance) use properties of the image to correct for errors. Physical models on the other hand take into account the dynamic nature of the environmental phenomenon and incorporate parameters that may interfere with reflectance of radiation.

For Landsat, the USGS does radiometric and geometric corrections of images and makes them publicly available. Following download of an image, the user needs to carry out atmospheric correction in order to remove error from scattering or misrepresentation of pixels. Most of the statistical and physical models for atmospheric correction come as extensions of image processing software packages such as ENVI and ArcGIS. Some of the widely utilized physical models include fast line-of-sight atmospheric analysis of spectral hypercubes (FLAASH), second simulation of satellite signals in the solar spectrum (6S), low resolution atmospheric radiance and transmittance (LOWTRAN), moderate resolution

atmospheric radiance and transmittance (MODTRAN), and quick atmospheric correction (QAC).

A key component of satellite imagery is the development of products that end users can apply in their project management efforts. Scientists build these products through machine learning applications; one such application is open Python scripting. Python is useful in remote sensing applications because it has both analytical and object oriented applications. It interfaces with a variety of extension programs such as GDAL (a translator library for raster and vector geospatial data), NumPy (the fundamental package for scientific computing with Python), and shapely (a spatial data model for points, curves, and surfaces).

Barrett and Frazier (2016) used open Python scripting to develop an automated method of extracting remotely sensed reflectance values from Landsat imagery to pinpoint water sample locations and their respective quality parameters with universal applicability (Barrett & Frazier, 2016). The criteria used for utilization of their automated method include:

1) In-situ water quality parameters collected after 1 March 1984;
2) Landsat TM and ETM+ images downloaded from the USGS Earth Explorer and GloVis, temporally coincident with water quality parameters within ± one day, and covering the lake(s) of interest; and
3) Lake-boundary shape files: the authors used automated image processing built in the open Python scripting language in ArcMap via the Arcpy (the Python extension in ArcGIS mapping software) module.

Image processing followed four stages: minimum value extraction and image subsetting, radiometric correction including water and cloud masks, extraction and averaging of spectral

reflectance values in sample point windows, and statistical regression analysis (Barrett & Frazier, 2016).

They tested their approach on a set of lakes in eastern Oklahoma and the results of reflectance in the short wave infrared (SWIR) region of the EMS had significant relationships ($\alpha < 0.01$) with both chlorophyll and turbidity through ratios with other bands. Even though USGS now processes and provides Landsat data at no cost to the user, the work of Barret and Frazier (2016) serves as a useful reference for quality control and quality assurance.

In a 1999 study, Allee and Johnson processed their Landsat images for 30 sampling points using global positioning system (GPS) and pseudo invariant features (PIF) (Allee & Johnson, 1999). The study utilized geometric measurements of Landsat scenes using a vector-based hydrology map obtained from the USGS with mean digital numbers from a 3x3-pixel window for Bands 1 to 5 and 7 for each station. The resulting pixel values accounted for boat drifting and erroneous GPS coordinates. Results of their predictive models for CHLa showed a good coefficient of determination (R^2= 0.80) in the July 1994 set of samples and also in the December 1994 samples (R^2 = 0.84); the February 1995 data for SDZ also had strong R^2 (0.96). The historical data did not quite support these models probably because of differences in species composition during different times of satellite flyover.

Kallio et al (2008) rectified their ETM+ images to national geographic coordinates based on 25 ground control points (GCPs). Using nearest neighbor, they resampled the images to 25 m with positional accuracy of about 0.5 pixel. Digital numbers were useful in calculating the top-of-atmosphere (TOA) radiances and they applied the gain and offset

values of the header files associated with each image. The authors used the simplified method of atmospheric correction (SMAC) model to minimize errors from the atmosphere.

The study simulated underwater reflectance using the Finnish national water quality dataset for 2000–2002 including the routine monitoring results of 1,670 stations representing 1,113 lakes. Kallio et al (2008) used the bio-optical models concentration of total suspended solids (CTSS), the absorption coefficient of colored dissolved organic matter at wavelength λ = 400 nm (aCDOM400), and the sum of concentrations of CHLa and phaeophytin a (CChl-a) as input to measure reflectance for turbidity, Colored Dissolved Organic Matter (CDOM), and SDZ.

For estimation errors, the image-specific empirical algorithms improved on accuracy by 14% compared to using *in situ* data without algorithm training. The results also revealed that a better atmospheric correction method was needed as SMAC had minimal improvement compared to the original Top-of-Atmosphere radiance. The under-water simulation of reflectance revealed the need for region-specific algorithms, particularly in the case of SDZ. Overall, this reflectance model has been tested and proven to work in Finnish lakes (Kallio, et al., 2008).

1.1.1.8 Ground reference information

Ground reference data make it possible for image enhancement, image correction using ground reference points or pseudo-invariant features, and accuracy assessment. Ground reference data is also important because it combines with remotely sensed data to validate the spectral signature of substances under study (Jensen, 2015).

A typical data gathering technique in remote sensing is the use of in-situ sampling through transducers (Jensen, 2015). The transducer comes into physical contact with the

medium and records a signal that represents the presence and magnitude of a specified parameter in that medium. The signal is usually energized by pressure, electric charge, magnetic induction, or temperature change. The instrument displays concentrations of parameters of interest on the detector screen (Jensen, 2015). In order to ensure true representation of situations on the ground, studies usually collect field data that are temporally coincident with remotely sensed data (Jensen, 2015).

Collecting field data at temporally coincident time with Landsat overpass has proven useful in the literature. Allee and Johnson's study (1999) derived SDZ and CHLa from Landsat spectral data by developing an algorithm that relates the two sets of data. The authors recognized that atmospheric conditions vary on a daily basis and have an impact on the nature of spectral data. In addition, ground conditions have impacts on the magnitude and properties of parameters measured. Due to these dynamics, the authors decided to collect their field data on dates temporally coincident with Landsat overpasses.

Carpenter and Carpenter (1983) utilized spectral data from Landsat MSS to build multiple linear predictors for turbidity and chlorophyll pigment in freshwaters in southeastern Australia (Carpenter & Carpenter, 1983). The objective was to develop a remotely sensed monitoring tool that would help alleviate the burden of covering costly and inaccessible monitoring sites. Since the study used Landsat data as surrogate to ground based monitoring, ground reference information at coincidental times was imperative. This is because environmental conditions change on a daily basis and may not reflect the true nature of conditions during sampling time before or after Landsat overpass (Carpenter & Carpenter, 1983). In their 2008 study, Kallio et al investigated the estimation accuracy of Landsat

imagery for turbidity, CDOM, and SDZ and asserted this was possible through ground based monitoring temporally coincident with image acquisition (Kallio, et al., 2008).

It is also typical to have some flexibility in temporal coincidence for field and Landsat data provided there is no major change between the acquisition dates. Major changes may be due to biophysical conditions of the water body and its surroundings or atmospheric conditions. The number of flexible days reported in the literature range from ±1 day (Barret and Frazier, 2016) to ± 7 days (McCullough, Loftin, & Sader, 2012) of satellite overpass.

1.1.1.9 Image errors

Water quality monitoring through satellite remote sensing includes planning and design of appropriate methodologies and analytical protocols that ensure significant reduction in error (Jensen, 2015). Several sources of error exist in satellite remote sensing. These errors come from geometric and radiometric distortions from the Earth's complicated systems and imperfect sensors (Jensen, 2015).

Sensor errors are systematic and correction protocols exist to help improve image quality. One source of sensor error is in the type of scanner used. The Landsat sensors have either whiskbroom or pushbroom scanners. Whiskbroom mirrors move across a track to reflect light on a single detector. The mirror moves back and forth to collect measurements one pixel at a time. These back and forth movements give angles of reflections at the nadir different from those at the edges. These differences in angles at which the mirror scans an object creates a distortion at the edges of the image. All Landsat sensors prior to Landsat 8 had whiskbroom scanners on their platforms.

Pushbroom scanners have fewer moving parts and they move along the track of the Landsat platform collecting images of many pixels at a line perpendicular to the flight path.

This gives them increased sensitivity and fewer edge errors compared to whiskbroom scanners. The Earth Resources Observation and Science (EROS) Center in South Dakota does correction of all sensor edge errors before posting images on the USGS website (USGS, 2016).

Bad pixels (shot noise) and line dropout (line stripping) are two important sources of error. Bad pixels result when the scanner skips certain areas and records wrong pixel values. Typical correction methods include interpolation from neighboring pixel values or comparison to images taken from the same spot on previous dates. One issue with these corrections is in the heterogeneous nature of land cover types. Interpolating values from neighboring pixels that may represent different land cover types may be misleading, especially giving the low spatial resolution of Landsat. Another issue is that changing characteristics of a particular land cover over time may give misleading information about the bad pixel (Jensen, 2015).

The fate of radiation from the sun also introduces error in pixel values recorded by the sensor. The ideal way of avoiding sources of error resulting from the fate of reflected solar radiation is to select spectral bands that are less susceptible to atmospheric scattering as well using images less affected by cloud cover. Studies have shown that cloud cover less than 10% is ideal for natural resource remote sensing (Sano, Ferreira, Asner, & Steinke, 2007). The five main fates and their characteristics include (Jensen, 2015)

1) Solar radiation is incident on the target pixel, reflects and makes its way to the Landsat sensor, and sensor records the correct pixel value. This is the ideal route of solar radiation for remote sensing of the environment.

2) Solar radiation is incident on the atmosphere, it is scattered, makes its way to the Landsat sensor, and wrongly represents target pixel values. This gives misleading spectral signatures and is very common with short waves radiant energy. That is why ultraviolet (UV) and Blue bands are not very useful in remote sensing of the environment.
3) Solar radiation is scattered by the atmosphere, part of it becomes incident on the target pixel, makes its way back to the Landsat sensor, and sensor records spectral signature representing that target pixel. This will give the expected spectral signature under study.
4) Solar radiation is scattered by the atmosphere, part of it becomes incident on the wrong pixel, makes its way back to the Landsat sensor, and sensor records spectral signature representing the target pixel. This will give misleading results of the spectral signature under study.
5) Solar radiation is scattered by the atmosphere, part of it becomes incident on the wrong pixel, bounces on to the target pixel, makes its way back to the Landsat sensor, and sensor records spectral signature representing the target pixel. This will give the expected spectral signature under study.

Another source of error is distortion in synchronicity between the orbit of the Earth and the sensor orbit. This leads to shift in pixel positions on the surface of the Earth. The Earth is spherical, making it impossible to have a 90^{o} angle of incidence at nadir, which creates a source of spatial error. An important type of spatial error is circular error of probability, which defines the average distance between a target and the terminal end of the signal's path of travel. When signals are recorded, it is possible to miss the target pixel several times.

Calculation of circular error considers the distance of each missed target from the intended target (Kim, 2017). The acceptable distance depends on the type of satellite mission and type of image correction routine. The USGS Landsat data gap study team accepts a circular error less than 65 m for image processing (USGS, 2017).

Correction of errors due displaced pixels is done by repositioning them to their original locations with GCPs and mathematical models. It is easy to identify GCPs with the use of reference maps or georeferenced images. Using the map or georeferenced image, correction follows the use of an appropriate warping model, a transformation matrix, and resampling of the BV to restore accuracy of data obtained. The EROS center does all these image corrections before the USGS provides the readily available images to the public.

Ensuring accuracy in ground-based data minimizes errors like misrepresenting pixels during field monitoring. Sometimes the pixel values do not represent the true picture of variations in the land cover types. Low spatial resolution pixels may have a mix of land cover types that make it difficult to record values representing one spectral signature. In addressing these issues, researchers use empirical tests to confirm the right spectral signature (Theologou, Patelaki, & Karantzalos, 2015).

1.1.2 Algorithm development for mapping water quality

In an algorithmic approach to problem solving, the computer programs give an output of the defined relationship between the independent and response variables. Any change in information may require modification of the algorithm to accommodate for that change (Jensen, 2015). Selection of appropriate algorithms is critical in building automated tools for remotely sensed natural resource monitoring. Algorithms can be object based, supervised, or unsupervised input-output relationships (Jensen, 2015).

Regression analysis gives the significance of those relationships even though it sometimes drops the most important variable due to computational issues like multi-collinearity (Carpenter & Carpenter, 1983). An important consideration is that environmental processes are complex and may violate some of these modeling requirements. The need for more flexible but accurate mapping tools becomes obvious in some cases (Dormann, et al., 2013). Theologou et al (2015) confirmed the use of one or more of the following algorithms in establishing relationships between in-situ field and Landsat data (Theologou, Patelaki, & Karantzalos, 2015).

1) Empirical algorithm: the creation of regression models using satellite imagery and water quality parameters. The primary sources of data are principally the satellite data (the independent variable) and field in-situ data (the dependent variable). The process is essentially an input-output analysis.
2) Semi-empirical approach: This approach embodies the use of spectral water quality characteristics in the statistical analysis. There are inherent sets of information that help map the deployment of information into the model.
3) Analytical approach: In this approach, key parameters relate to the inherent optical properties, the apparent optical properties, and top-of-atmosphere radiance.

1.1.2.1 Band ratios and the development of indices

A remarkable application of remotely sensed data in natural resource studies is the development of indices from equations derived from ratios of spectral bands. The process utilizes information from feature pixels of different bands and their relationships to translate into useful information (Jensen, 2015). Most indices make use of a normalized relationship between two bands that concurrently interact with matter. In a 1973 study, researchers

developed the normalized differential vegetation index (NDVI) to infer the health of vegetation in terms of changes over time (Rouse, Haas, Schell, & Deering, 1973). The index is based on the assumption that greater biomass equates to better health of an ecosystem. It has a range of values defined as $-1 \leq NDVI \leq 1$. The lesser the value, the less healthy is the vegetation. Values closer to or equal to one indicate healthy vegetation (Jensen, 2015).

In 2010, a group of researchers in India developed a MERIS (MEdium Resolution Imaging Spectrometer) Terrestrial Chlorophyll Index (MTCI) to map the spatio-temporal variation of vegetation phenology using the equation (Jensen, 2015): $\rho_{band\ 10} - \rho_{band\ 9} / \rho_{band\ 9} - \rho_{band\ 8}$ (ρ represents reflectance). The equation derives from MERIS bands 8, 9, and 10. With an 8-day temporal composite of MERIS MTCI data, the authors suggested that the MTCI combined information on leaf area index and the chlorophyll concentration of leaves to produce an image of chlorophyll content (Jensen, 2015).

1.1.2.2 Remote sensing of water quality in reservoir ecosystems

The availability of remote sensing datasets and the understanding of their benefits and limitations provide the potential to assist in overcoming some water quality monitoring challenges. These include meeting the cost of additional sampling space/frequency and inaccessibility to important areas (Barnes, Hua, Holekamp, Blonski, & Spiering, 2014). This has led to several studies that use algorithms to establish relationships between remotely sensed and ground based data. Birth and McVey (1968) were among the first scientists to utilize remote sensing techniques to reveal new findings in natural resource management. They evaluated the color of grass turf using a ratio of NIR (750-nanometer [nm]) to Red (650-nm) reflectance and called it the turf color index. The authors developed this index in order to serve as a means of determining from an image the density and distribution of grass

turf in an area. They measured the index with a two-filter instrument, called ratiospect, on eight samples of turf collected from three species. The results showed a correlation coefficient of 0.984 between the ratiospect readings and the visual score of turf color. This mathematical relationship became a useful reference for development of remotely sensed natural resource models in ecosystems studies (Birth & McVey, 1968).

Several studies have followed Birth and McVey (1968) in utilizing remote sensing to overcome natural resource monitoring challenges. The need for satellite remote sensing in the study area is rooted in information from the literature regarding utilization of Landsat data for estimating water quality trends in reservoir ecosystems.

1.1.2.3 Remote sensing of chlorophyll pigments

Chlorophyll is optically active, having spectral signatures of Green reflectance and absorbance in Red and Blue (CHLa). These signatures make it possible to remotely sense chlorophyll pigments (Jensen, 2015). Figure 3 presents a plot of the spectral signatures of CHLa (present in green algae and BGA) and CHLb (present only in green algae):

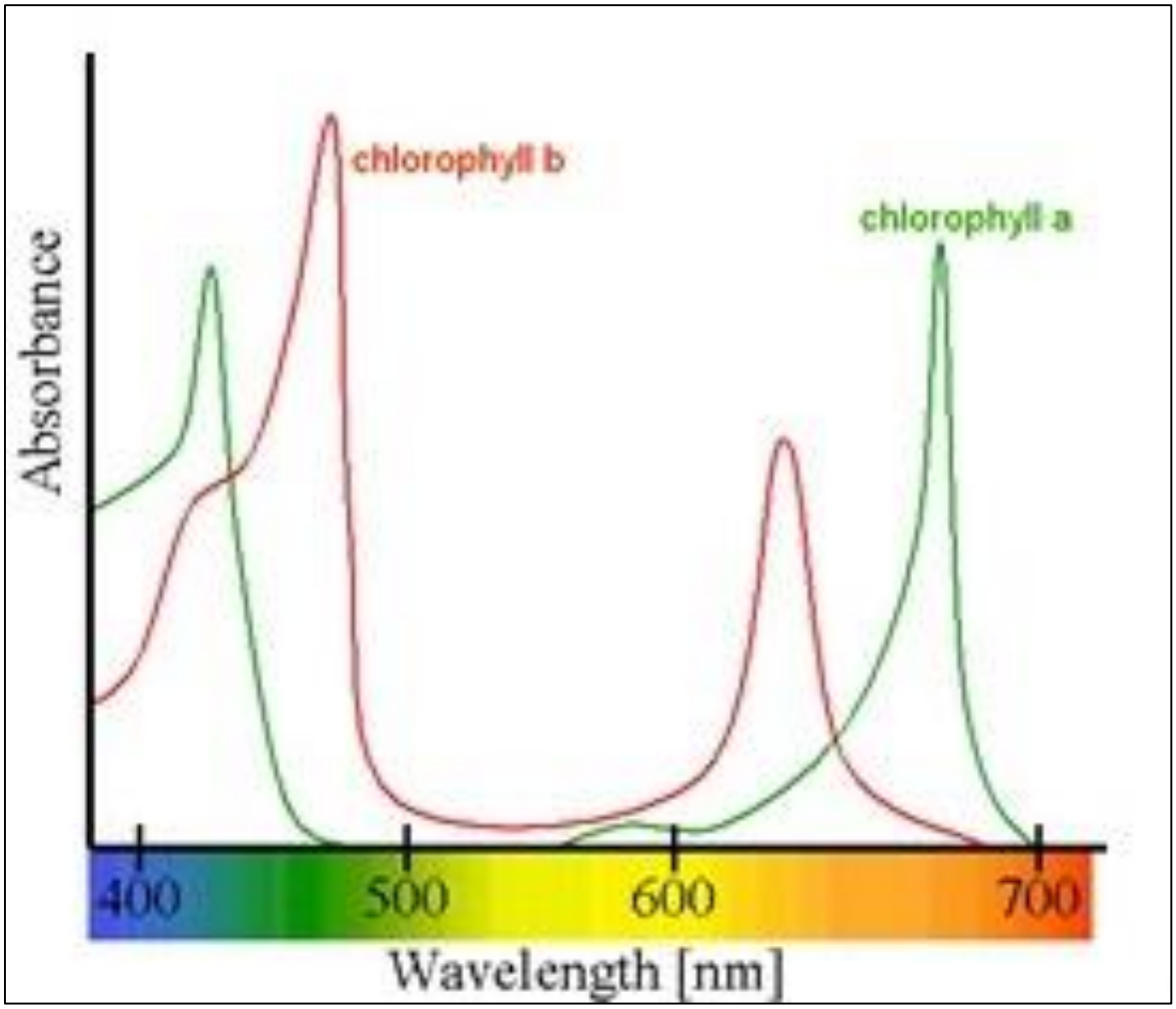

Figure 3. Spectral signatures of CHLa & CHLb (Jensen, 2015)

A major challenge to remote sensing of chlorophyll in inland waters is the difficulty to register pixel values at low concentrations (Yacobi, Giltelson, & Mayo, 1995) or when mineral turbidity masks sensor detection of chlorophyll reflected bands. Ruddick et al (2001) proposed four steps to utilize satellite sensors in measuring CHLa concentrations by analytical methods (Ruddick, Gons, Rijkeboer, & Tilstone, 2001):

1. Carrying out atmospheric correction to discriminate above-water upwelling radiance derived from satellite sensors;

2. Air-water interface correction to differentiate subsurface irradiance reflectance from the above-water upwelling radiance and downwelling irradiance;
3. Estimating the phytoplankton absorption coefficient at a designated wavelength from subsurface irradiance reflectance; and
4. Removing errors from conversion of the phytoplankton absorption coefficient into CHLa concentration.

Some studies combine data from high spectral resolution images with Landsat multispectral data to develop the optimum spectral index that can estimate the concentration range of water quality parameters. Yacobi et al (1995) used algorithms to explain chlorophyll concentrations in Lake Kinneret, a large freshwater body in Israel, by means of high spectral-resolution radiometer and spectral reflectance of Landsat TM (Yacobi, Giltelson, & Mayo, 1995). The authors tested the influence of varying chlorophyll concentrations on surface reflectance and the index of spectral bands that would serve as benchmark for chlorophyll determination from remotely sensed data.

The results showed that chlorophyll reflectance spectra did not necessarily depend on concentration as much as it depended on the region of the EMS. Chlorophyll absorbed Blue and Red bands and reflection was high in Green and NIR bands. Their study confirmed a positive relationship between high reflectance from chlorophyll and an increase in its concentration only in the Green and NIR bands (Yacobi, Giltelson, & Mayo, 1995). These results confirmed expected chlorophyll-spectra relationships. Chlorophyll reflects Green light and absorbs high in the Blue and Red regions of the EMS (Jensen, 2015). The authors used these results to build regression equations for estimating chlorophyll concentrations in Lake Kinneret. Appendix 1 shows the coefficient of determination for the predictive equation.

In order to use spectral data in determining chlorophyll in their lake under review, Yacobi et al (1995) saw the need to develop a chlorophyll index with little or no interference from other water quality parameters. The authors factored in spectral bands with minimal sensitivity to variation in chlorophyll concentration and ruled out influence by survey conditions. Using high spectral-resolution data from the radiometer used in the study, they considered the wavelength at which only one dominant factor would influence spectral feature variation as the most useful for determining chlorophyll concentration.

According to Yacobi et al (1995), the Red reflectance maximum at nearly 700 nm was the only feature that met those criteria. One reason was that the position of the peak, as well as its magnitude, had a close relationship with chlorophyll concentration. The standard deviation of reflectance values for the 400 to 850 nm EMS, as well as the coefficient of variation, showed that sensitivity to chlorophyll variation in the range near 700 nm was up to 3-fold higher than in the Blue region of the spectrum.

Han and Rundquist (1997) tested to see whether the well documented ratio of reflectance in the NIR (705 nm) to that in the Red (670 nm) region was a good predictor of chlorophyll content in relatively turbid Midwestern reservoirs in the United States (US). The authors compared their 2-year study results to those obtained by first derivative of reflectivity near 690 nm, to see which of the two would better predict chlorophyll concentration. In calculating the first derivatives, they divided the difference between successive reflectivity values by the wavelength interval separating them. In this case study, only in one occasion did they find the NIR/Red ratio to be a good predictor of chlorophyll content. The first derivative of reflectivity was found to be a good predictor of chlorophyll concentration (Han & Rundquist, 1997).

In a more recent study in Lake Bogoria in Kenya, reflectance values for both NIR (835 nm) and NIR:Red (835 nm/660 nm) showed strong linear correlations with in-situ CHLa concentrations (Tebbs, Harper, & Remedios, 2013). The NIR/Red ratio gave a better fit to CHLa compared to the single NIR (Appendix 1). The band ratio produced a better indication of water quality with top of atmosphere (TOA) reflectance compared to atmospherically corrected data (Tebbs et al, 2013). The advantage of TOA reflectance is that it reduces the in-between scene variability through a normalization for solar irradiance since it combines surface and atmospheric reflectance (Jensen, 2015).

The studies discussed above show that NIR and Red bands are common for chlorophyll determination in the literature. Other studies have shown that other combinations can yield acceptable results. Torbick et al (2008) used different combinations of Landsat 7 ETM+1 (450-520 nm) and ETM+3 (630-690 nm) to develop equations for CHLa concentrations in West Lake, China (Torbick, et al., 2008). For single bands, ETM+3 was a better predictor ($R^2 = 0.78$) compared to ETM+1 ($R^2 = 0.45$). A ratio of ETM+3/ETM+1 gave the best model ($R^2 = 0.81$). All the other combinations gave poor water quality models.

In addition to band combinations, studies have also compared results from different Landsat sensors. In a 2014 study in Lebanon, algorithms derived from Landsat 7 and Landsat 8 showed different results for CHLa (Deutsch, Alameddine, & El-Fadel, 2014). The results revealed better predictive tendencies of Landsat 8 ($R^2 = 0.70$) than either Landsat 7 ($R^2 = 0.11$) or Landsat 7+8 ($R^2 = 0.46$). The authors attributed the differences to dissimilar band spacing in the two satellite sensors. They asserted that Landsat 8 seemed more capable of characterizing the chlorophyll fluorescence peak in the Red to NIR boundary than Landsat 7.

1.1.2.4 Remote sensing of water clarity

Using satellite data as indicator of clarity in water bodies can be challenging because clarity depends on dynamic processes such as limnetic characteristics and natural or anthropogenic activities in a watershed (Torbick, et al., 2013; McCullough, Loftin, & Sader, 2012). Accessibility and frequency of monitoring is particularly challenging for a large number of water bodies in some watersheds (McCullough et al, 2012). The use of satellite remote sensing in overcoming this challenge has been widely documented. Some of those findings were useful in the development of the objectives for monitoring water quality in this research.

In mapping inland lake water quality across the Lower Peninsula of Michigan, Torbick et al (2013) used Landsat TM imagery to build models for a number of water quality parameters, including SDZ. The authors applied a suite of preprocessing routines to help come up with the best mapping model for water quality in the study area. The preprocessing routines included digital number (DN), radiance, Landsat Ecosystem Disturbance Adaptive Processing System (LEDAPS) protocol, dark object subtraction (DOS), and subsurface volumetric reflectance. Each routine combined water quality results to build algorithms for the modeling. For SDZ, the following were the R^2 values for the routines: 0.56 for DN, 0.77 for LEDAPS, 0.58 for DOS, 0.82 for subsurface volumetric modeling, and 0.81 for radiance. All routines showed strong correlation with SDZ, using the band combination TM1+TM3+TM3/TM1 (Torbick, et al., 2013).

McCullough et al (2012) asserted that remotely sensed data could efficiently estimate clarity of lakes on a regional scale. They developed equations for use in monitoring the clarity of 1511 lakes in Maine, USA. Their research combined a 20-year (1990-2010) dataset of Landsat 5 TM and Landsat 7 ETM+ brightness values for TM bands 1 (Blue) and 3 (Red)

with SDZ. They took SDZ readings temporally coincident with Landsat schedule and having a flexibility of 1–7 days' field data gathering before or after the overpass. Their results indicated that Landsat TM bands 1 and 3 were good predictors of SDZ; this was supported by data from 119 sample stations on the lakes under study. They also tested the TM1/TM3 ratio and found it to be a good predictor of water clarity.

Researchers have also compared different Landsat sensors to estimate water clarity. In comparing sensors on Landsat 7 ETM+ and Landsat 8 OLI, Olmanson et al (2016) developed predictors for SDZ in Minnesota. They compared September 1, 2008 Landsat 7 and August 22, 2013 Landsat 8 images using stepwise regression to identify the best predictor for water clarity. Their results asserted that the best model for water clarity with Landsat 8 accounted for 82% (R^2=0.82) of the data from the relationship, water clarity = OLI band-2/OLI band-4 + OLI band-1. This result was nearly identical to the relationship, water clarity = OLI band-2/OLI band-4 + OLI band-2. The best model for the ETM+ sensor was, water clarity = ETM+ band-1/ETM+ band-3 + ETM+ band-1. The researchers found that both sensors worked well for water clarity measurements (Olmanson, Brezonik, Finlay, & Bauer, 2016).

1.1.2.5 Strength of regression models

Linear regression models attempt to minimize the deviation of measured values from the predicted values through a line of best fit. The smaller the differences between the observed and the predicted values, the stronger is the model (Frost, 2013). Some studies use residual plots to determine the strength of a model. It reveals unwanted residual patterns that indicate biased results more effectively than numbers (Frost, 2013). Remote sensing studies often utilize the coefficient of determination (R^2) to evaluate how close the measured values are to the fitted regression line with values ranging 0-100% (0.0-1.0). The closer R^2 is to 1.0,

the more reliable is the model. Appendix 1 presents a list of studies and their regression results.

1.1.3 Social and economic impacts of satellite remote sensing

In 2008, the DOI authorized release of all Landsat images for free public utility. The DOI made this policy in order to allow researchers provide better explanation of trends that affect the social and economic welfare of societies around the world. By 2015, there were about 30 million downloads of Landsat scenes for variety of uses (Campbell J. , 2015). The data from those images provided useful information for government agencies, learning institutions, private entities, and individuals. These help address major issues in agriculture, forestry, disaster risk management, climate change, and settlements.

The US Federal Government allocates an annual budget of $ 3.5 billion to civil earth observation, management of the data obtained thereof, and support to similar programs at state level. These programs contribute an estimated $30 billion dollars to the US economy through projects that utilize satellite data (Campbell J. , 2015).

Albeit these social and economic benefits from utilizing satellite data, a major barrier is slow acceptance by end users (Schaeffer, et al., 2013). According to Schaeffer et al (2013), managers still rely on periodic ground based monitoring, which typically utilize limited sample locations and frequencies. Additionally, some potential end users have concerns over errors from the atmosphere, the environment, and the sensors. These in addition to uncertainties regarding the fate of future satellite missions, and the perceived high-tech nature of satellite data make it hard to integrate satellite-based information into policy decisions. There appears to be the need to integrate cost/benefit analysis into all satellite remote sensing projects and their products.

Watkins (1978) presented three basic principles of cost/benefit analysis for remotely sensed data. The first principle evaluates the costs and benefits in terms of how much change the remote sensing project brings. Secondly, the amount of money that is equivalent to those costs and benefits will determine the value of the remote sensing project. The third principle requires evaluating the market value of products derived from a remote sensing project (Watkins, 1978). Studies over the years have shown that direct monetary evaluation of costs and benefits is more difficult than the other principles. Indirect monetary value seems to be the most feasible form of analysis.

Hellegers, Soppe, Perry, and Bastiaanssen (2010) showed that remote sensing was useful in delineating the economic indicators of water resource management. Remote sensing helped track consumption patterns of water, irrigation needs, and crop yields. This approach made it simple to forecast market trends for agricultural products and improve water consumption by means of equity in access to water resources (Hellegers, Soppe, Perry, & Bastiaanssen, 2010). Rauniker, Forney, and Benjamin (2013) showed an indirect economic benefit of satellite remote sensing by estimating the value of information derived from such data. The estimated value was $858 million ± $197 million per year, and this could increase to $38.1 billion ± $8.8 billion in the future (Raunikar, Forney, & Benjamin, 2013). In the carbon market, Cunningham, Little, and Montgomery (2013) compared satellite remote sensing to auditing in accounting firms. Utilization of satellite data helps investors keep track of trends in forest cover and its economic impact. Satellite imagery is helping an estimated growth of $100 billion in the carbon market by 2020 (Cunningham, Little, & Montgomery, 2013).

A major economic growth in satellite remote sensing has been in the market value of its products. Commercial earth observation programs and products significantly contribute to the satellite industry (more than 70%), which was worth $314.17 billion in 2013 (Orban, 2015). This growth is expected to continue as more countries lunch space programs, and as the technologies become simpler.

However, the industry's future is not that certain giving a number of factors. Competition between countries is increasing and no one seems to have control over trends in the market. The type and magnitude of change will depend on which direction the competition takes. Additionally, declassification of satellite data in the US gave momentum to commercial programs and products. However, most of those products are expensive and it is not clear whether prices may reduce significantly in the future. This could be achieved if the technologies become more user friendly and are useful to a wide variety of end users (Weber & O'Connell, 2011).

In the Grand Lake watershed, there has been no study on the social and economic impacts of satellite remote sensing on ecosystem services of lakes. Ghimire, Boyer, Sheilder, Melstrom, and Stoecker (2017) estimated amenity values on Grand Lake O' The Cherokees to residential homeowners in the area. Values estimated included lake view, lake access, proximity, frontage, and dock capacity. They found out that, residential sales with docks worth on average $46,599 more than those without. The value of houses near the shoreline of the lake sold for $88,568 more than those located far away from the shore, and the value dropped as the property became more remote. Other variables that affected value were the age of the house, presence of septic sewer, and the need for possession of flood insurance (Ghimire, Boyer, Shideler, Melstrom, & Stoecker, 2017).

However, Ghimire et al (2017) did not consider the effect of Grand Lake's water quality on the housing market in that area. A future study could take a close look at the impact of lake water quality on the value of amenities that depend on it. It seems water quality to the housing industry is only an issue when it becomes an aesthetic (example, HABs) or a public health problem. A study in 2017 shows that people are willing to pay extra for assurance of minimal likelihood of HABs (Boyer, Daniels, & Melstrom, 2017). Additionally, the scenery of HABs and their uncertainties pose a challenge to lake managers when planning for recreation (Roberts, Boyer, & Lusk, 2008). The automated monitoring tool developed in this study will help address most of these issues.

CHAPTER II

LANDSAT-8 BASED INDICES OF ALGAE AND TURBIDITY FOR INLAND WATER BODIES IN SOUTHCENTRAL USA

Mansaray, Abubakarr S.[1]; Stoodley, Scott H.[1]; Dzialowski, Andrew D[1]; Storm, Daniel E[1]; Torbick, Nathan[2]; and Wagner Kevin L.[1]

[1]Oklahoma State University; [2]Applied GeoSolutions

Abstract

Point and nonpoint sources of pollution introduce pollutants that can impair water quality and pose health risks to humans and aquatic organisms. Managing these sources requires monitoring the spatial and temporal extent of water quality to help identify impaired water bodies. In the Grand Lake Watershed situated in Oklahoma, Kansas, Arkansas, and Missouri, there is concern over repeated harmful algal blooms (HABs) in recent history. A new monitoring strategy that ensures timely HABs detection will help resolve this concern. Our objective was to develop indices for photosynthetic algae and mineral turbidity using spectral bands in Landsat 8. We measured chlorophyll a (CHLa) and water clarity *in situ* in four lakes in the Grand Lake Watershed using an EXO-1 YSI multi-parameter probe and Secchi disc. We used regression analysis to compare *in situ* results to the indices. The results revealed relationships varying temporally with significant relationships and strong R^2 on some dates. For those days with strong relationships, there may have been minimal mixed pixel problems or less interference from other inherent optical properties. Mixed pixel problems are the most probable cause of poor model performance for dates that recorded insignificant relationships. Using concentrations from single points as ground truth for radiation representing a 900-m^2 area may be misleading. However, these need confirmations in future studies, which could involve accounting for interference; determining low, medium, and high values for the indices; lab-based clarification of CHLa reflectance in the near infrared (NIR) spectrum; and fusion of different satellite sensors.

2.1 Introduction

Point and nonpoint sources of pollution introduce pollutants such as sediments, nutrients, and microorganisms that can impair water quality and pose health risks to humans and aquatic organisms (Brooks, et al., 2016). Managing these sources requires monitoring the spatial and temporal extent of water quality to help identify and characterize impaired water bodies (Cord, et al., 2017). A major challenge to lake monitoring is the limitation in space and time for water quality characterization (Karpatne, et al., 2016). This challenge is particularly true for algal blooms, which result from erratic biophysical conditions including elevated nutrient levels (Gilbert & Burford, 2017), changing climate (Paerl, et al., 2016), and the rate of physiological activity of algal pigments in relation to wavelengths of light (Tamburic, et al., 2014).

In the Grand Lake Watershed (located in Oklahoma, Kansas, Arkansas, and Missouri), the Grand River Dam authority (GRDA) is concerned over the repeated cases of harmful algal blooms (HABs) in recent history. The agency is interested in new monitoring strategies that would help identify and explain the spatial and temporal extent of such algal blooms. Developing new tools that pinpoint priority areas for algal pollution monitoring will help the GRDA save time and cost in future water quality monitoring.

Satellite remote sensing datasets provide a potential data source for overcoming certain water quality monitoring challenges. The increased costs associated with *in situ* data collection at additional sampling sites, higher sampling frequencies, and the inability to access important areas (Barnes, Blonski, Hua, Holekamp, & Spiering, 2014) are some of the challenges. Several studies have established statistical relationships between remotely sensed spectral signatures and ground based data for algal pigment detection

(Allee & Johnson, 1999; Chen, et al., 2010; Han & Rundquist, 1997; Kirk, 2011; Mishra & Mishra, 2012; Ruddick, Gons, Rijkeboer, & Tilstone, 2001; Tebbs, Harper, & Remedios, 2013; Thu Ha, Koike, Nhuan, Parsons, & Thao, 2017; Torbick, et al., 2008; Yacobi, Giltelson, & Mayo, 1995). In particular, chlorophyll-a (CHLa) is an optically active pigment in algae and other green plants that has spectral signatures of reflecting Green light and absorbance in Red and Blue. These unique signatures make it possible to remotely sense chlorophyll pigments (Jensen, 2015).

A major limitation to the use of remotely sensed images to predict chlorophyll content in inland waters is the difficulty in registering reflectance/absorbance values at low chlorophyll concentrations (Yacobi, Giltelson, & Mayo, 1995). Discerning the region of the reflectance spectrum resulting from chlorophyll versus the region resulting from other effects like mineral turbidity (Jensen, 2015; Ruddick, Gons, Rijkeboer, & Tilstone, 2001) is also a challenge. The fate of radiation from the sun may also introduce errors in reflectance values recorded by the sensor, creating the need for atmospheric correction (Jensen, 2015). Geometric correction is also required due to errors introduced from external sources including wind, temperature, humidity, tidal waves, and the shape of the Earth (USGS, 2018). Correction of circular error (i.e. the distance between target pixel and actual pixel of measurement) ensures accurate representation of the pixels under consideration.

When relating remotely sensed data to algal pigments, it is important to collect field data that are spatially and temporally coincident with the satellite flyover. This gives a reliable representation of statistical relationships between data from satellite imagery and field monitoring data (Carpenter & Carpenter, 1983; Kallio, et al., 2008). It could be

acceptable to sample before or after Landsat overpass if there is no major change in water quality conditions between the acquisition and sampling dates. Major changes may result from biophysical conditions of the water body and its watershed (Mosley, 2015). The number of flexible days reported in the literature range from ±1 day (Barrett & Frazier, 2016) to ± 7 days (McCullough, Loftin, & Sader, 2012) of satellite overpass.

Studies relating satellite remote sensing to water quality typically utilize correlation between spectral band ratios and ground based *in situ* parameters. The most common band ratio is that between near infrared (NIR) and Red (Han & Rundquist, 1997; Mishra & Mishra, 2012; Thu Ha, Koike, Nhuan, Parsons, & Thao, 2017). Some studies also mix band ratios with different types of band combinations in order to get the best coefficient of determination (Torbick, et al., 2008). Even though these studies have reported proven methods to confirm the use of multispectral band combinations and band ratios for a linear relationship between chlorophyll content and reflectance, some of the assertions remain unclear.

It is an established fact that algae have pigments that reflect or absorb radiation with specific wavelengths in the visible region of the electromagnetic spectrum (Kirk, 2011). However, it seems unclear if NIR radiation is also reflected in photosynthetic algae. A 2010 study gave a different result when the authors reported that chlorophyll-f absorbed NIR radiation (Chen, et al., 2010). This contradicts studies that have reported NIR reflectance spectral of algal pigments, except if chlorophyll-f is not universally distributed in algae.

There has been no universally accepted band ratio to represent chlorophyll reflectance even though spectral properties, chlorophyll structures, and image processing

routines all remain the same. The differences lie in the wavelengths selected. However, the idea of chlorophyll having a spectral signature that allows reflectance in multiple wavelengths needs further clarification.

Based on these uncertainties, this study did not include IR reflectance as one of the bands representing chlorophyll concentration in inland water bodies. Absorption in IR seems more realistic because there is absorption of an even shorter-wavelength band, Red, during photosynthesis. The reported IR reflectance values may be coming from a different optically active object, especially from a 900-m^2 pixel that is susceptible to mixing from multiple optically active objects.

We used relationships between bands that are photosynthetically active in order to develop a universally acceptable photosynthetic algal index (PAI). The objective is to develop an index for CHLa that can qualitatively determine, on a $0 \leq PAI \leq 1$ scale, the spatial extent of photosynthesis on the water body. This will guide ground based monitoring and enhance resource use efficiency. We also present and index for mineral turbidity to account for interference from turbidity in those waters.

2.2 Materials and methods

2.2.1 The Grand Lake Watershed

The Grand Lake Watershed (Figure 4) situates in three Landsat path/row combinations (Appendix II) and Council Grove Lake and Marion Lakes in the Neosho River watershed fall in two path/row combinations (Appendix II). All the lakes under study, except Marion, share path 27 with varying rows. The Landsat path/row combinations have minimum swath width of 185 km and the sensor takes images with an instantaneous-field-of-view (IFOV) of 30 m x 30 m. The IFOV is also known as pixel,

the smallest unit of an image (Jensen, 2015), and ranges between 7,000 and 9,000 pixels per Landsat scene.

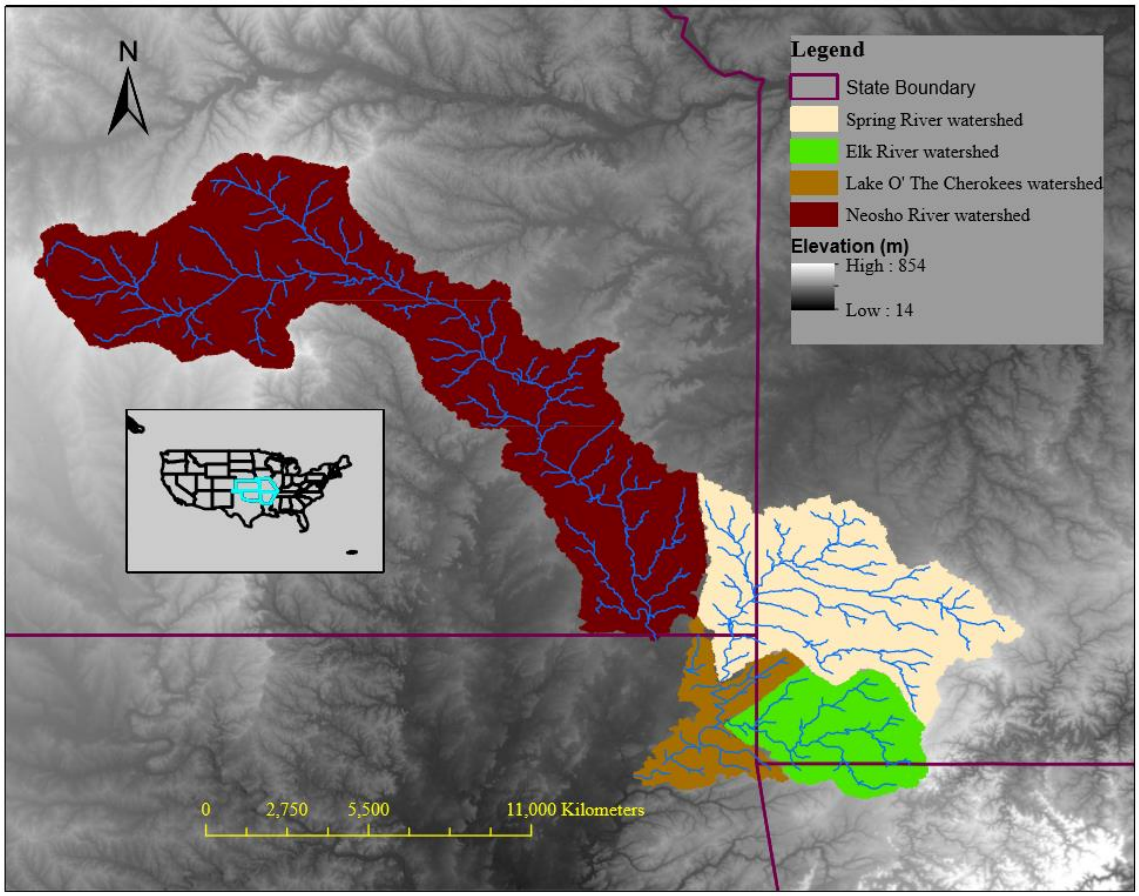

Figure 4. The Grand Lake watershed and its sub-watersheds

Officially named Grand Lake O' The Cherokees hereafter referred to as Grand Lake, it is located in Delaware, Ottawa, and Mayes counties in northeastern Oklahoma. Grand Lake is in the foothills of the Ozark Mountains and receives its water from the Grand (Neosho), Elk, and Spring Rivers (LakeHub LLC, 2018). Table 2 shows the surface area, shoreline length, average depth, and water volume of Grand Lake (Johnson & Luza, 2008) and the other lakes under study.

Table 2. Characteristics of Lakes under study

Lake	Surface area (km^2)	Shoreline length (km)	Mean Depth (m)	water volume (m^3)
Grand Lake	188.2	2,092.147	11.0	2,062,378,560
Council Grove Lake	13.27	64.374	4.0	59,823,869.121
Marion Lake	0.62	96.561	3.4	98,560,132.747
John Redmond Lake	38	94.951	2.7	83,016,000

Figures 5 and 6 show maps of the Grand Lake sub watershed and sampling sites on the lake, respectively.

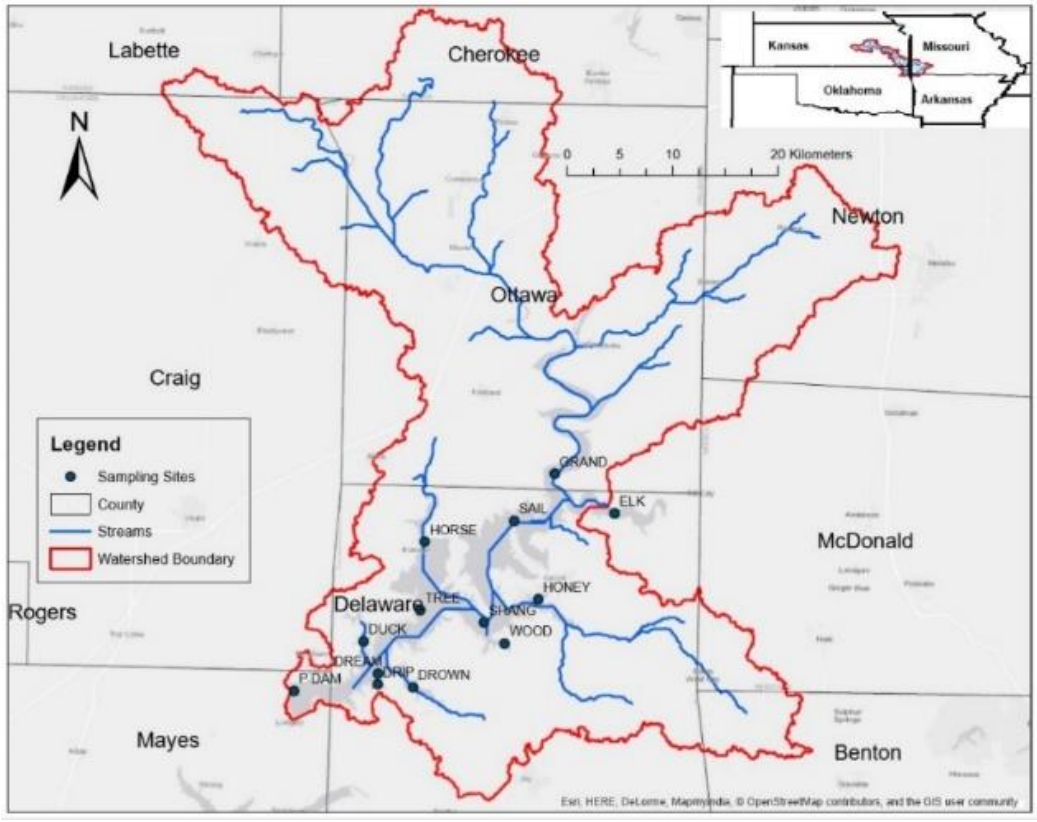

Figure 5. Grand Lake sub-watershed

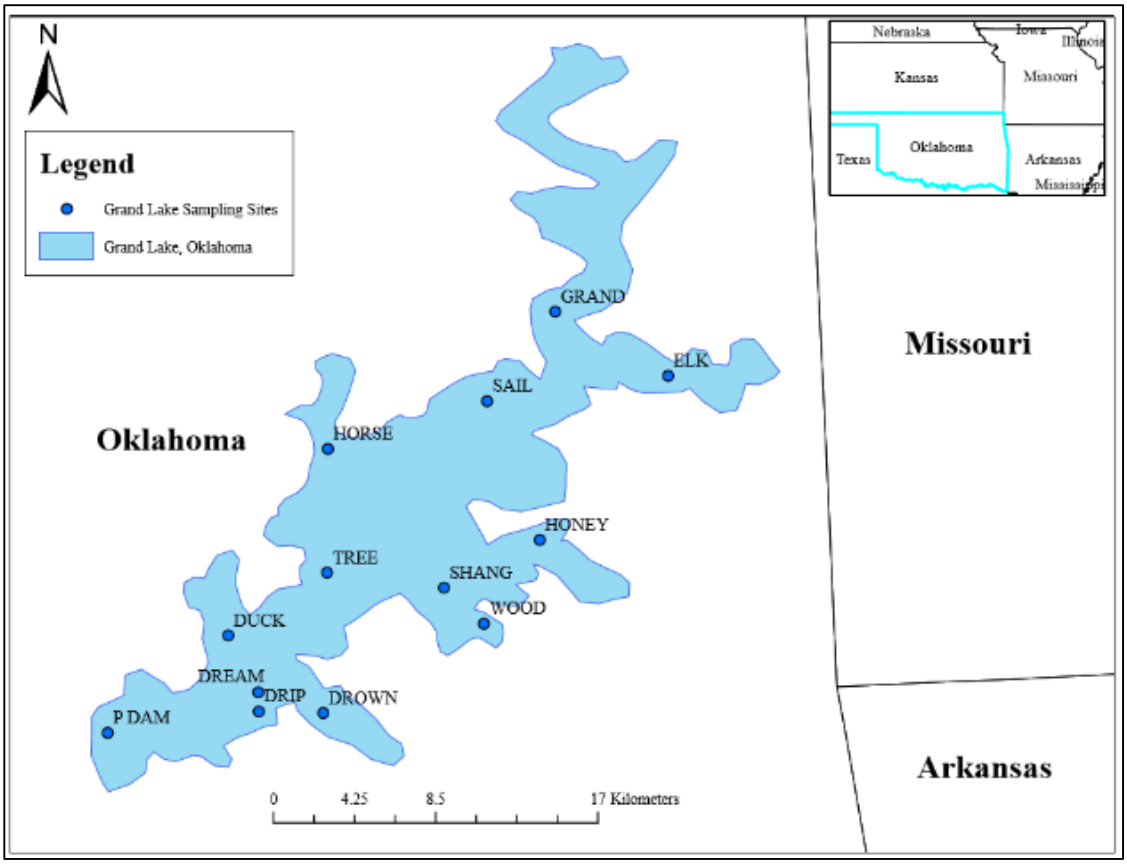

Figure 6. Sampling sites of Grand Lake in Oklahoma

Council Grove Lake in Morris County is located in the scenic Flint Hills region of Kansas and lies in the Neosho River basin. Table 2 shows the surface area, mean depth, shoreline length, and volume of water in the lake (U.S. Army Corps of Engineers, 2011). Figures 7 and 8 show maps of the Council Grove sub watershed and sampling sites on the lake, respectively.

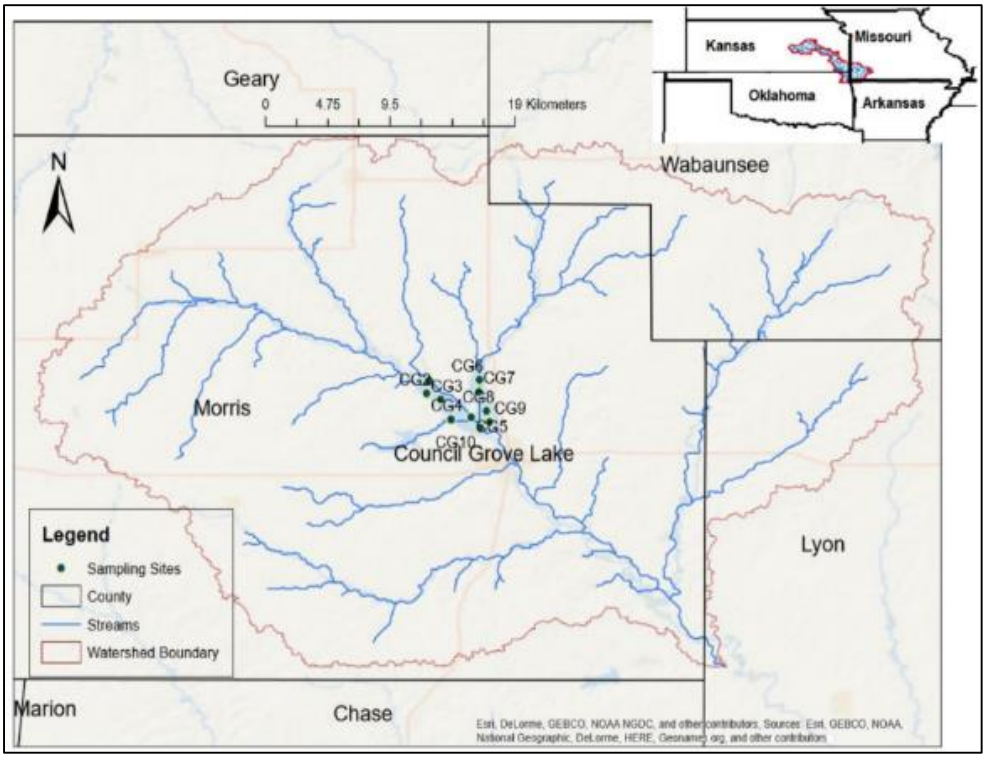

Figure 7. Map of Council Grove Lake sub-watershed

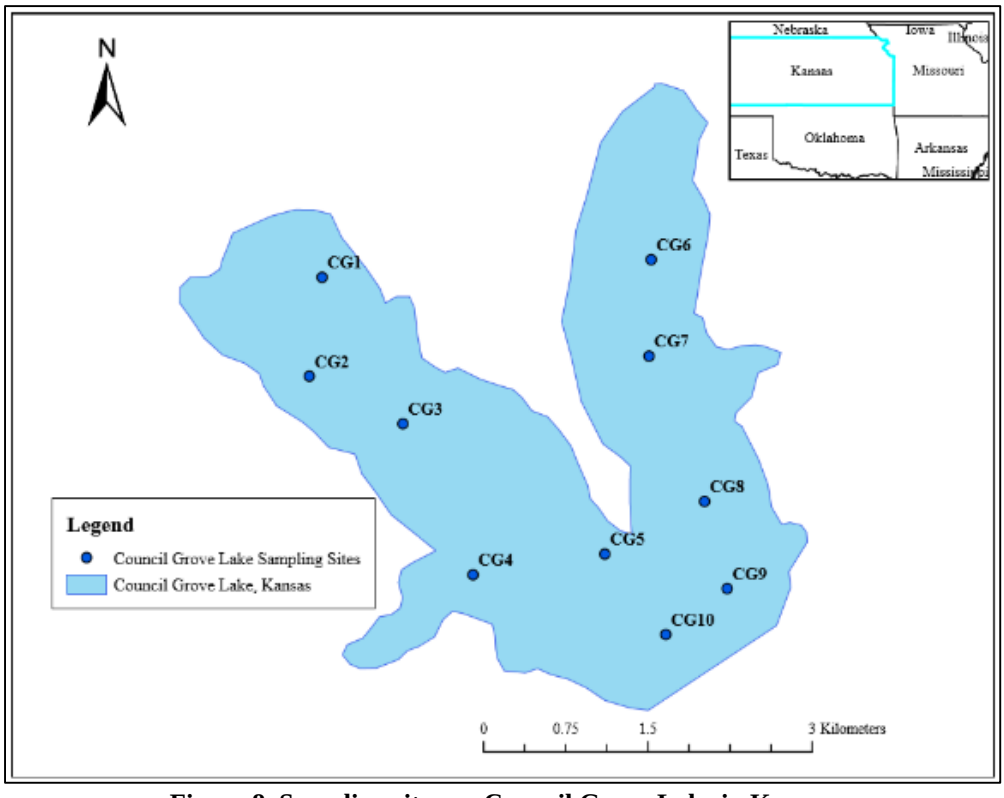

Figure 8. Sampling sites on Council Grove Lake in Kansas

Marion Lake lies between the cities of Marion and Hillsboro in Marion county, central Kansas. It is situated in the North Cottonwood River basin, which drains most of the watershed. Figures 9 and 10 show maps of the watershed and lake sampling sites, respectively. The surface area, shoreline length, mean depth, and water volume are shown in Table 2 (US Army Corps of Engineers, 2018).

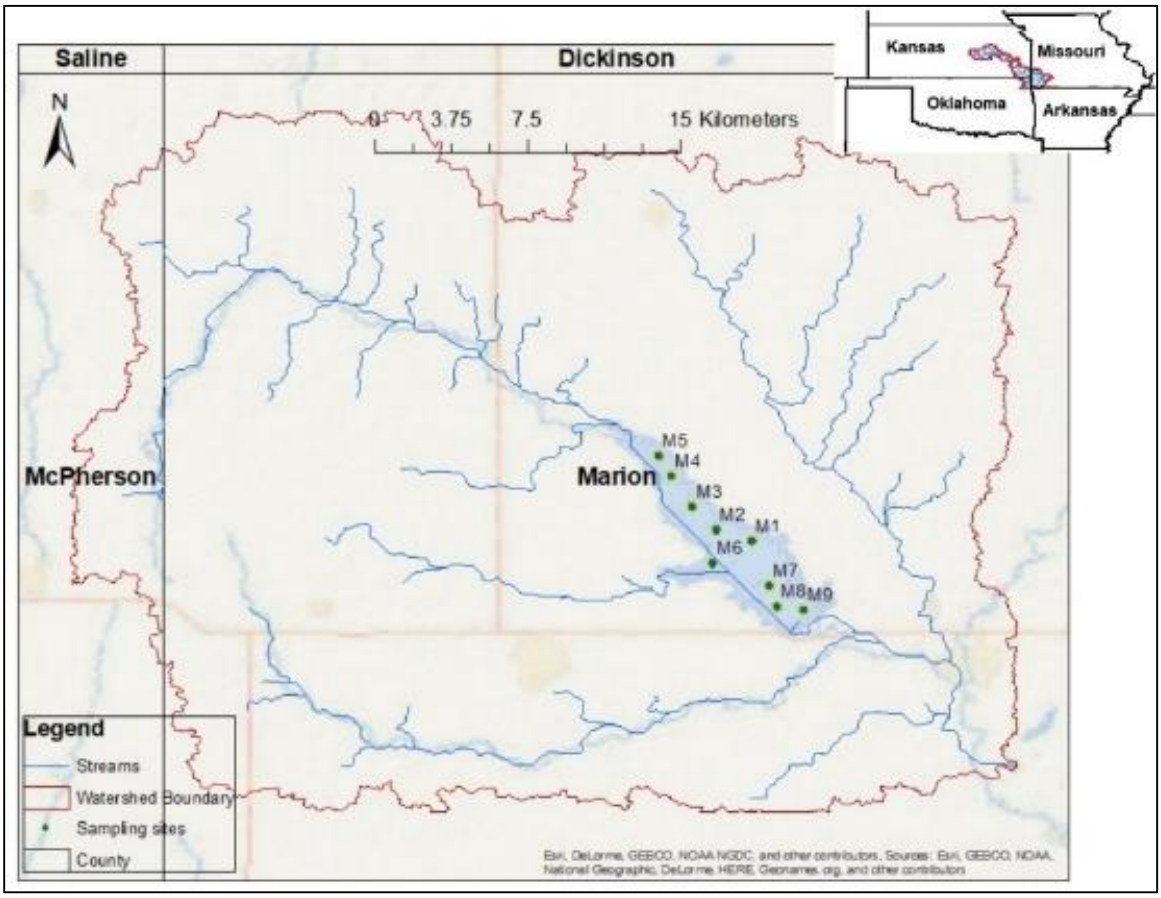

Figure 9. Maps of Marion Lake sub-watershed

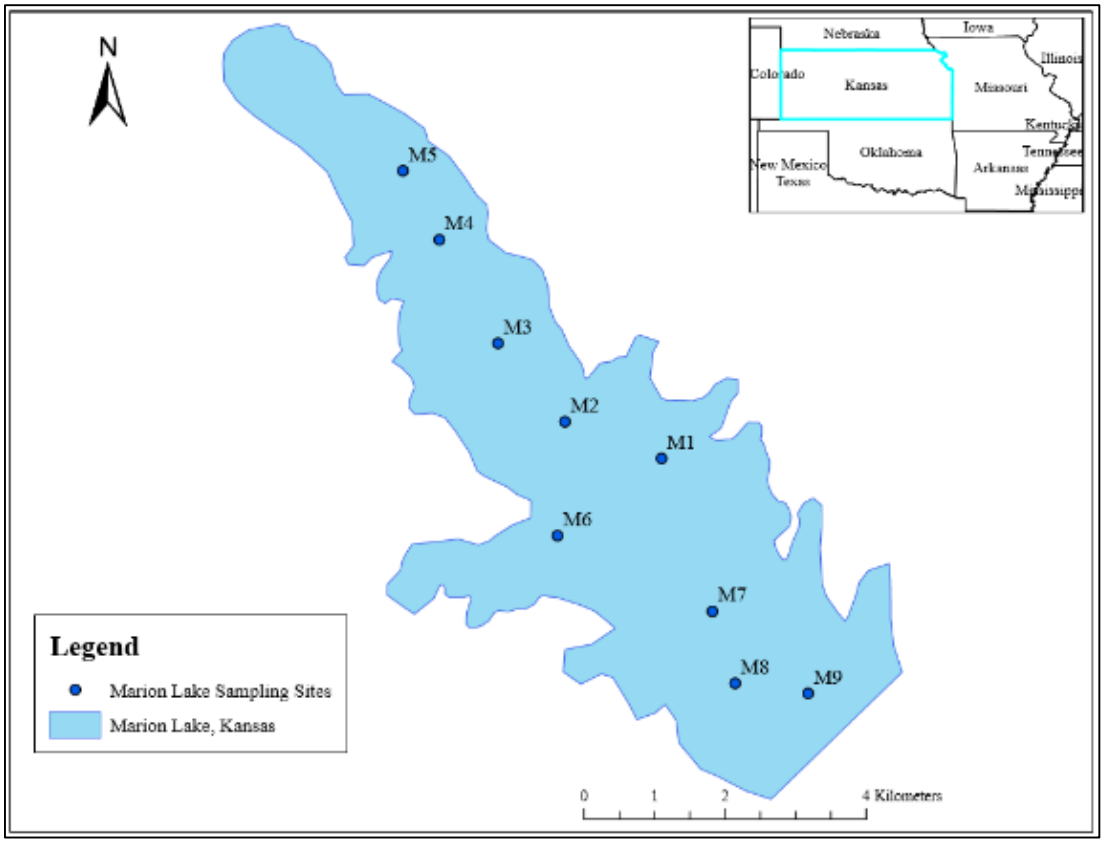

Figure 10. Sampling sites on Marion Lake in Kansas

The Neosho River serves as both the recharge in the northwest and discharge in the southeast for the John Redmond Lake (Figure 11), which lies within Coffey County in eastern Kansas. Table 2 shows the reservoir's surface area, mean depth, shoreline length, and volume (US Army corpse of Engineers, 2018).

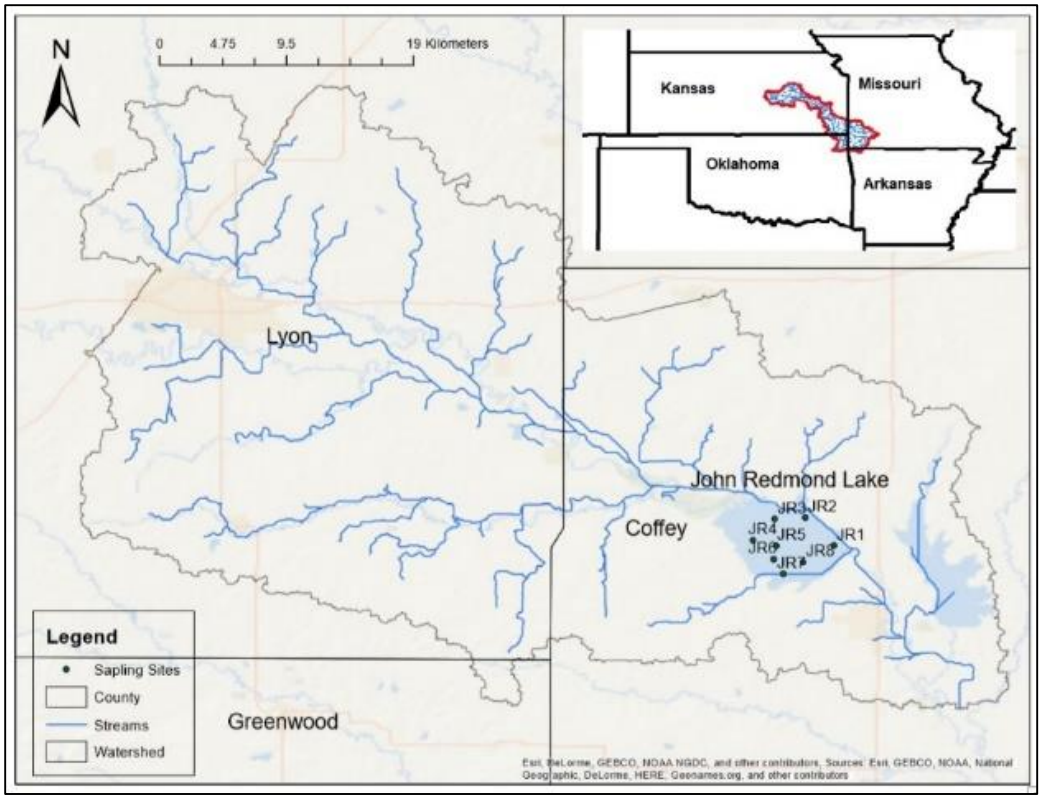

Figure 11. Maps of the John Redmond Lake sub watershed

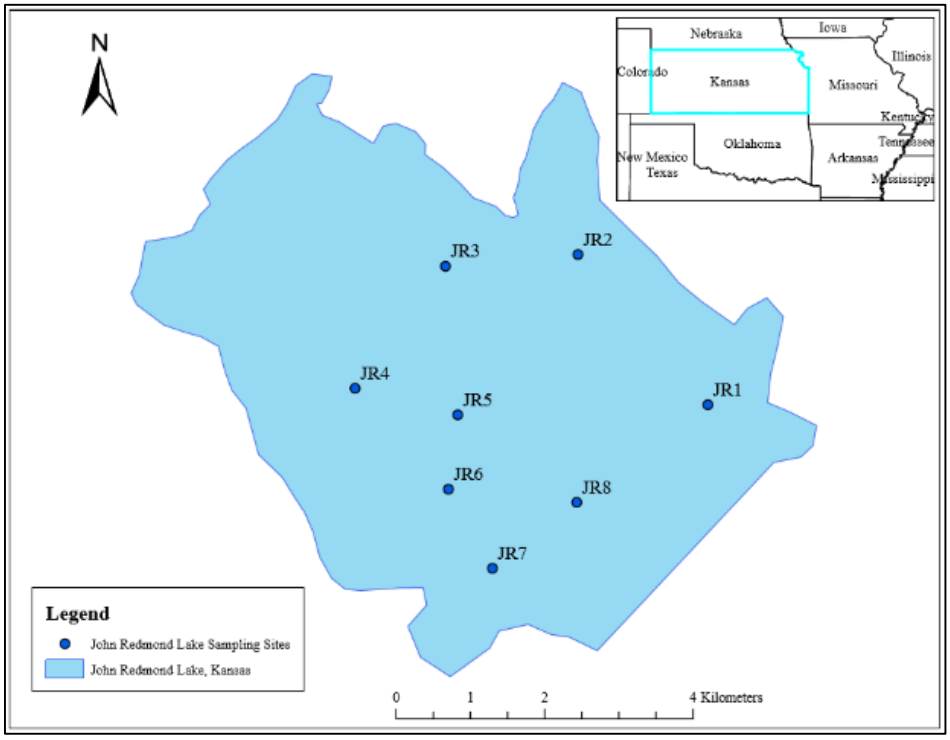

Figure 12. Sampling sites on John Redmond Lake in Kansas

2.2.2 Image acquisition

We downloaded radiometric and geometrically corrected Landsat 8 images from the USGS Earth Explorer website at no cost. Details of the image dates, sites, reflectance values as well as the details of *in situ* samples are presented in the appendices (Appendix III – Appendix X). All the images selected had scene cloud cover less than 10%. In areas where cloud cover was over 10%, we ensured that it did not affected the area of interest. The software packages utilized were ENVI 4.5 and ArcGIS 3.5 for all image analysis and mapping.

2.2.3 Image processing

For brevity, this section summarizes the processing workflow succinctly. We started with computation of the top of atmosphere radiances, L_{TOA}, from Digital Number (DN): $L_{TOA} = M_L * DN + A_L$; with M_L (multiplicative factor, gain) and A_L (additive factor, offset) values provided in the metadata. The next step is computing the TOA reflectances (ρTOA) by normalizing L_{TOA} to the band averaged irradiance: $\rho TOA = \frac{\pi * L_{TOA} * d^2}{F0 * cos\theta_0}$; where $F0$ is the band averaged extraterrestrial solar irradiance, d the sun-earth distance in Astronomical Units, and θ_0 the sun zenith angle. The ρTOA is assumed the sum of aerosol reflectance (ρ_a), Rayleigh reflectance (ρ_r) and the water-leaving radiance reflectance just above the surface (ρw^{0+}): $\rho TOA = \rho_a + \rho_r + t * \rho w0+$; with t the two-way diffuse atmospheric transmittance. Note for more recent scenes processed with Level-1 Product Generation System (LGPS), top of atmosphere reflectances are directly computed from DN using the provided scaling factors (MR, AR): $\rho TOA = M_R * DN + A_R$. The ρw^{0+} defines as $\rho w0+ = \frac{\pi * Lw0+}{Ed0+}$; where Lw^{0+} is the water-leaving radiance, and Ed^{0+} the down-welling irradiance, both just above the water surface. The Rayleigh

correction of Vanhellemont & Ruddick (2014), and Vanhellemont & Ruddick (2015), implements a look-up-table (LUT). The LUT is generated for all bands (square bandpass) using 6SV v1.1 modified to disable the ocean contribution but including surface reflectance (sky- and sunglint) for a nominal wind speed of $1\ m\ s^{-1}$ (Vanhellemont & Ruddick, 2015). For Landsat 8 OLI the relative spectral response applies as opposed to square band passes. The Rayleigh reflectance is then from the LUT using sun and sensor geometry. Wang and Shi (2006) suggest cloud and land masking to be performed using a threshold on the reflectance in the 1609 nm SWIR band (Wang & Shi, 2006). Pixels are classified as not being water when the Rayleigh-corrected reflectance ($\rho c = \rho TOA - \rho r$) in band 6, $\rho \frac{6}{c} > 0.0215$. Ultimately, for aerosol correction we applied a simple correction scheme leveraging SWIR, which has negligible signals in water, a moving average smoothing filter (kernel=32), and nominal fixed per pixel epsilon for batch processing of Landsat scenes.

To complement the empirical modeling, we employed machine-learning techniques. This algorithm framework will rely upon open Python scripting for development of the automated monitoring tool. Chapter III presents a detailed description of the Python based tool for satellite based water quality monitoring.

2.2.4 Sampling

The sampling sites used in this study (Figures 5-12) are the same as those designated and used by the lake managers. Water quality sampling took place on dates and times temporally coincident with Landsat flyover (Appendix III – Appendix X). If no major change in water quality occurred, and when there was the need, sampling dates

extended to ±2 days of Landsat overpass; this is consistent with the number of days reported in the literature (Barrett & Frazier, 2016).

2.2.4.1 In-situ water quality sampling

The sampling instrument used was the EXO1 YSI multi-parameter probe to collect water quality data at each sample site. The sonde consists of replaceable sensors and pressure transducers, which pick signals and send to the detector that displays the signals as concentrations of the different parameters. Parameters measured include turbidity, dissolved oxygen, pH, temperature, chlorophyll fluorescence, and phycocyanin (cyanobacteria) fluorescence. The water quality data were recorded in field notebooks in addition to logging them on to the EXO1 storage system. The procedures for assembling, preparing, and calibrating the EXO1 probe are detailed in the instrument's operation manual (EXO, 2017).

2.2.4.2 Collection of water samples for laboratory analyses

This research utilized brown bottles, a depth integrated tube sampler, and a Van Dorne water sampler to collect water samples. The samples were stored in a cooler and transported to the laboratory for sample analysis. Sample collection and analyses followed procedures adapted from the USEPA's sampling and analysis plan guidance and template (USEPA, 2014).

2.3 Landsat 8 spectral indices for photosynthetic algae and mineral turbidity

2.3.1 Photosynthetic Algal Index (PAI)

During photosynthesis, there is maximum CHLa reflectance in Green light and absorption of Blue and Red lights (Tamburic, et al., 2014). A Landsat based qualitative confirmatory test for algae would indicate reflectance in Green and absorption of Red

radiation. Presence of healthy photosynthetic algae in the water would expectedly agree with a chlorophyll index given in Equation 1.

$$PAI \propto \frac{\rho_G - \rho_R}{\rho_G + \rho_R} \qquad \textit{Equation 1}$$

Where ρ_G is Green reflectance and ρ_R, Red reflectance of light in the sun's electromagnetic spectrum (EMS). This chlorophyll index ranges between -1 and +1. Healthy photosynthetic algae would skew towards +1 while low values would indicate reflectance from substances other than photosynthetic algae. Equation 2 introduces k, the constant of proportionality, accounting for visible reflectance from water and other substances in the water.

$$PAI = k\left(\frac{\rho_G - \rho_R}{\rho_G + \rho_R}\right) \qquad \textit{Equation 2}$$

Turbidity, a major water quality issue in the study area (Holt, et al., 2008), is the main water quality parameter (in addition to water) that reflects visible light and may diminish the accuracy of the algal index developed in this study. The variable k in Equation 2 accounts for other reflectance sources of visible light. The value of k was assumed to be one because determination of visible reflectance from other optical active objects (other than PAI and mineral turbidity) was beyond the scope of this study. On a scale of $-1 \leq PAI \geq 1$, values that skew towards negative one (-1) indicate either minimal algal activity in the lake or there is high mineral turbidity. There is maximum likelihood of algal bloom for a photosynthetic algal index that skews to positive one (+1).

Since Blue light has a shorter wavelength range compared to Green and Red light, it is more susceptible to Rayleigh scattering in the atmosphere (Jensen, 2015). Its

inclusion in a Landsat based photosynthetic algal index may increase the likelihood of random error.

2.3.2 Mineral Turbidity Index (MTI)

Since clear water absorbs all three bands of IR light: NIR, shortwave IR 1 (SWIR1) and shortwave IR 2 (SWIR2), its reflectance indicates the presence of substances that may interfere with the accuracy of the algal index developed in this study. Thus, spectral a relationship that would qualitatively represent mineral turbidity is

$$MTI = k\left(\frac{\rho_{SWIR2}-\rho_G}{\rho_{SWIR2}+\rho_G}\right) \quad \textit{Equation 3}$$

A replacement of ρ_R in equation 1 with ρ_{SWIR2} and rearranging, gave the normalized difference mineral turbidity index in equation 3. The SWIR2 reflectance was suitable in this case because it has the longest wavelength range making its reflectance the least likely except in highly turbid waters.

On a scale of $-1 \leq MTI \geq 1$, values that skew towards negative one (-1) indicate either high algal activity in the lake or the water is clear; the reverse is the case for a mineral turbidity index that skews to positive one (+1). We present the following rules for interpreting the two indices (Table 3).

Table 3. MTI and PAI interpretation scenarios

SN	Scenario	MTI value	PAI value	Comments
1	Algal bloom	Low	High	High means MTI or PAI is skewed towards +1; low means MTI or PAI is skewed towards -1
2	Possible algal bloom	Medium, Low	High	Medium means MTI or PAI value cluster around zero
3	No algal bloom	Medium, Low	Medium, Low	
4	Water is clear	Medium, Low	Medium, Low	Ground-based monitoring required
5	Turbid water	Medium, High,	Medium, Low	MTI or PAI could be medium if there is high visible reflectance from turbidity;

2.4 Empirical relationship between *in situ* CHLa & PAI and between SDZ & MTI

This study utilized simple linear regression models to determine the significance of relationships between PAI and *in situ* CHLa concentration and also between MTI and SDZ, within the pixel in which sampling was done. This study used a 95% confidence level (p-value, $\alpha = 0.05$) to demine significance between predictors and response variables in the models. The null hypothesis was that there was no linear relationship between the predictor and the response variable. When $\alpha \leq 0.05$, we rejected the null hypothesis and concluded there was significant relationship; the reverse was the case when $\alpha > 0.05$.

This assumption was tested using statistical significance and coefficients of determination of the regression models. Where there was no significant relationship, it may have been that the concentration captured in the *in situ* measurement was different from the actual concentration reflecting the water leaving radiance. Additionally, there was probably a mixing pixel problem interfering with CHLa reflectance. Mixed pixels (when a pixel has heterogeneous optically active objects) can result in confusion when interpreting properties of an image (Choodarathnakara, Kumar, Koliwad, & Patil, 2012). The coefficients of determination were R^2 (strength of the relationship between the predictor and response variable) and predicted R^2 (strength of such relationship in future application of the model). The R^2 values ranged between $-1 \leq R^2 \leq +1$.

Each designated sampling site was located within a Landsat pixel with an area of 30 m x 30 m on the lake. PAI and MTI values were used as predictors for CHLa concentrations and SDZ, respectively. A lake's SDZ is an indication of how deep light

penetrates the water body (Alikas & Kratzer, 2017) and is inversely related to turbidity (Bachmann, Hoyer, Croteau, & Canfield Jr., 2017).

2.5 Results and discussions

2.5.1 Laboratory data versus *in situ* data

This research involved validation of chlorophyll concentrations measured *in situ* via the YSI multi-probe. The team randomly selected dates on which water samples were collected alongside *in situ* measurements for laboratory analysis. Comparison of *in situ* data to the laboratory-analyzed data for CHLa in Grand Lake showed moderate to high correlation (Figure 13) demonstrating the accuracy of the *in situ* measurements.

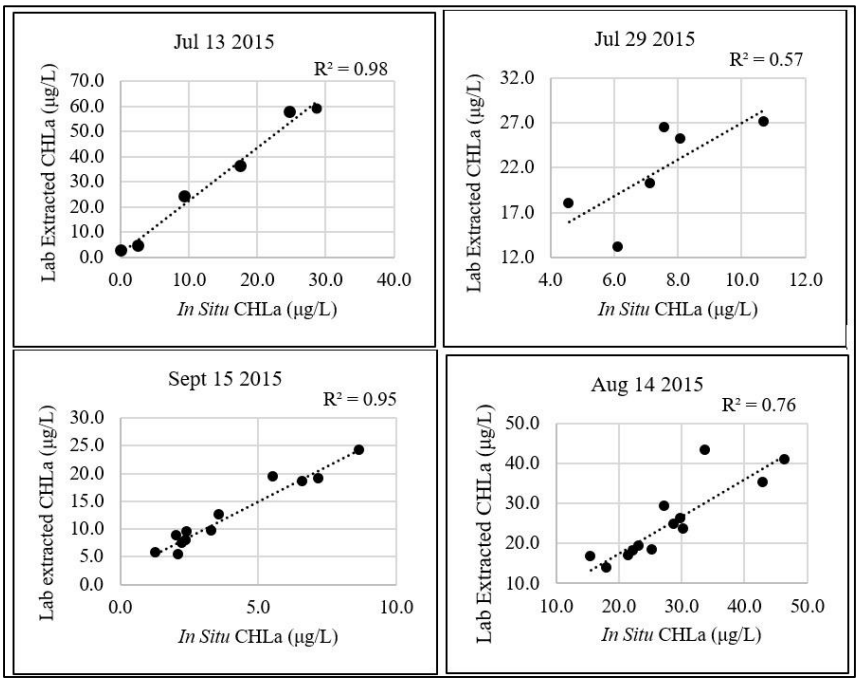

Figure 13. *In situ* vs. laboratory CHLa concentrations on selected dates in Grand Lake

2.5.2 Results of relationships between CHLa & PAI and SDZ & MTI

Table 4 presents results of sampling dates on which Landsat 8 spectral data were collected. Discussions of the results follow in the subsections. There was also a

comparison of images of PAI to those of true color images (Figures 17, 19, 19, & 20). The expectation was that green vegetation on true color images would have the same locations as relatively high values on a PAI image.

Table 4. Regression models showing p-values, R^2, predicted R^2 and equations of PAI vs CHLa & MTI vs SDZ on different sampling dates in the study area.

Lake	Date	Regression analysis (PAI vs. CHLa)			Regression analysis (MTI vs. SDZ)			Regression equations
		p-value	R^2	Predicted R^2	p-value	R^2	Predicted R^2	
Grand Lake	2015/07/13	0.004	0.579	0.275	0.011	0.462	0.304	CHLa = 14.32 + 162PAI SDZ = 1.29 + 1.05MTI
Grand Lake	2015/07/29	0.078	0.278	0.007	0.165	0.168	0.000	CHLa = 29.08 - 79.0PAI SDZ = 1.486 + 0.375MTI
Grand Lake	2015/08/14	0.512	0.004	0.000	0.033	0.352	0.003	CHLa = 37.30 - 37.7PAI SDZ = 2.17 + 1.52MTI
Grand Lake	2015/09/15	0.156	0.174	0.000	0.001	0.640	0.555	CHLa = 7.25 - 19.3PAI SDZ = 3.23 + 2.97MTI
Council Grove Lake	2017/08/01	0.001	0.738	0.607	0.315	0.125	0.000	CHLa = 1.74 - 12.23PAI SDZ = 0.69 + 0.39MTI
Council Grove Lake	2017/08/17	0.003	0.679	0.474	0.780	0.010	0.000	CHLa = 5.10 - 40.46PAI SDZ = 0.59 + 0.14MTI
John Redmond Lake	2017/08/10	0.210	0.248	0.000	0.226	0.233	0.000	CHLa = 4.21 + 98.1PAI SDZ = -294 - 341MTI
John Redmond Lake	2017/08/26	0.984	0.000	0.000	0.132	0.336	0.000	CHLa = 11.10 + 3PAI SDZ = 168.70 + 158MTI
Marion Lake	2017/08/01	0.066	0.403	0.100	0.852	0.000	0.000	CHLa = 7.04 - 47.9PAI SDZ = 0.552 + 0.21MTI
Marion Lake	2017/08/17	0.005	0.707	0.406	0.098	0.343	0.000	CHLa = 6.61 – 34.38PAI SDZ = 1.32 + 1.44MTI

2.5.2.1 Grand Lake

On July 13, 2015, the data showed significant relationship between CHLa and PAI ($\alpha = 0.004$). Compared to previous studies (Appendix II) we saw a good linear relationship between PAI and CHLa ($R^2 = 0.58$) and a predictive strength of 28% (predicted $R^2 = 0.28$). Concentrations ranged from 0.09 µg/L to 47.5 µg/L (Figure 14). It was not clear from the results whether PAI could predict more or less CHLa data if the

concentrations changed in range. In a future study, the spatial distribution of CHLa within a pixel will help capture the maximum concentration that may give a better R^2 value (Yacobi, Giltelson, & Mayo, 1995).

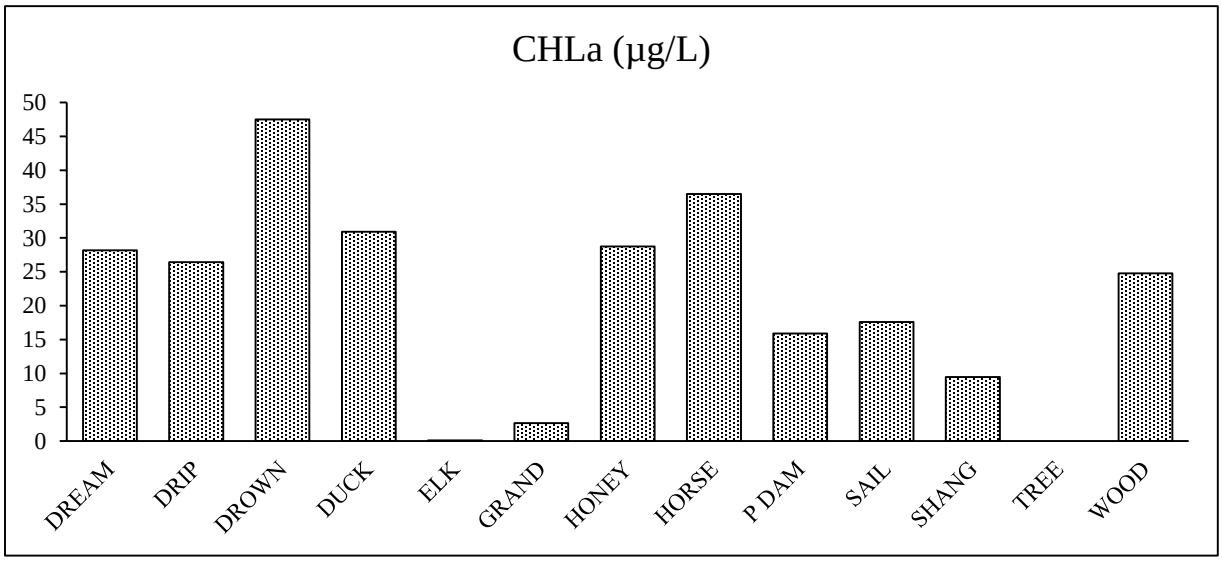

Figure 14. CHLa concentrations (µg/L) in Grand Lake on July 13 2015

The regression analysis also supported a significant relationship between SDZ and MTI ($\alpha = 0.011$) on July 13, 2015. This significance might be supported by the trophic condition, having SDZ less than 3.0 m (Figure 15) and chlorophyll concentration greater than 8 µg/L (Istvánovics, 2013). The R^2 was lower (0.46) than that of PAI while the predicted R^2 (0.3) was comparable.

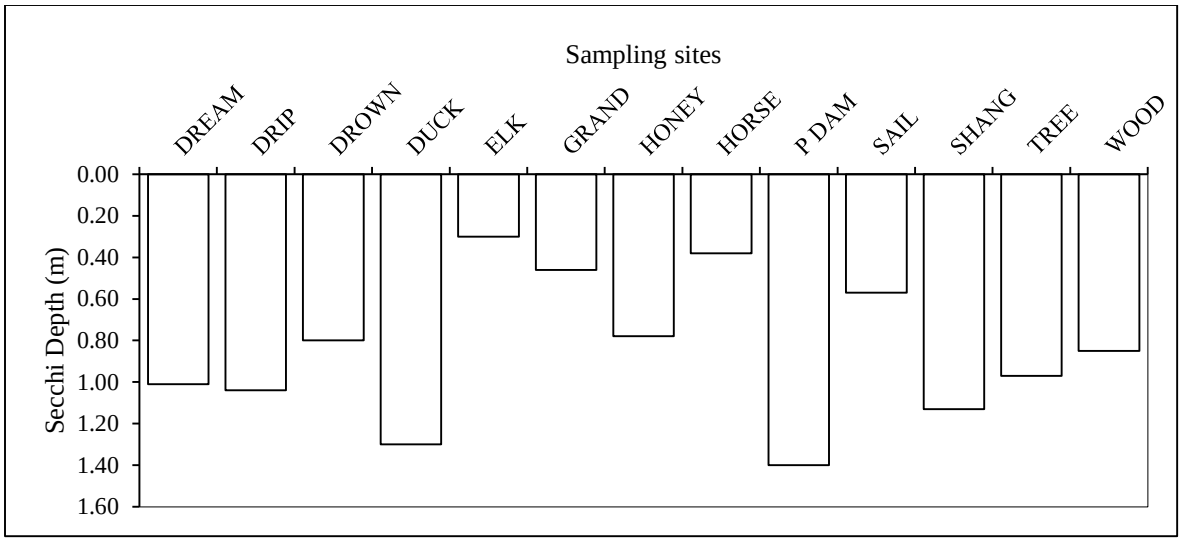

Figure 15. SDZ (m) in Grand Lake on July 13 2015.

On July 29, 2015, there was no significant relationship between CHLa and PAI ($\alpha = 0.08$). The coefficients of determination were also low ($R^2 = 0.28$; R^2-predicted = 0.007). Similar results were recorded for the MTI on this date even though cloud cover was low (0.05%), and the image was taken at nadir while CHLa and SDZ remained comparable to the July 13 samples. The predictive model recorded for PAI ($\alpha = 0.51$; $R^2 = 0.004$; R^2-predicted = 0.00) on August 14 was even further off target. However, MTI, on August 14, showed a significant relationship with SDZ ($\alpha = 0.003$; $R^2 = 0.35$) although the predictive tendency was significantly low (R^2-predict = 0.003). A mixed pixel problem may have affected the regression relationships between CHLa and PAI/MTI (Jones & Sirault, 2014) on these dates.

On September 15, 2015, similar conditions were observed for PAI as on July 29. However, the model supported a significant relationship between MTI and SDZ, with strong R^2 (0.64) and predicted $R^2 = 0.56$. This could mean that the water was too turbid to allow sensor recording of chlorophyll reflectance; CHLa concentrations were relatively

low and SDZ relatively shallow at most sampling sites on that date (Figure 16). Alternatively, there could have been a mixed pixel problem (Jones & Sirault, 2014)

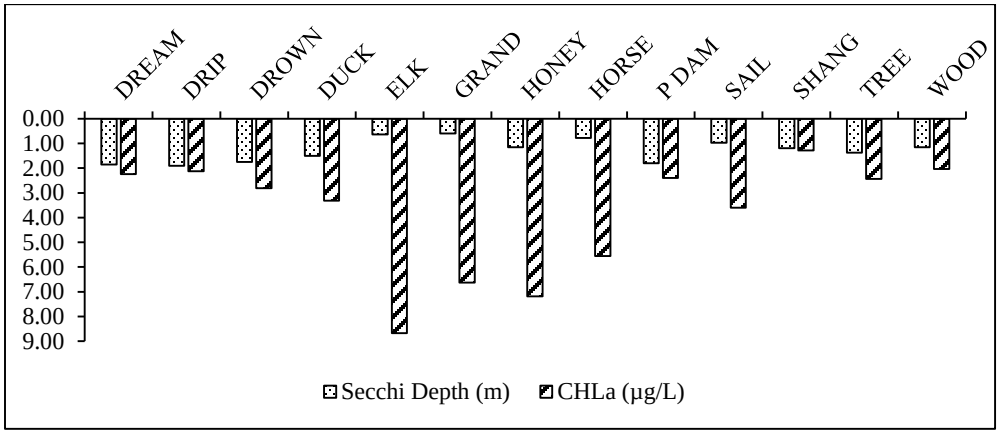

Figure 16. CHLa (µg/L) and SDZ (m) in Grand Lake on September 15 2015

2.5.2.2 Kansas reservoirs

There were favorable cloud conditions for two ground based monitoring trips to Council Grove Lake, Kansas, in the summer of 2017 (08/01/2017 and 08/17/2017). The clouds were greater than 10% on August 1, but did not cover the lake and there were clear skies on August 17. The analysis showed significant relationship between CHLa and PAI on both days ($\alpha = 0.001$ and 0.003 on the 1st and 17th, respectively). There were good R^2 values as well on these dates (August 1: $R^2 = 0.74$; predicted $R^2 = 0.61$; August 17: $R^2 = 0.68$; predicted $R^2 = 0.47$). Relationship between MTI and SDZ was insignificant ($\alpha = 0.78$ and 0.23, respectively) on both days and the R^2 values were very low as well (0.23 or lower). The reverse was expected on these dates because of the low CHLa concentration (Table 6) and seemingly turbid condition (low SDZ) on the lake. Apparently, the turbidity was not as significant to give high reflectance in SWIR2 (i.e. SWIR2 was probably absorbed by water more than it was reflected by mineral turbidity) Also, mixed pixel problems may have been minimal to enhance CHLa reflectance (Jones & Sirault, 2014).

Table 5. CHLa (µg/L) and SDZ (m) in Council Grove Lake with data collected from the 10 sample sites on 08/01/2017 and 08/17/2017.

	08/01/2017		08/17/2017	
Sampling Site	SDZ (m)	CHL (µg/L)	SDZ (m)	CHLa (µg/L)
CG1	0.35	3.83	0.35	5.03
CG2	0.35	5.09	0.31	4.51
CG3	0.45	3.88	0.48	3.28
CG4	0.35	3.05	0.46	2.79
CG5	0.45	1.97	0.60	1.61
CG6	0.35	5.03	0.40	2.68
CG7	0.35	3.5	0.54	2.59
CG8	0.50	2.26	0.57	2.35
CG9	0.50	1.34	0.70	2.07
CG10	0.65	2.21	0.59	1.96

Unlike Council Grove Lake, analysis of data from John Redmond Lake showed no significant relationship between either pair (PAI and CHLa or MTI and SDZ). All R^2 values were very low as well. These were the cases for both sampling dates (08/10/2017 and 08/26/2017).

In Marion lake, there were no significant relationships between the variables using data collected from this lake on August 1, 2017. One of the two datasets (08/17/2017) showed significant relationship between PAI and CHLa ($\alpha = 0.005$) with $R^2 = 0.71$ and predicted $R^2 = 0.41$. The relationship between SDZ and MTI was not significant on the same date; this meant photosynthesis was active within the pixel under review.

2.5.2.3 Interpretation of the regression models

The slope of each model is the ratio of variations in PAI and CHLa, and it gives the extent to which the variables can change along the vertical and horizontal axes; the intercept (or constant) gives the CHLa concentration at which PAI becomes zero (Piñeiro, Perelman, Juan P. Guerschman, & Paruelo, 2008). These are useful pieces of

information in determining the minimum and maximum PAI/CHLa values within the predictive range of the model.

Table 6 gives the regression models on the various sampling dates at the lakes under study and p-values of their slopes and intercepts. Inferring from the regression model for Grand Lake on July 13, 2015, the CHLa concentration would be 14.32 µg/L when PAI became zero at a slope of 162. Extrapolating the line negatively or positively would give the minimum and maximum possible PAI values for this concentration range and giving the prevailing circumstances. Based on this model, it is impossible to use a PAI value as low as negative one (-1) because CHLa will give a negative result. Using the model, the maximum CHLa concentration at which PAI became positive one (1) would be 176.32 µg/L. However, a series of run tests should follow to give the practical implications of the predictive tendencies revealed on this date (and all the other dates) albeit the statistical significance of the slope (α=0.004) and intercept (α=0.002).

In Grand Lake, the dates on which the slopes were insignificant corresponded to slopes that had values less than one. In the Kansas reservoirs, however, significance in the slope or intercept did not depend on the magnitude of their values. The number of sampling dates in each of the Kansas lakes were smaller than in Grand lake. Several test runs are required to show the practical implications of the scenarios observed in Table 6.

Table 6. The p-values of slopes and intercepts of the regression models developed between PAI and CHLa and between MTI and SDZ

Lake	Date	Regression equations	p-value (Slope)	p-value (Constant)
Grand Lake	2015/07/13	CHLa = 14.32 + 162PAI	0.004	0.002
		SDZ = 1.29 + 1.05MTI	0.011	0.000
Grand Lake	2015/07/29	CHLa = 29.08 - 79.0PAI	0.078	0.002
		SDZ = 1.486 + 0.375MTI	0.165	0.000
Grand Lake	2015/08/14	CHLa = 37.30 - 37.7PAI	0.512	0.020
		SDZ = 2.17 + 1.52MTI	0.033	0.001
Grand Lake	2015/09/15	CHLa = 7.25 - 19.3PAI	0.156	0.009

		SDZ = 3.23 + 2.97MTI	0.001	0.000
Council Grove Lake	2017/08/01	CHLa = 1.74 - 12.23PAI	0.001	0.000
		SDZ = 0.69 + 0.39MTI	0.315	0.022
Council Grove Lake	2017/08/17	CHLa = 5.10 - 40.46PAI	0.003	0.000
		SDZ = 0.59 + 0.14MTI	0.708	0.099
John Redmond Lake	2017/08/10	CHLa = 4.21 + 98.1PAI	0.210	0.635
		SDZ = -294 - 341MTI	0.26	0.270
John Redmond Lake	2017/08/26	CHLa = 11.10 + 3PAI	0.984	0.252
		SDZ = 168.70 + 158MTI	0.132	0.080
Marion Lake	2017/08/01	CHLa = 7.04 - 47.9PAI	0.066	0.003
		SDZ = 0.55 + 0.21MTI	0.852	0.459
Marion Lake	2017/08/17	CHLa = 6.61 – 34.38PAI	0.005	0.000
		SDZ = 1.32 + 1.44MTI	0.098	0.031

2.6 Comparison of PAI images to true color images

The Landsat 8 images in Figures 17-20 show the landscape of PAIs in comparison to true color on the sampling dates that showed significant relationships between PAI and CHLa. Values range between low PAI values (dark colored) and high values (green). PAI, an indication of where photosynthesis is taking place, is comparable to the landscape of the true color images in all scenarios. (Jensen, 2015). Areas with green vegetation show high PAI values because photosynthesis is a process that reflects green light. Compared to areas with green vegetation, the values of PAI are low on the lakes because there is no algal bloom during the time of image acquisition. When there is an algal bloom on a lake (i.e. high photosynthetic activity in CHLa), we expect PAI to increase in value on the lake.

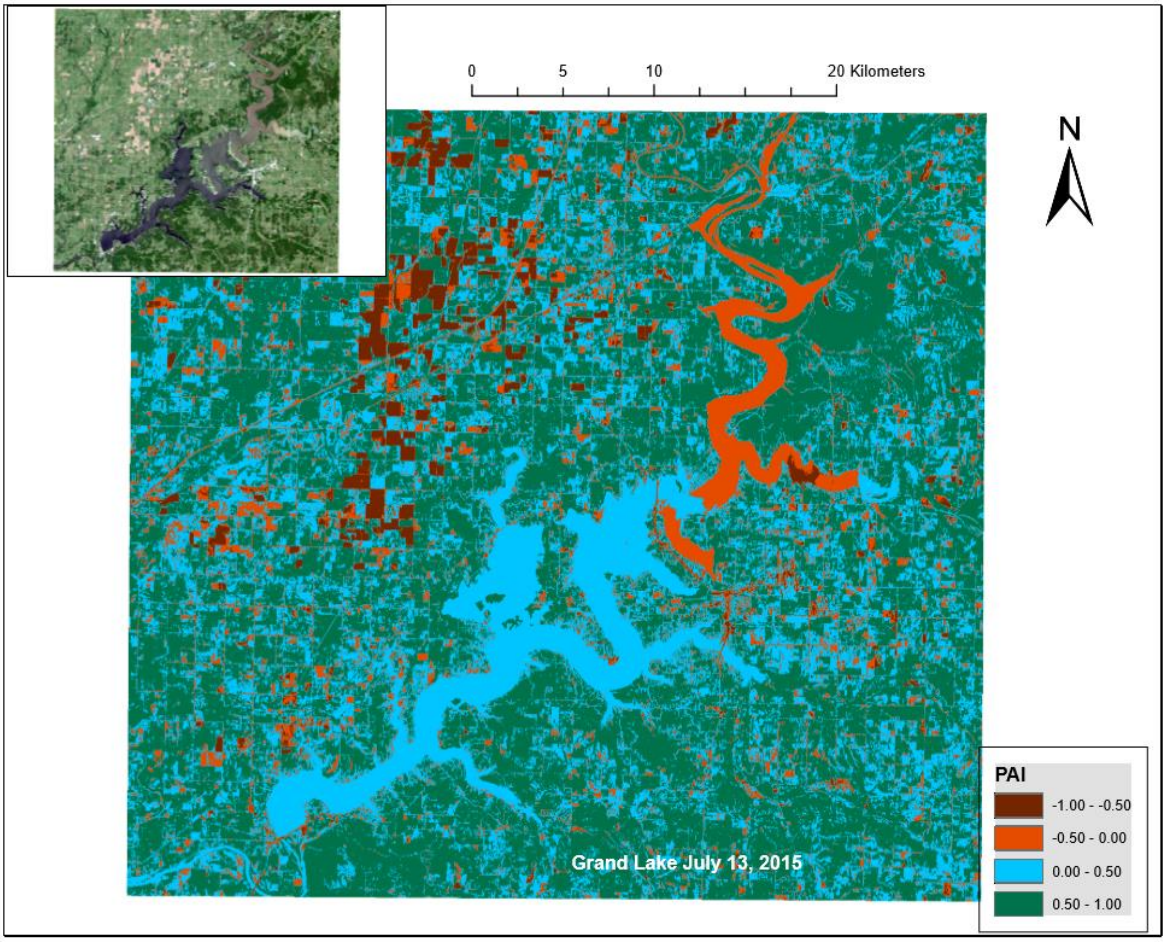

Figure 17. PAI compared to true color (Grand Lake, July 13, 2015).

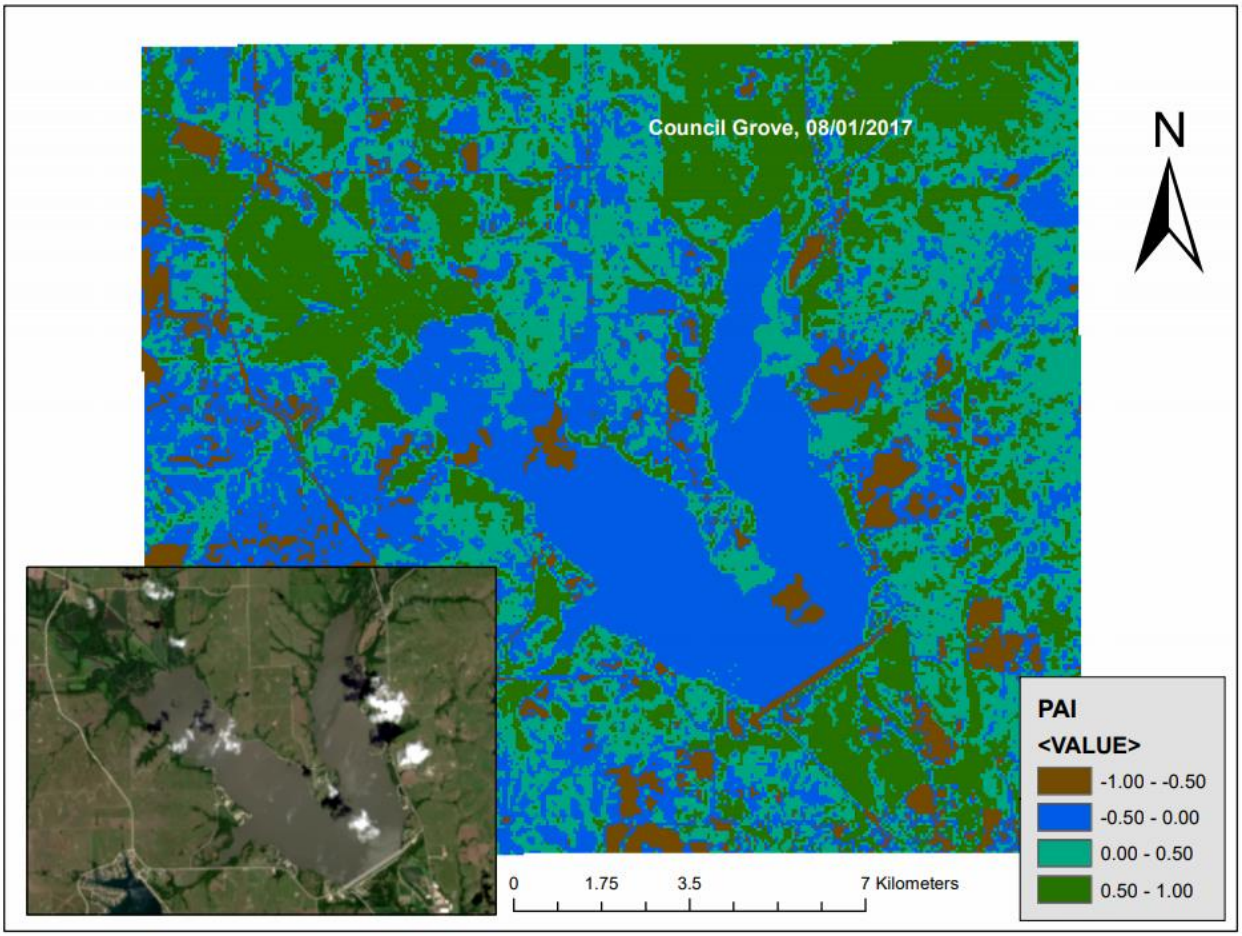

Figure 18. PAI compared to true color (C. Grove, August 1, 2017). Cloud cover is not different from bare soil because they both reflect high in red.

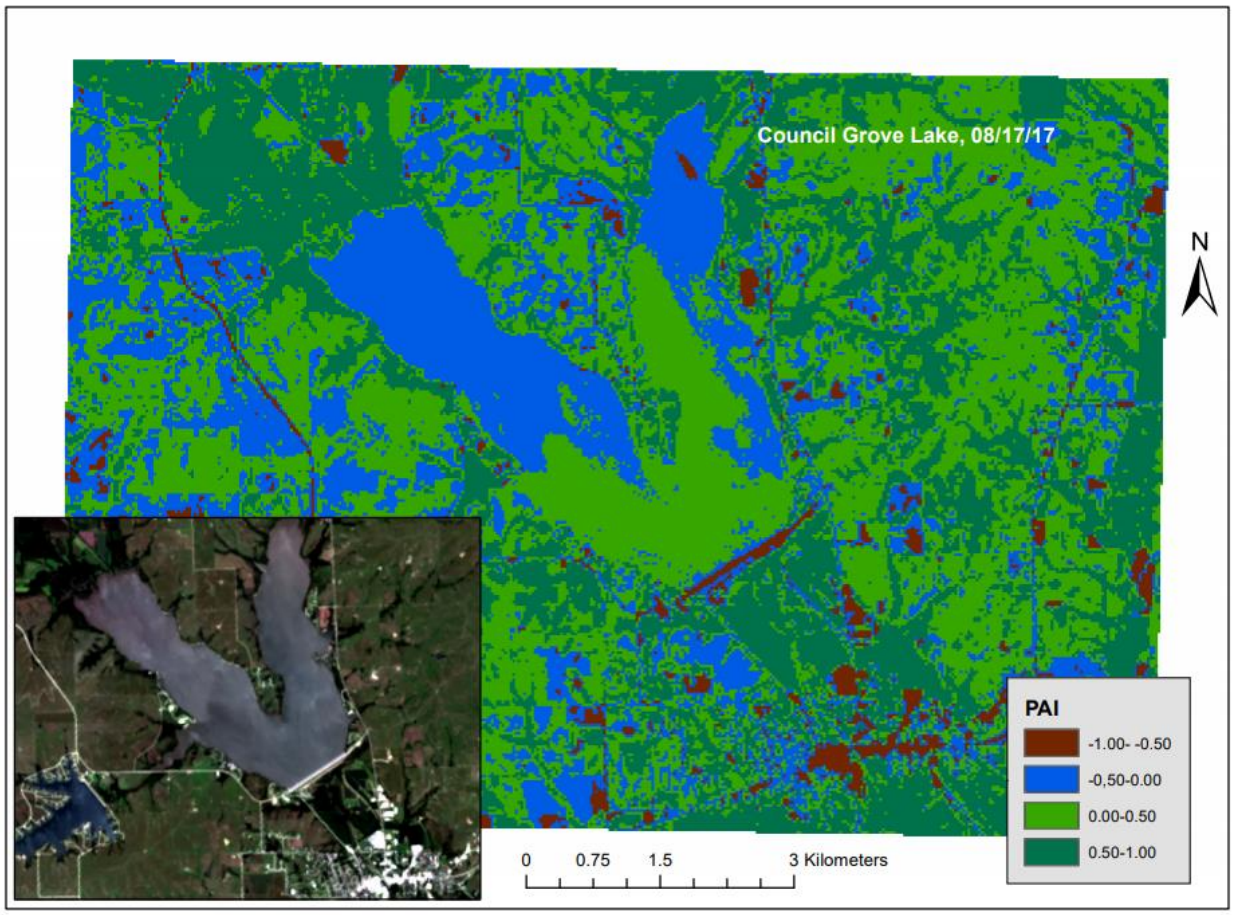

Figure 19. PAI compared to true color (C. Grove, August 17, 2017).

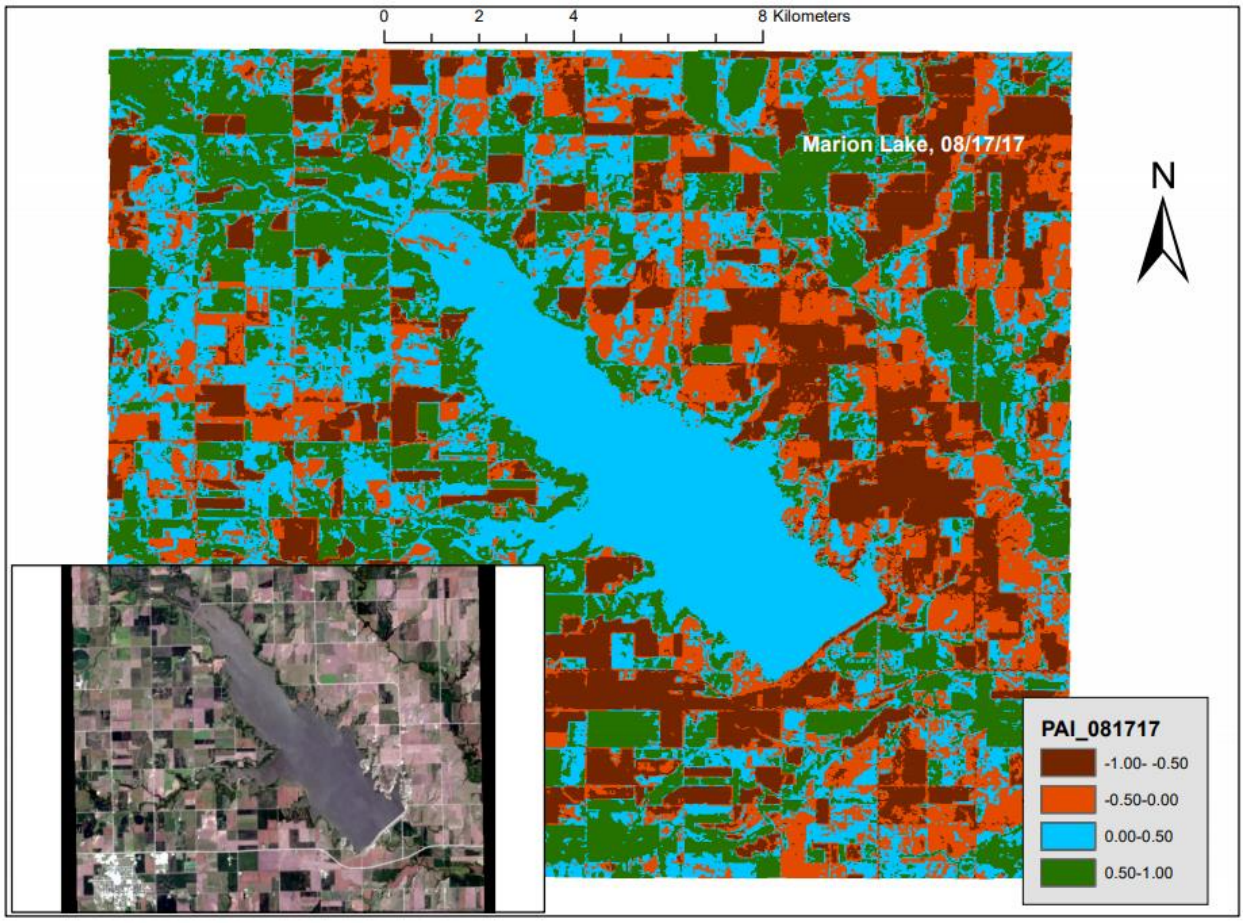

Figure 20. PAI compared to a true color (Marion Lake, August 17, 2017).

2.7 Conclusions

The objective of this study was to develop indices for photosynthetic algae and mineral turbidity using Landsat 8 operational land imager (OLI). The goal was to develop indices for inclusion in a monitoring tool for automated characterization of HABs on lakes managed by the GRDA. A photosynthetic algal index (PAI) was developed using water leaving radiance in Green and Red giving active spectrum plots for these two bands in the photosynthetic pigment, CHLa. For the mineral turbidity index (MTI), SWIR2 and Green bands were used since SWIR2 has the longest wavelength and it is expected to be absorbed by water except if it is incident upon waters with high mineral turbidity.

The *in situ* results were compared to the PAI and MTI developed in this study using regression analysis. The results revealed temporally variable relationships. On some dates, significant relationships were observed with strong R^2. However, this was not observed in all sampling dates.

For those days on which strong relationships were found, there may have been minimal mixed pixel problems and less interference from other inherent optical properties with similar spectral signatures. Even though concentrations were low on some of those days, the model still had significant p-values and R^2. Photosynthesis may have been active in those chlorophyll pigments despite their low concentrations.

Mixed pixel problems are the most probable causes for poor model performance for the dates in which insignificant relationships were observed. Using concentrations from a single sampling point as ground truth for radiation representing a 900-m^2 area may be overly optimistic. For a more accurate spectral signature for water leaving radiance, the goal would be sampling in as many points within a pixel as possible to estimate the concentration range and how much influence a parameter has on reflected radiation from that pixel.

There were a number of other limitations to this study. A lab based clarification on whether CHLa can reflect NIR radiation was beyond the scope of this study. Conclusions were drawn based on literature reviewed. A future study would involve laboratory scale determination of IR spectral signatures for CHLa.

Computation of PAI and MTI did not take into account the constant of proportionality. We assumed k to have carried the value of one. A lab-based study that gives a linear plot between CHLa and PAI and between SDZ and MTI would give a slope

that represents interference from water and other optically active objects with comparable spectral signatures.

Determination of cutoff points for low, medium, and high values were also beyond the scope of this study. These were limited to range of values between negative and positive one. A future lab based experiment would develop a calibration curve with various concentrations of CHLa and turbidity to determine those cutoff points.

CHAPTER III

SOFTWARE TOOL FOR MONITORING HARMFUL ALGAL BLOOMS USING LANDSAT DATA

Mansaray Abubakarr S.[1], Swatelle Mitchell[1], Lampard Dave[1], Torbick Nathan[2], Stoodley Scott H.[1], Wagner Kevin L. [1], and Dzialowski Andrew D. [1]

[1]Oklahoma State University, [2]Applied GeoSolutions

Abstract

Lake managers need more resources to address challenges of increased frequency and spatial extent in detecting harmful algal blooms (HABs). Land use practices such as agriculture and urbanization cumulatively introduce nutrients into downstream water bodies and increase the likelihood of HABs. They also introduce organic carbon leading to increased rates of microbial metabolism, oxygen demand, and subsequent bioavailability of nutrients. Pinpointing these sources is a difficult task, which complicates prioritizing monitoring locations and frequency for HABs detection. In responding to the susceptibility of Oklahoma lakes to these uncertainties, we developed an automated tool that can help address these spatial and temporal challenges for HABs monitoring. In this study, we developed an open source software tool in Python to monitor HABs using a satellite based photosynthetic algal index (PAI). To account for interferences from other optically active objects, a mineral turbidity index (MTI) was also developed. The Python tool downloads Landsat images from the United States Geological Survey's (USGS) Earth Explorer website and saves them onto a desktop. It then extracts spectral data and input into the equations that characterize photosynthetic algae and mineral turbidity. These computational results for photosynthetic algae and mineral turbidity determine whether there is a bloom on the lake.

3.1 Introduction

Lake managers today need more resources to address challenges of increased frequency and spatial extent in detecting harmful algal blooms (HABs). Increasing land use practices such as agriculture, settlements, and forestry cumulatively introduce nutrients directly and through metabolism of organic carbon into downstream water bodies (Machmuller, et al., 2015). Agricultural practices and land clearing introduce organic carbon into water bodies and lead to an increase in oxygen demand resulting from increased rates of microbial metabolism (Findlay, Pace, Lints, & Howe, 1992). Phosphorus becomes bioavailable in these anoxic aquatic conditions (Pettersson, 19989) and triggers exponential algal growth (Bormans, Maršálek, & Jančula, 2016). Nitrogen is also a limiting factor to HABs occurrence (Filstrup & Downing, 2017) and it is supplied through fixation from the atmosphere (Howarth, Marino, Lane, & Cole, 1988), groundwater inflow (USGS, 2016), and surface runoff (Filstrup & Downing, 2017). These nonpoint nutrient sources make it challenging to pinpoint priority areas for HABs monitoring in inland water bodies. New monitoring tools that capture spatial and temporal variability of these HABs are needed in agriculturally productive regions such as Oklahoma, where more than 200 lakes are susceptible to impairment from these pollutants.

In the Grand Lake watershed in Oklahoma, Kansas, Arkansas, Missouri, the development of an automated monitoring tool for HABs detection has become a priority in pursuit to addressing the repeated cases of unprecedented blooms in jurisdictional waters. The goal is to use this new monitoring strategy to identify and characterize the spatial and temporal extent of such algal blooms. Developing this tool will help agencies

pinpoint priority areas for algal pollution monitoring and save time and cost in future water quality monitoring.

The development of such automated monitoring tool is possible through machine learning, which is a sequence of instructions (algorithms) that are built in a computer programming language. The script is coded according to specific instructions and input information derived from analytical and/or empirical data (Alpaydın, 2010). Machine learning has been used in remote sensing and geographic information systems (GIS) for natural resource management. Huang and Jensen (1997) asserted that the use of decision trees and minimal human input help computers learn how to generate information on remote sensing and GIS of the environment (Huang & Jensen, 1997). Several studies have used similar methods in developing workflows of image acquisition, processing, and analysis with minimal human input (Melgani & Bruzzone, 2004; Ahmad, Kalra, & Stephen, 2010; Lary, Alavi, Gandomi, & Walker, 2016; Cracknell & Reading, 2014; Yong Hoon, Ho Kyung, Jong-Kuk, Jungho, & Sunghyun, 2014).

A limitation to machine learning in remote sensing is the difficulty in generalizing the code to be universally applicable. The algorithms are limited to specific geographical, analytical, and empirical boundaries (Brassel & Weibel, 2007). This makes it limiting to use a software developed in a different study area since their algorithms have spatial differences in water quality. The objective of this study is to develop an automated satellite based monitoring tool for HABs detection in the Grand Lake Watershed. Ultimately, lake managers in the entire southcentral US will be able to use this tool in detecting and characterizing HABs.

3.2 Materials and methods

3.2.1 Description of the study area

The Grand Lake Watershed (Figure 21) has an area that lies in three Landsat path/row areas (Appendix II). The Landsat path/row areas have minimum swath width of 185 km and the sensor takes images with an instantaneous-field-of-view (IFOV) of 30 m x 30 m. The IFOV is also known as pixel, the smallest unit of an image (Jensen, 2015), and ranges between 7,000 and 9,000 pixels per Landsat scene.

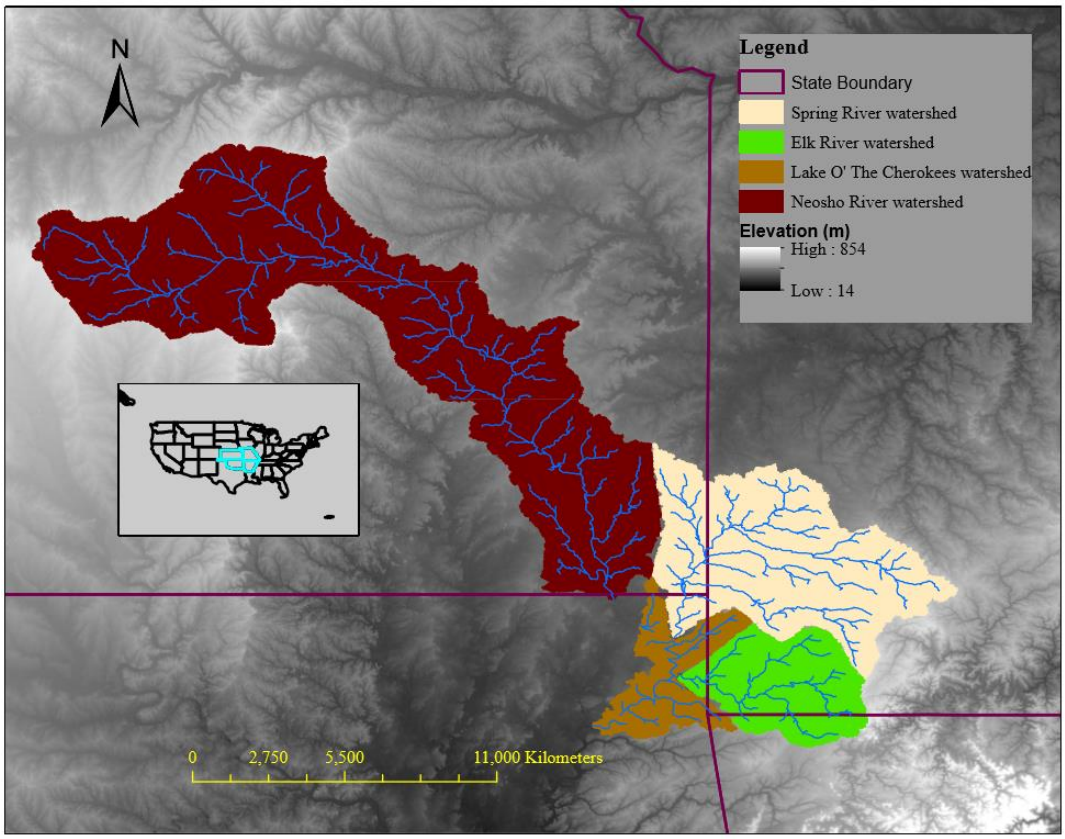

Figure 21. Map showing the Grand Lake watershed and its sub-watersheds

Officially named Grand Lake O' The Cherokees hereafter referred to as Grand Lake, it is located in Delaware, Ottawa, and Mayes counties in northeastern Oklahoma. Grand Lake is in the foothills of the Ozark Mountains and receives its water from the Grand (Neosho), Elk, and Spring Rivers (LakeHub LLC, 2018). Table 7 shows the

surface area, shoreline length, average depth, and water volume of Grand Lake (Johnson & Luza, 2008) and the other lakes under study. Figure 22 shows a map of the Grand Lake and sampling sites on the lake.

Table 7. Characteristics of Lakes under study

Lake	Surface area (km^2)	Shoreline length (km)	Mean Depth (m)	water volume (m^3)
Grand Lake	188.2	2,092.147	11.0	2,062,378,560
Council Grove Lake	13.27	64.374	4.0	59,823,869.121
Marion Lake	0.62	96.561	3.4	98,560,132.747
John Redmond Lake	38	94.951	2.7	83,016,000

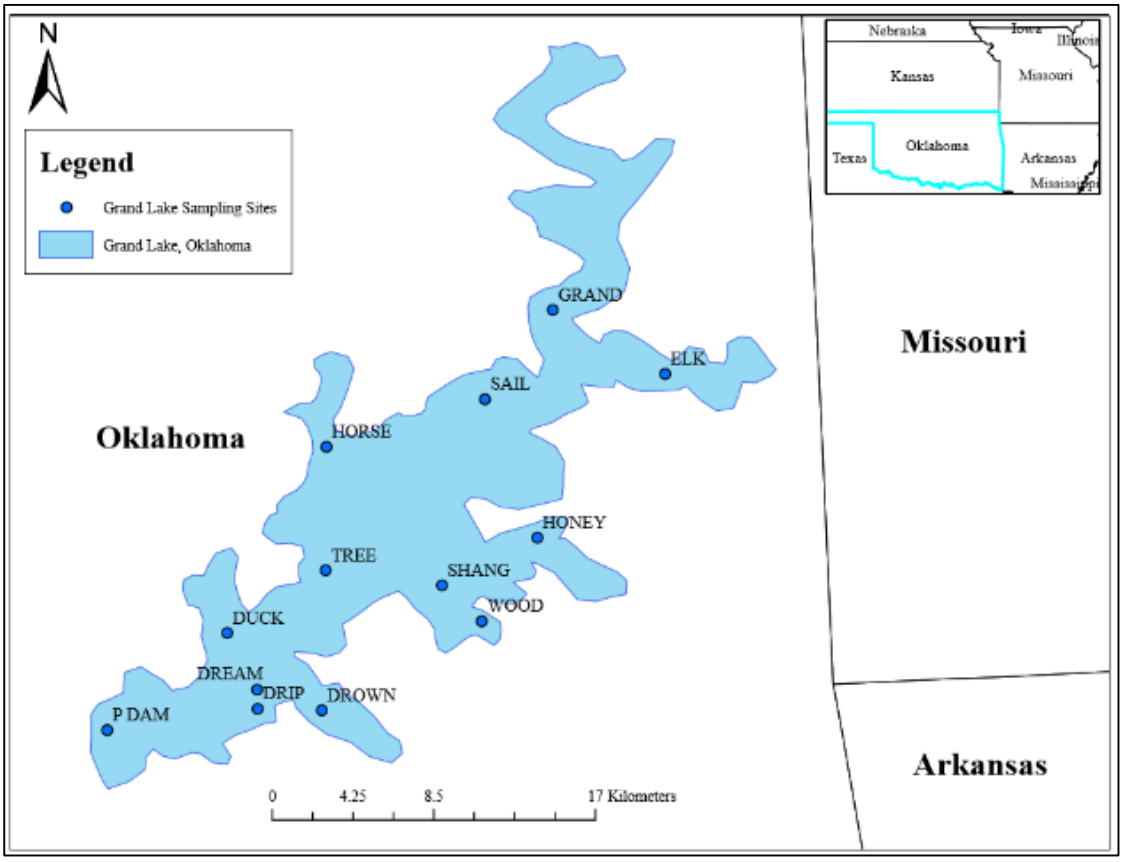

Figure 22. Sampling sites of Grand Lake in Oklahoma

Council Grove Lake, in Morris County, is located in the scenic Flint Hills region of Kansas and lies in the Neosho River basin. Table 7 shows the surface area, mean depth, shoreline length, and volume of water in the lake (U.S. Army Corps of Engineers,

2011). Figure 23 shows a map of the Council Grove Lake and sampling points on the lake.

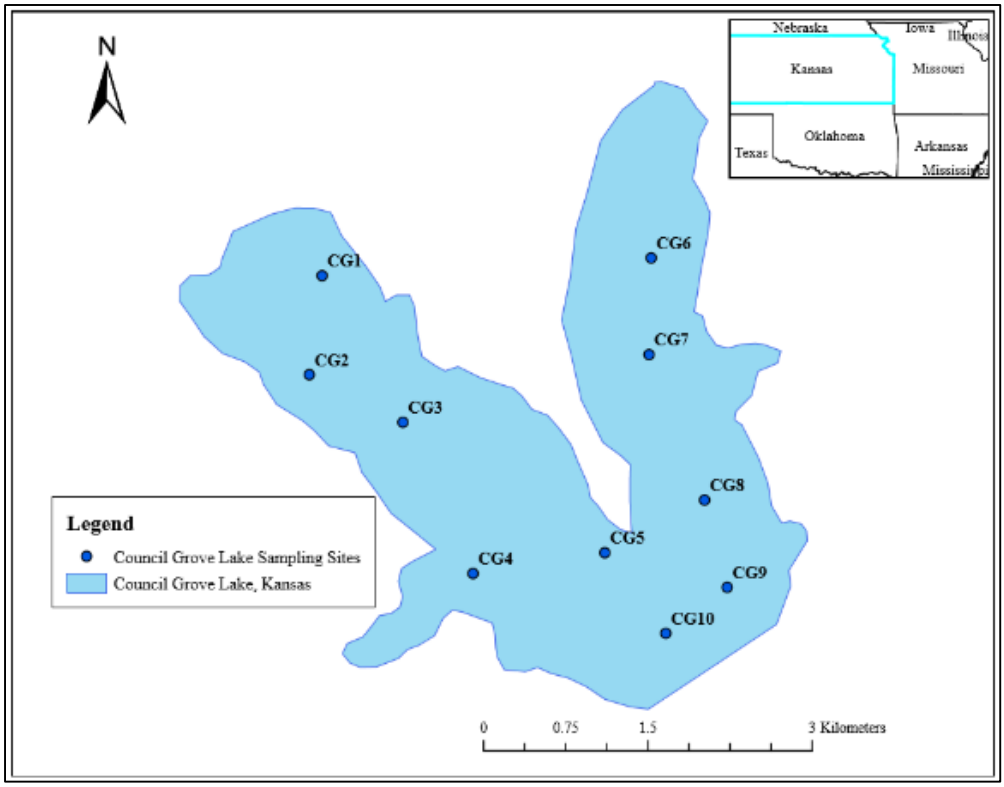

Figure 23. Sampling sites on Council Grove Lake in Kansas

Marion Lake lies between the cities of Marion and Hillsboro in Marion county, central Kansas. It is situated in the North Cottonwood River basin, which drains most of the watershed. Figures 24 shows a map Marion Lake and the lake sampling sites. The surface area, shoreline length, mean depth, and water volume are shown in Table 7 (US Army Corps of Engineers, 2018).

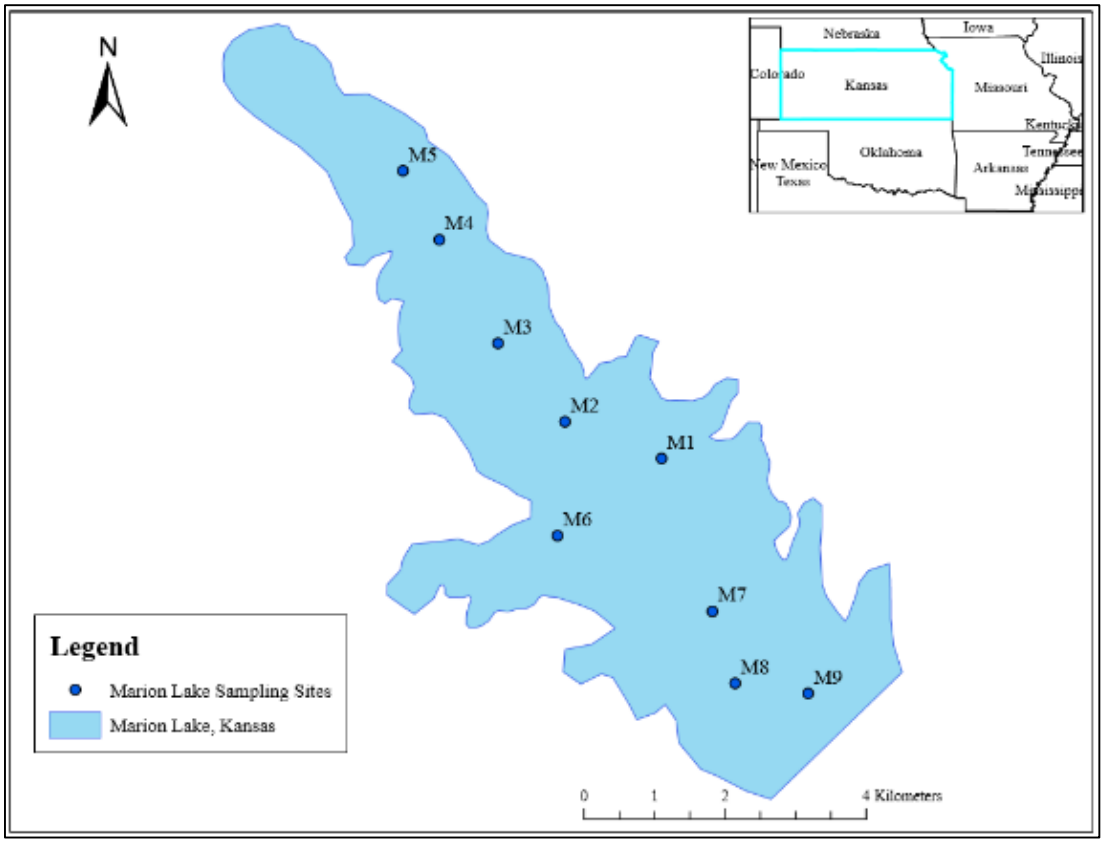

Figure 24. Sampling sites on Marion Lake in Kansas

The Neosho River in the John Redmond sub watershed serves as both the recharge in the northwest and discharge in the southeast for the John Redmond Lake (Figure 25), which lies within Coffey County in eastern Kansas. Table 7 shows the reservoir's surface area, mean depth, shoreline length, and volume (US Army corpse of Engineers, 2018).

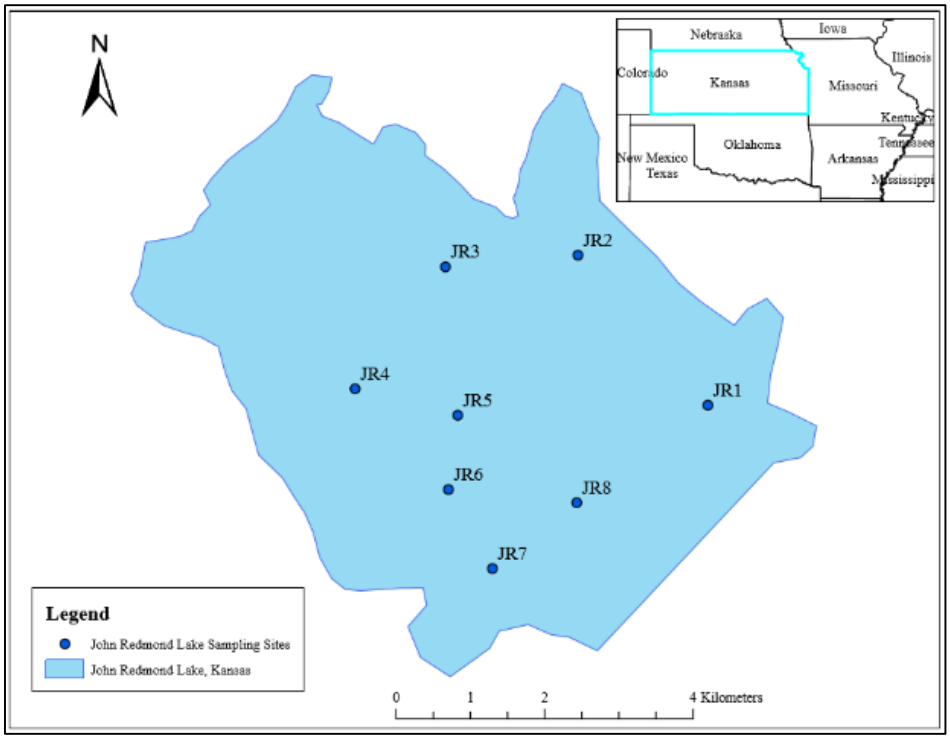

Figure 25. Sampling sites on John Redmond Lake in Kansas

3.2.2 In-situ water quality sampling

The programming workflow provides for validation through *in situ* water quality data plotted against temporally and spatially coincident extracted spectral data. The EXO-1 YSI multi-parameter water quality probe is used to collect data for CHLa, and the Secchi disc is used to collect data for SDZ. These data are used for routine quality assurance (QA) tests when running the tool. In a previous study (Chapter II), indices were developed, for use in this tool. The data used to develop the indices were collected using the EXO1 YSI multi-parameter probe at designated sample sites on lakes in the study area. The probe consists of replaceable sensors and pressure transducers, which pick signals and send to the detector that displays the signals as concentrations of the different parameters. The procedures for assembling, preparing, and calibrating the EXO1 probe are detailed in the instrument's operation manual (EXO, 2017).

3.2.3 Collection of water samples for laboratory analyses

In the development of the indices, we collected samples for analysis in the laboratory. These data were compared to *in situ* water quality data collected from the same sites and dates as quality control and quality assurance. We utilized brown bottles, a depth integrated tube sampler, and a Van Dorne water sampler to collect water samples. The samples were stored in a cooler and transported to the laboratory for sample analysis. Sample collection and analyses followed the USEPA's sampling and analysis plan guidance and template (USEPA, 2014).

3.2.4 Software

The software developed in this study is written in Python 3.4. Python is free and open source, and it is extensively utilized for scientific applications because of its object-oriented, interpretive, and interactive programming tendencies (Wichmann, 2017). Python 3 has all recent standard library improvements available by default in version 3.4 (Wichmann, 2017).

With Python, the user does not have to be an expert in computer programming. The language is generic and its script can be easily interpreted. The standard Python programming language can support a large set of spatial and temporal raster data files and can run and display iterative temporal models (Karssenberg, de Jong, & van der Kwast, 2007). The program is an open source with a large number of library modules that make it suitable for our satellite based monitoring (Oliphant, 2007).

3.2.5 Theoretical and empirical bases of the tool

In a previous remote sensing study (Chapter II), indices were developed for photosynthetic algae and mineral turbidity as shown in the equations below.

$$PAI = \frac{\rho_G - \rho_R}{\rho_G + \rho_R}$$

Where PAI is photosynthetic algal index, ρ_G is Green reflectance, and ρ_R is Red reflectance of light in the sun's electromagnetic spectrum (EMS). The PAI has values ranging between -1 and +1. For the mineral turbidity index (MTI),

$$MTI = \left(\frac{\rho_{SWIR2} - \rho_G}{\rho_{SWIR2} + \rho_G}\right)$$

Where ρ_{SWIR2} is shortwave infrared 2 and MTI ranges between -1 and +1. The PAI is incorporated into the Python script to delineate the active spectrum of photosynthetic algae and guide mapping of HABs in the lakes under study. The MTI was developed to account for interference from other optically active objects in the water body. Turbidity, a major water quality issue in Oklahoma, is regarded the main interference to PAI measurement. These two indices were empirically tested with ground based data on temporally coincident dates of Landsat 8 OLI (Chapter II).

3.3 Structure and work flow of the python script

3.3.1 Image acquisition

The tool is customized to obtain satellite images from the USGS earth explorer website. Specific instructions include searching for the uniform resource locator (URL), signing in with a username and password; specifying image types and quality, and downloading to a computer desktop. The tool also has the capability of ordering and downloading surface reflectance images from USGS. It displays update on the status of orders whenever the user logs on to their computer. This software has instructions that enhance the complete ordering and downloading procedures set by the USGS.

3.3.2 File extensions (dependencies)

There is a wide range of extension libraries that the Python program depends on for full operation. The type of file extension used depends on the purpose for which the script is written. We utilized eight extensions in order to ensure smooth operation of the automated HABs monitoring tool. Table 8 shows a list of the file extensions used in this study.

Table 8. File extensions for Python scripting

File Extension	Description/function
NumPy	The fundamental package for scientific computing with Python
GDAL	A translator library for raster and vector geospatial data formats
PyProj	Performs cartographic transformations and geodetic computations
Shapely	A licensed Python package for manipulation and analysis of planar geometric objects
Requests	Allows the user to send HTTP requests, without the need for manual labor, i.e. there is no need to add query strings manually to your URLs, or to form-encode your POST data
Rasterio	Geographic information systems use GeoTIFF and other formats to organize and store gridded raster datasets such as satellite imagery and terrain models. Rasterio reads and writes these formats
Matplotlib	A Python 2D plotting library which produces publication quality figures in a variety of hardcopy formats and interactive environments
USGS	A Python module for interfacing with the USGS website

3.3.3 Interpretation of PAI and MTI values

Figure 26 shows a simple flow diagram describing the workflow of the software and its interpretation rules. Following are detailed descriptions of the workflow.

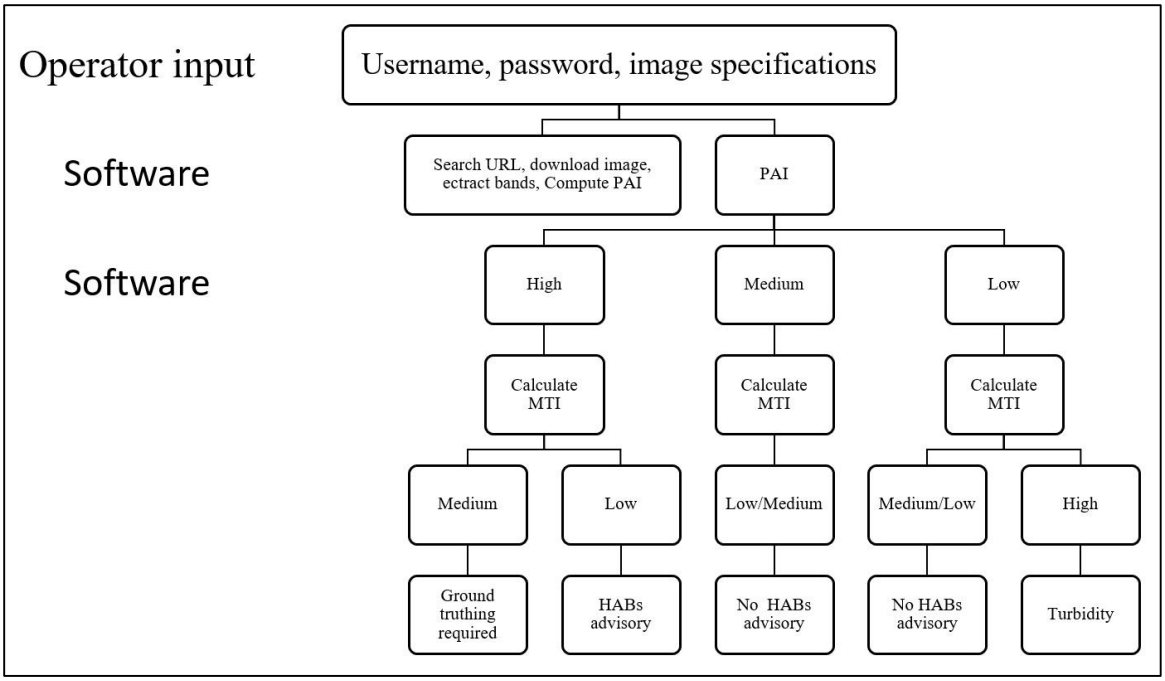

Figure 26. Flow diagram showing the operational structure of the software developed for automated monitoring of HABs in the Grand Lake watershed

The Python tool extracts spectral data for input into the indices developed for photosynthetic algae and mineral turbidity. The first step is computation of PAI followed by a quality assurance (QA) test. The workflow is built such that QA tests are done routinely and when necessary. The frequency of this routine is determined through empirical data, which will be compiled in due course alongside utilization of the monitoring tool. In-between the routine QA tests, it is optional to the user to execute the test. The QA test is based on a Pass/Fail standard. Regression analysis is done on the PAI against *in situ* chlorophyll-a data. If the results show regression error, $\alpha \leq 0.05$, coefficient of determination $R^2 \geq 0.6$ and predicted $R^2 \geq 0.5$, the tool will indicate a Pass. If, on the other hand, $\alpha > 0.05$, $R^2 < 0.6$, and predicted $R^2 < 0.5$, the tool will indicate a Fail and report details of the failed QA test. In this case, the user has the ability to override the failed test and continue with the analysis. These standards are based on values reported in the

literature and from confidence intervals that assume normal distribution of data (Allee & Johnson, 1999; Chen, et al., 2010; Han & Rundquist, 1997; Kirk, 2011; Mishra & Mishra, 2012; Ruddick, Gons, Rijkeboer, & Tilstone, 2001; Tebbs, Harper, & Remedios, 2013; Thu Ha, Koike, Nhuan, Parsons, & Thao, 2017; Torbick, et al., 2008; Yacobi, Giltelson, & Mayo, 1995). Future studies will involve development of a Pass/Fail standard based on both empirical and analytical evidences.

Following the pass/fail test is interpretation of high, medium, or low PAI values. High PAI values have range 0.5-1, medium PAI values have range (-0.5)-0.49, and low PAI values have range (-1)-(-0.49). The expectation is that these ranges will correspond to scenarios as summarized in Table 9. However, these standards require verification by empirical evidence through series of test runs in future monitoring programs.

Table 9. Interpretation rules for both PAI and MTI in the automated monitoring tool

Caveat	If PAI is:	And MTI is:	Report
QA test, no MTI computation required	High	Low	Algal bloom
QA test, MTI computation is necessary	High	Medium, Low	Possible algal bloom
QA test, MTI computation is required	Medium, Low	Medium, Low	No algal bloom
QA test, MTI computation is required	Medium, Low	Medium, Low	Water is clear
QA test, MTI computation is required	Medium, Low	Medium, High	Turbid water

These resulting PAI and MTI values at designated monitoring sites are exported to a csv file for further analysis and decision-making. Additionally, shape files for all lakes under investigation have been included in the software for overlay on the satellite image. Mapping of PAI and/or MTI on the lakes are possible through masking and plotting in a GIS software.

The Python code for the software will post at GitHub (https://github.com/) upon approval from the owners (GRDA). The next step will be series of test runs of the software to validate its functionality. Additionally, results of trials will be useful in the

development of standards and a completed manuscript for publication in peer reviewed journals.

3.4 Conclusions

The objective of this study was to develop an automated tool for detection of HABs in the Grand Lake Watershed and, potentially, the southcentral USA. This study used open source Python to build a software that automates a number of steps from image acquisition to displaying the spatial extent of a photosynthetic algal index on lakes through GIS mapping software.

The software can order and download radiometric, geometric, and atmospherically corrected images (Level-2 LC images) and extract spectral values to compute PAI and/or MTI with set standards and QA requirements. The results indicate whether there is a bloom, a possible bloom, turbidity, or the water is clear. Resulting images can also be plotted in a GIS platform (e.g. QGIS or ArcMap).

CHAPTER IV

LAKE WATER QUALITY BY ECOREGION AND HYDROLOGIC UNIT IN OKLAHOMA

Mansaray Abubakarr S[1], Stoodley Scott H[1], Dzialowski Andrew D[1], Wagner Kevin L[1], and Torbick Nathan[2]

[1]Oklahoma State University; [2]Applied GeoSolutions

Abstract

The goal of water quality monitoring at a regional level is to determine the magnitude and spatial distribution of pollutants across a region. In Oklahoma, most of the more than 200 lakes are susceptible to impairment from sediments, nutrients, and microorganisms causing economic and ecological concerns to state agencies and other stakeholders. The Oklahoma Water Resources Board (OWRB) monitors over 130 lakes on a quarterly rotational basis over a five-year period through their Beneficial Use Monitoring Program (BUMP). In this study, we classified 20 of those lakes into ecoregions and/or hydrologic units to determine if a representative lake could be selected per ecoregion for ground-based water quality monitoring. The OWRB's lake monitoring staff collected and analyzed the water quality samples. Lakes were compared for turbidity and CHLa using single factor analysis of variance (ANOVA) and two-sample t-test. The results indicate that selecting representative lakes by ecoregion or hydrologic unit is a plausible approach. These lakes are located within Landsat flyover path/rows. This makes it possible to combine ground based and Landsat data for input into the satellite based water quality monitoring tool developed in a previous study (Chapter II). This combination of ground based and automated satellite-based monitoring will increase sampling frequency in lakes and expand the spatial extent of OWRB's lake monitoring program.

4.1 Introduction

A major challenge to water quality monitoring is using limited resources to sample many areas at a time. Usually agencies are limited in budgets and human resources. This makes it hard for accurate and comprehensive sampling of water bodies throughout a region (Rodríguez, et al., 2006). Nonetheless, successful water quality monitoring at regional scale requires consideration of the spatial extent of many water bodies as opposed to measuring a single point over time (Urquhart, Paulsen, & Larsen, 1998). Deciding which water body to choose in a rotational monitoring program is also challenging as the possibility exists to miss out on major pollution events (Harvey, Kratzer, & Philipson, 2015). Oklahoma state agencies with water quality monitoring responsibilities face this challenge with over 200 reservoirs distributed throughout the state (Figure 27). There are approximately 55,646 miles of shoreline along lakes and ponds and 1,401 square miles of water area in those lakes and ponds (OWRB, 2018).

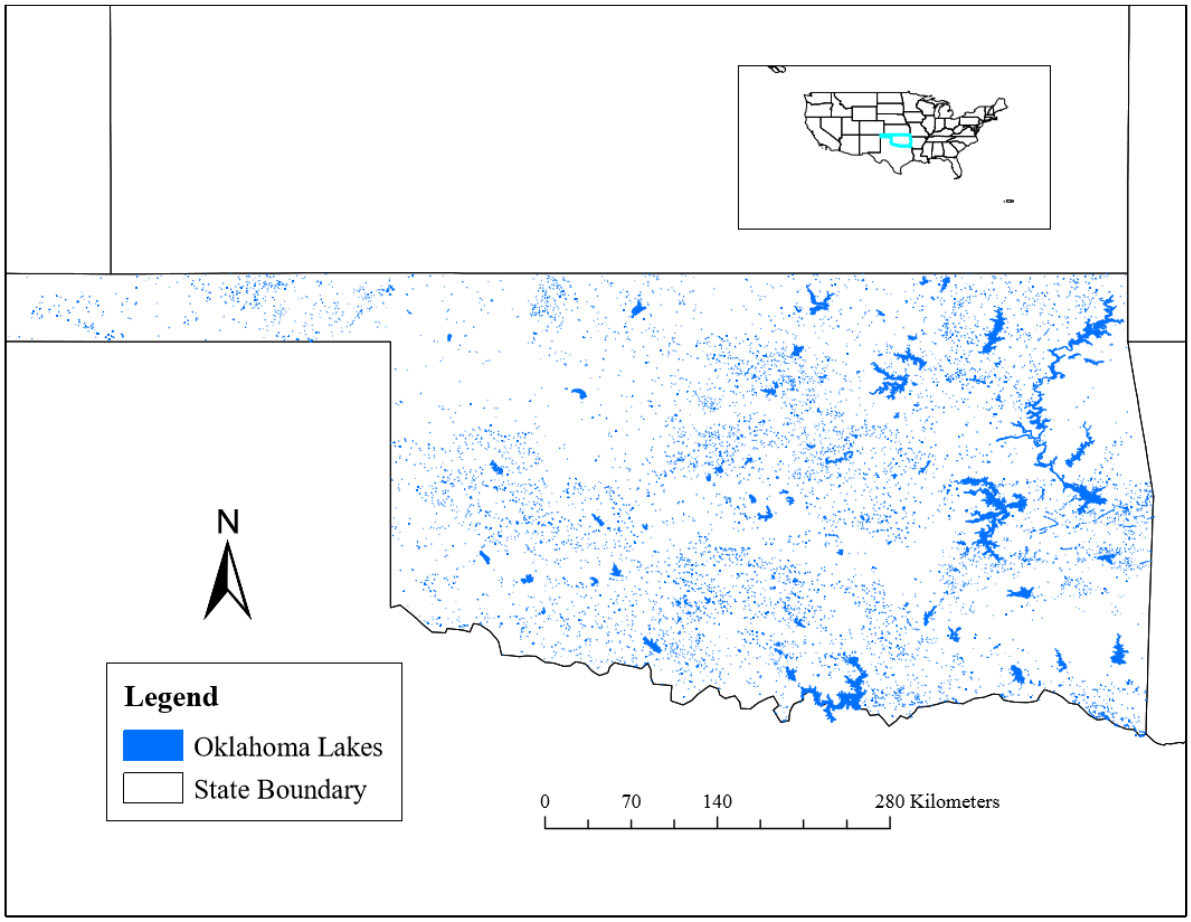

Figure 27 Map showing Lakes in Oklahoma

In Oklahoma, most of the lakes are susceptible to impairment from sediments, nutrients, and pathogens (OCC, 2014). This is a concern given the social, economic, and environmental benefits derived from those lakes. Estimates have shown that reservoir related recreation contributes an annual income of $2.2 billion to Oklahoma's economy. Fishing contributes $730,503,000 to the economy, while camping contributes another $10.7 million annually. Activities related to those reservoirs provide 32,100 jobs and 18,718,000 tourist days every year (OWRB, 2017). There is a need for monitoring programs that will delineate the magnitude and extent of pollution in as many of those lakes as possible. Such monitoring results will provide a useful guide for determining

where to implement beneficial management practices that will reduce pollution sources in the watersheds in Oklahoma.

The Oklahoma Water Resources Board (OWRB) developed the Beneficial Use Monitoring Program (BUMP) to ensure sampling of 130 lakes on quarterly basis with a five-year rotation schedule (OWRB, 2017). The monitoring program includes only lakes that are above 50 surface acres. These are broken up into two groups, those lakes that are greater than 500 surface acres and those below. Out of the 68 lakes with surface acres greater than 500, 14 are monitored during one of the quarters in a selected year and twice in the five-year rotational monitoring period. Ten lakes with areas less than 500 surface acres are randomly selected and monitored annually over the 5-year rotational period (OWRB, 2017).

Due to this small sample size relative to the number of lakes in the state, many of the Oklahoma lakes are not monitored during a quarterly BUMP schedule. This poses the challenge of uncertainties in delineating which reservoirs may or may not be supporting their beneficial uses and to what magnitude they matter. These uncertainties have been further confounded by unprecedented harmful algal blooms (HABs) in a number of those reservoirs (Holt, et al., 2008). These algal pollution events have been repeating every summer.

In 2015, the GRDA funded this research to develop a near real time Landsat 8 based water quality monitoring tool for timely detection and assessment of HABs in northeastern Oklahoma. The goal is to capacitate state agencies like OWRB to utilize this new monitoring tool to improve risk assessment through timely and extended characterization of HABs in lakes in southcentral USA. This will help improve resource

allocation by delineating hotspot areas for priority monitoring, maximizing customer satisfaction, and achieving water resource policy objectives.

This study looks into the potential for a ground based monitoring routine that covers the required spatial extent while combining with temporally coincident satellite flyovers. This monitoring capability is needed to integrate *in situ* water quality data, satellite data, and machine learning to calibrate and run the monitoring tool. The objective is to determine if representative reservoirs can be selected based on their ecoregion or hydrologic unit to coincide with satellite flyover schedules. Lakes in these regions are compared to each other over a 5-year period (2012-2017) in terms of CHLa and turbidity.

Water bodies within the same ecoregion are expected to be susceptible to similar ecological conditions (USEPA, 2017). Those water bodies in the same hydrologic unit are expected to have similar water quality trends since they all receive waters from the same upstream sources and have similar indirect source conditions (NRCS-USDA, 2007). Delineation of representative water bodies within a satellite fly-over path/row will ensure spatial and temporal coincidence in ground based and Landsat data. We hypothesize that reservoirs in the same ecoregion and/or hydrologic unit are not significantly different in Turbidity and CHLa concentrations at a 95% confidence level.

4.2 Materials and Methods

4.2.1 Description of study area

This study covered 20 reservoirs across the state of Oklahoma all of which are included in the OWRB's BUMP. Appendix XI presents a list of all 20 lakes, sampling sites, sampling dates, and water quality parameters. In order to capture the variations in

Oklahoma's ecoregions and hydrologic units, the selected lakes spread across the length and breadth of the state with the exception of the panhandle in the northwest; data were not available for this region. Figure 28 shows locations of the selected lakes across Oklahoma.

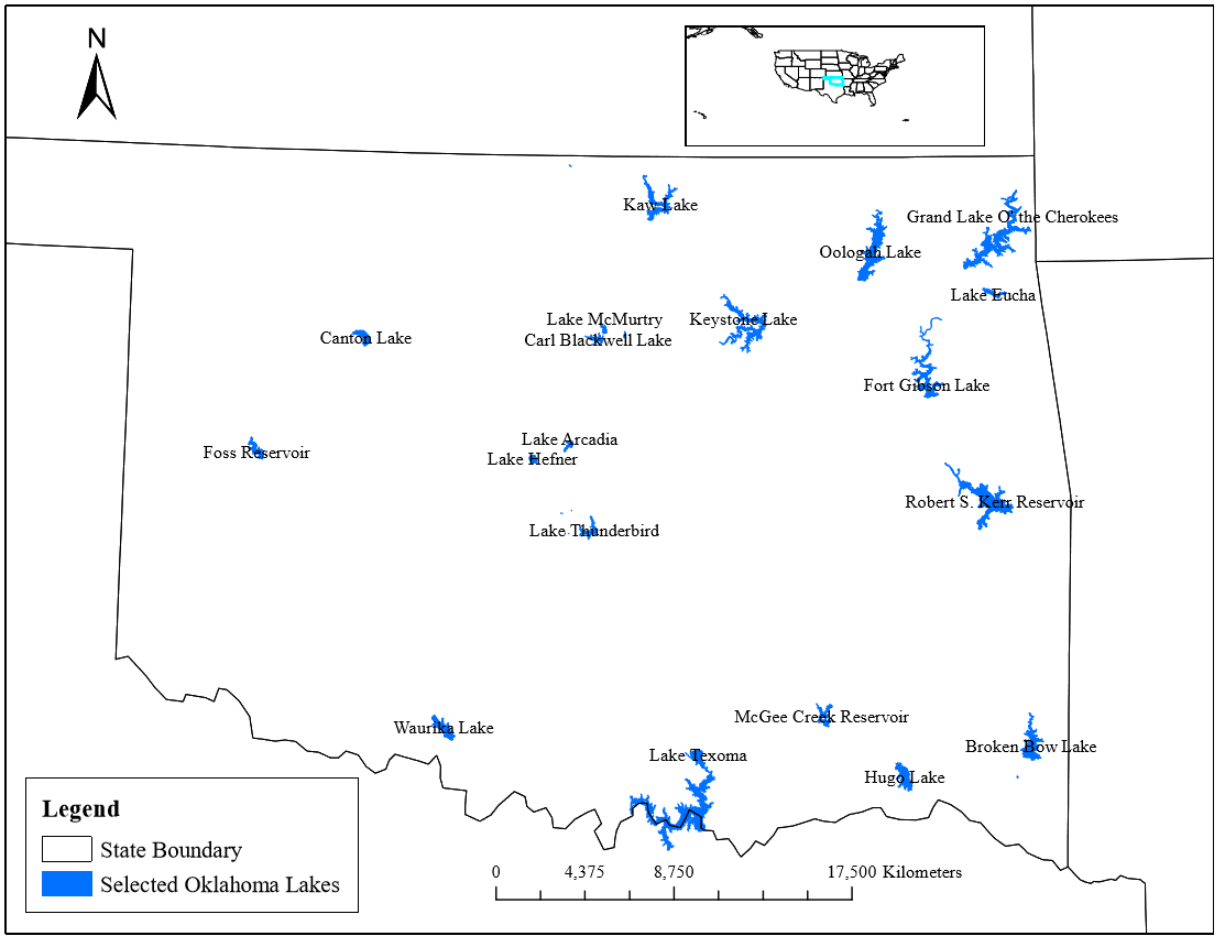

Figure 28 Selected Reservoirs across Oklahoma

4.2.2 Ecoregions

Oklahoma has 12 level III ecoregions (Figures 29) and 46 level IV ecoregions. Each ecoregion has characteristic spatial patterns of biotic and abiotic communities defined by their physiography, geology, climate, soils, land use, wildlife, fish, hydrology, and vegetation (USEPA, 2017). This ecological diversity in Oklahoma is due to the varied landscape in climate, terrain, geology, soil, and land use (USEPA, 2017). The variability

is characterized by vast plains, elevated karst plateaus, hills, and folded low mountains. The precipitation gradient starts from east to west ranging from high in the east to low in the west. There are higher temperatures and longer growing seasons in the south. The state is characterized by landscapes as summarized in table 10. The elevation gradient begins with 1,524 m on Black Mesa in the northwestern Panhandle down to about 91 m in the southeast (USEPA, 2017).

Table 10. Variations in landscape in Oklahoma

Landscape	Location/Description
Ouachita Mountains	forested and become progressively more stunted and open westward
Southern pine forests	Southeast
Tall grass prairie, mixed grass prairie, and short grass	Central and western parts of the state
mesquite and other xeric plants	characteristic of the dry southwest

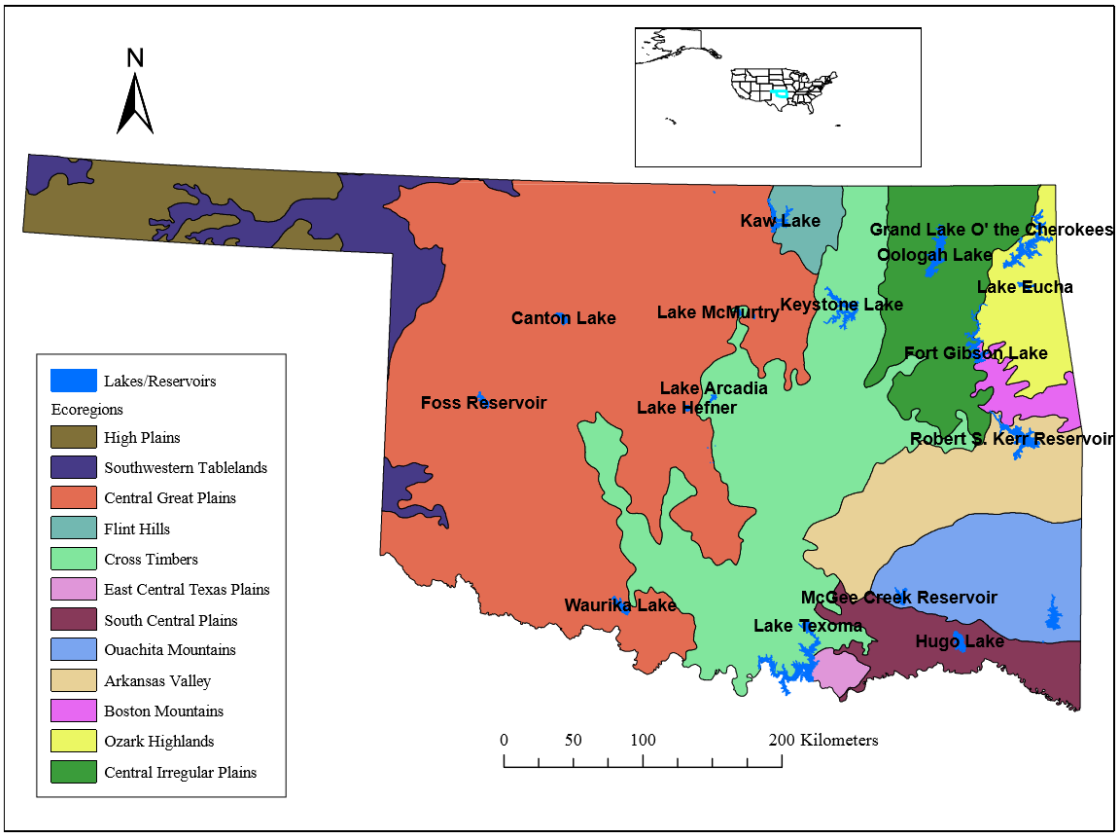

Figure 29. Level III Ecoregions and their constituent reservoirs in Oklahoma

4.2.3 River Basins and Hydrologic Unit Codes

Oklahoma lies within two major river basins, the Red River and the Arkansas River basins (Johnson & Luza, 2008). The Red River in Oklahoma, starts from the Texas Panhandle in the east and flows into Arkansas where it continues through Louisiana to join the Atchafalaya River. The Arkansas River enters Oklahoma in Kay County and flows into Arkansas near Fort Smith on its way to the Mississippi River in southeastern Kansas (Johnson & Luza, 2008). Figure 30 shows a map of Oklahoma's river systems. Most of these river systems were impounded to give rise to the lakes under study. These rivers and lakes divide into hydrologic unit codes based on their regional and drainage similarities (NRCS-USDA, 2007).

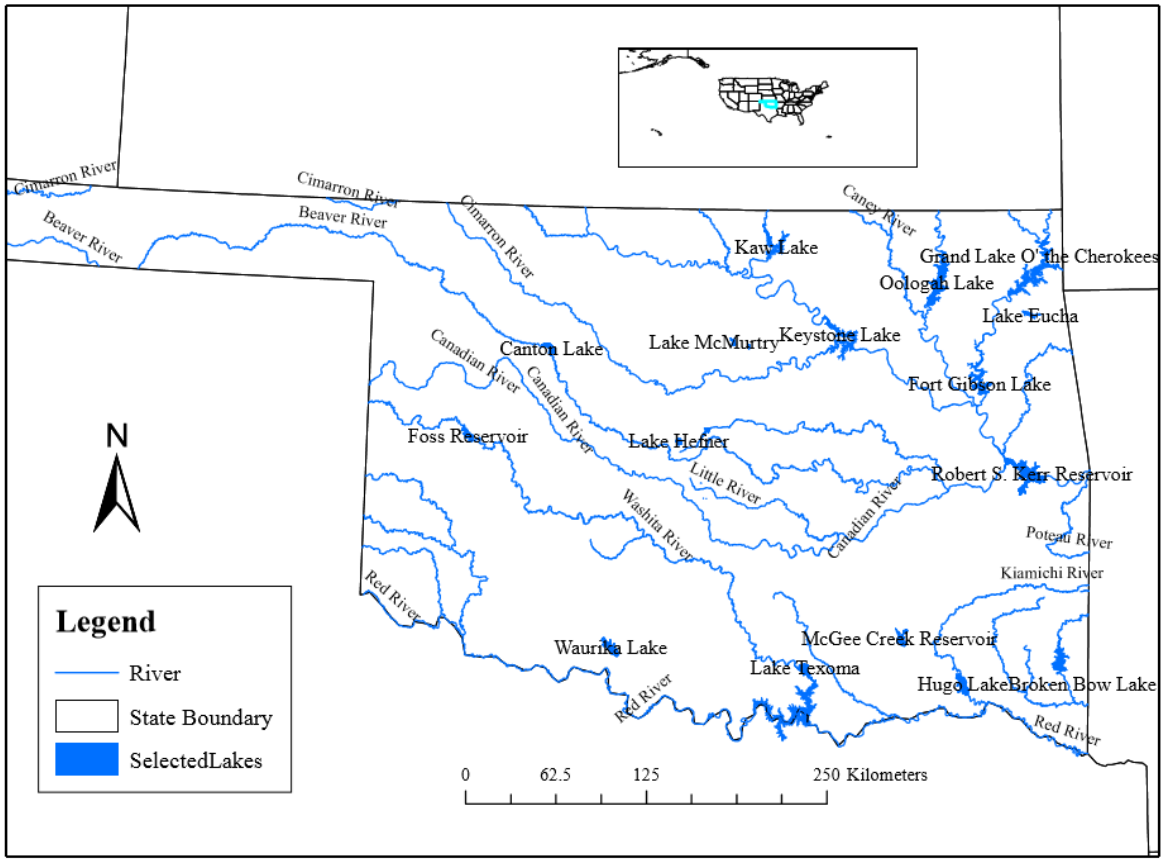

Figure 30. Map showing rivers and lakes across Oklahoma

This study considered Oklahoma's sub-regional level and accounting units with 4-digit and 6-digit hydrological unit codes, respectively. When lakes within an ecoregion were significantly different, they were divided further into these hydrologic units, which have areas that locate within those ecoregions. These units receive surface water from an upstream drainage system and associated surface areas and they form an area with single or multiple outlet points (NRCS-USDA, 2007). Figures 31 and 32 show the 4-digit and 6-digit hydrologic unit maps of Oklahoma, respectively.

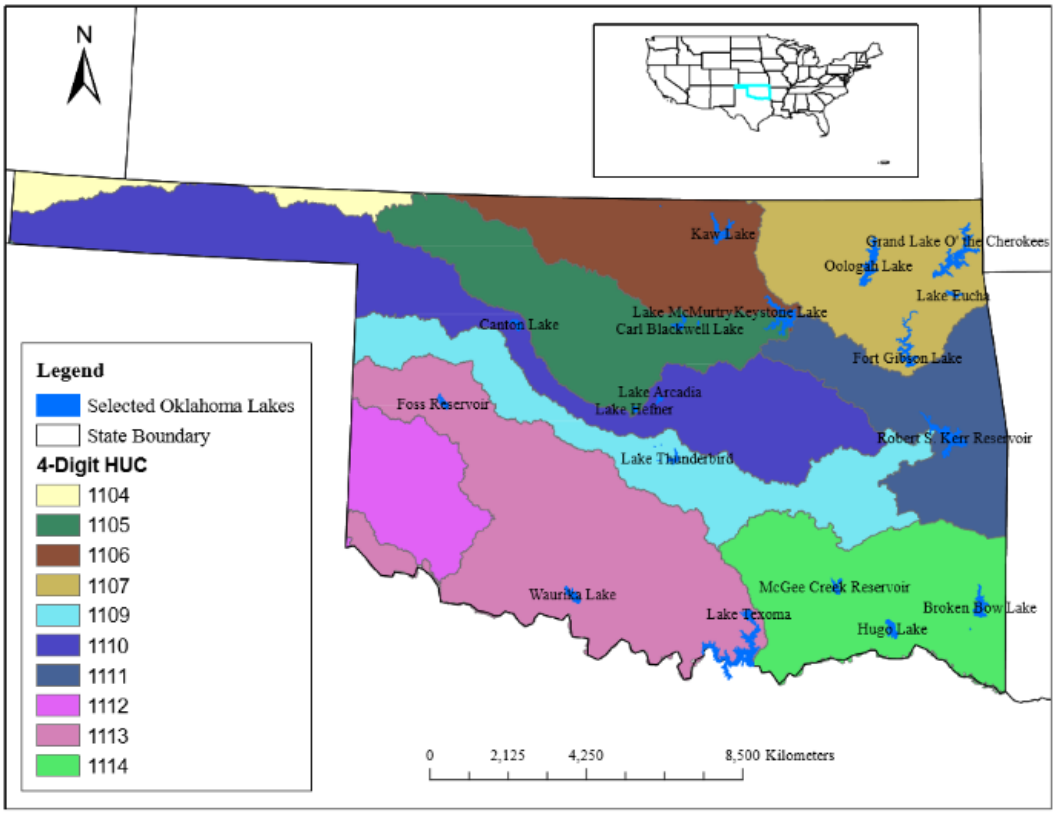

Figure 31. Maps showing 4-digi hydrologic units and their constituent reservoirs in Oklahoma

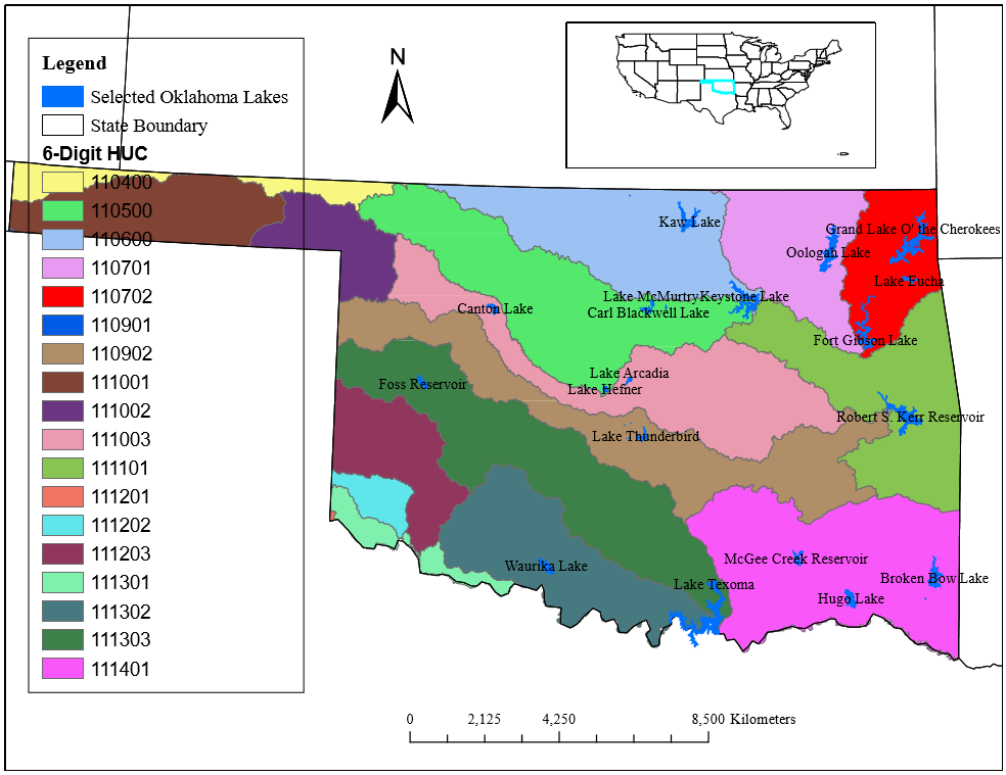

Figure 32. Maps showing 6-digit hydrologic units and their constituent reservoirs in Oklahoma

4.2.4 WRS2 Path/Row combinations for Landsat 8 in Oklahoma

The areas in Landsat flyover paths and rows as described in the World Reference System 2 (WRS2) have spatial coincidence with ecoregions in Oklahoma. Every ecoregion and, hence, every hydrologic unit and reservoir have areas that locate within specific Landsat path/row areas (Figure 33).

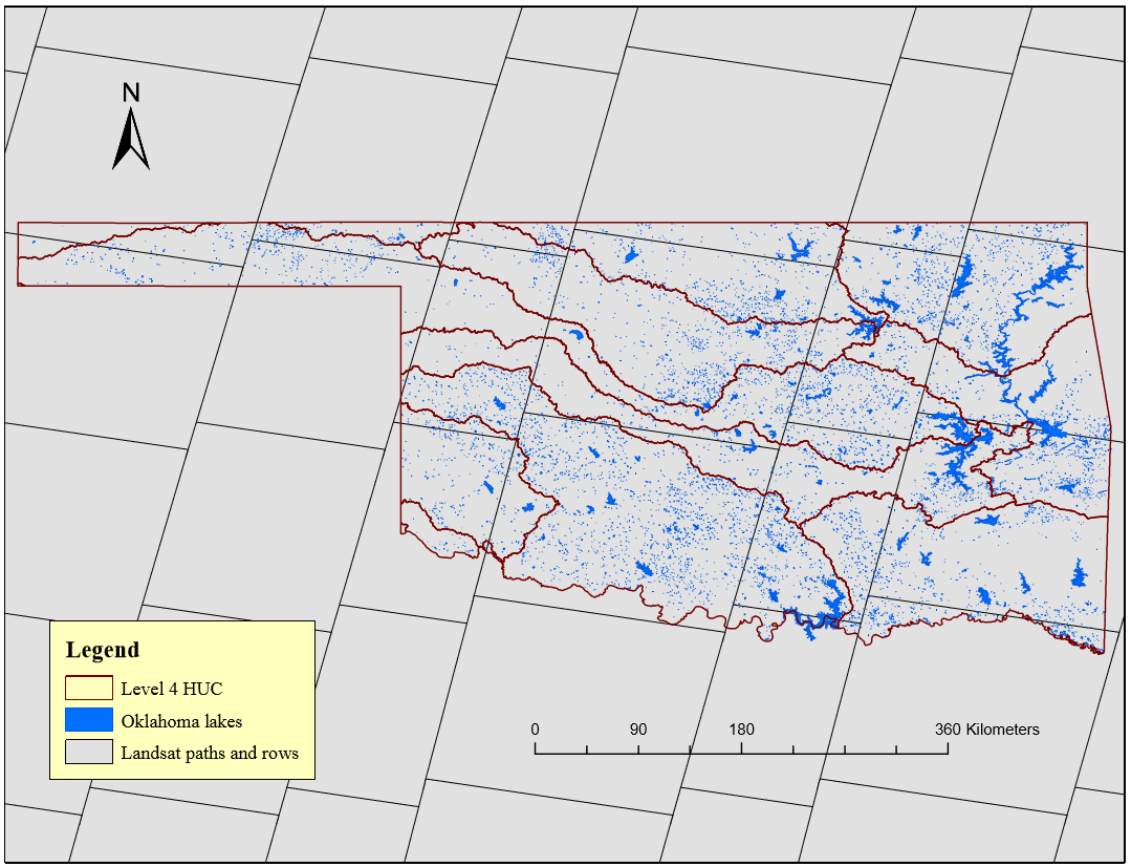

Figure 33. Reservoirs and Level 4 hydrologic units in Oklahoma's Landsat paths/row areas

Table 11 shows the list of lakes under review within each path/row.

Table 11. List of reservoirs in each WRS2 path/row combinations for Oklahoma

Path	Row	Oklahoma Lakes
25	36	Broken bow Lake
25	37	Broken Bow Lake
26	35	Grand Lake O' The Cherokees, Lake Eucha; Fort Gibson lake; Oologah Lake; Robert S Kerr Reservoir
26	36	Broken Bow Lake, Hugo Lake; Robert S Kerr Reservoir, McGee Creek Reservoir
27	34	Oologah Lake
27	35	Lake Arcadia, Boomer Lake, Kaw Lake, Keystone Lake, Lake Carl Blackwell, Fort Gibson lake, Lake McMertury, Oologah Lake
27	36	Lake Arcadia, Lake Thunderbird, Lake Taxoma, McGee Creek Reservoir
27	37	Lake Taxoma
28	34	Kaw Lake
28	35	Lake Arcadia, Boomer Lake, Canton Lake, Kaw Lake, Lake Carl Blackwell, Lake Hefner, Lake McMertury,
28	36	Lake Thunderbird, Waurika Lake
29	35	Canton Lake, Foss Reservoir

4.3 Sampling and Analysis

The OWRB did the sampling and analysis of data used in this study through their beneficial use monitoring program. Detailed description of procedures for sampling and analysis is available at the agency's water quality monitoring website (OWRB, 2018).

The monitoring team used high-resolution maps, landmarks, and thalweg (i.e. the deepest part of the water body) to designate sites for water sampling. A depth finder was used to locate a thalweg, details of which were recorded on a field sheet (location, depth, etc.). Samples were collected with sample bottles at 0.5 m depths; samples were also collected for quality assurance/quality control (QA/QC) analysis.

For CHLa analysis, 1-L samples were collected at each sample site starting with rinsing the containers with sample water. Sample collection was done by immersing the sample container's nozzle down to the 0.5-meter depth and slowly allowing sample container to fill and expelling all the air. The monitoring team ensured that shipping and analysis of samples in the laboratory was done within 24 hours because chlorophyll analysis has a 24-hour holding time. With overnight trips, the BUMP lake team did the analysis in the field. The detailed steps for CHLa analysis are available at the OWRB's website (OWRB, 2013).

The monitoring team used either the HACH® 2100P portable turbidity meter or the LaMotte 2020 portable turbidity meter. For immediate analysis, the water sample was collected using a vial in the turbidity meter kit. For subsequent analysis, a clean one-pint plastic bottle was rinsed and filled with sample for analysis within 24 hours. The bottles were placed on ice until analysis was conducted. During analysis, the water sample was

brought to ambient temperature for an accurate reading to be determined. Detailed description of this procedure is available at the OWRB website (OWRB, 2001).

Analysis of data followed either single factor analysis of variance (ANOVA) or two sample t-test. We assumed that differences within and between datasets were not significant on a 95% confidence level ($\alpha = 0.05$). Statistical analyses were completed for five years of data (2012-2017); the data were collected on specific dates within a quarter. Details of the data are shown in Appendix XI.

For each sampling date, we took average concentrations of parameters from all sampling sites per lake. For all the 20 lakes, we compared the means of those average concentrations per date to each other (i.e. we assumed that those means were equal). Using the Minitab-18 statistical software, comparison of those average values per sampling period in the 20 lakes gave the results of significance in similarities or differences of CHLa and turbidity between the lakes.

4.4 Results and Discussions

4.4.1 Water quality by ecoregion

Table 12 and Figure 34 show p-values that compare water quality in the lakes in each ecoregion. Five of the 12 ecoregions in Oklahoma include two or more of the 20 lakes in this study. Comparisons were not made in ecoregions in which there is only one lake.

Table 12. Differences/similarities in water quality between lakes in Oklahoma's ecoregions

Ecoregions	**Lakes**	**p-value**	
		CHLa	Turbidity
Central great plains	Lake McMurtry, Lake Hefner, Boomer Lake, Lake Carl Blackwell, Lake Thunderbird, Foss Lake, Kaw Lake, Waurika Reservoir	0.0258	0.1471
Cross Timbers	Keystone Lake, Lake Texoma, Lake Arcadia	0.1932	0.0779
Central Irregular Plains	Oologah Lake, Ft Gibson Lake	0.0307	0.0066
Ozark Highlands	Grand Lake O' The Cherokees, Lake Eucha, Fort Gibson Lake	0.3346	0.0542

Ouachita Mountains	McGee Creek Reservoir, Broken Bow Lake	0.1849	0.1495

In the Central Great Plains and Central Irregular Plains, we reject the null hypothesis that the mean CHLa concentration between lakes within these regions are equal. Their p-values ($\alpha = 0.0258$ and 0.0307, respectively) are lower than the required standard ($\alpha = 0.05$) and, hence, we say the differences in mean CHLa between lakes in those two regions are significant. This is probably because the areas in those ecoregions divide into hydrologic units that are different in drainage sources, and have different susceptibility to the conditions that cause algal growth on the lakes (NRCS-USDA, 2007). At the other ecoregions, we do not reject the null hypothesis for CHLa because their p-values are all greater than the required standard ($\alpha = 0.05$). This means concentrations in those lakes are not significantly different for the period under review. For a Landsat based regional monitoring tool, a representative lake could come from each of those ecoregions for ground-based data.

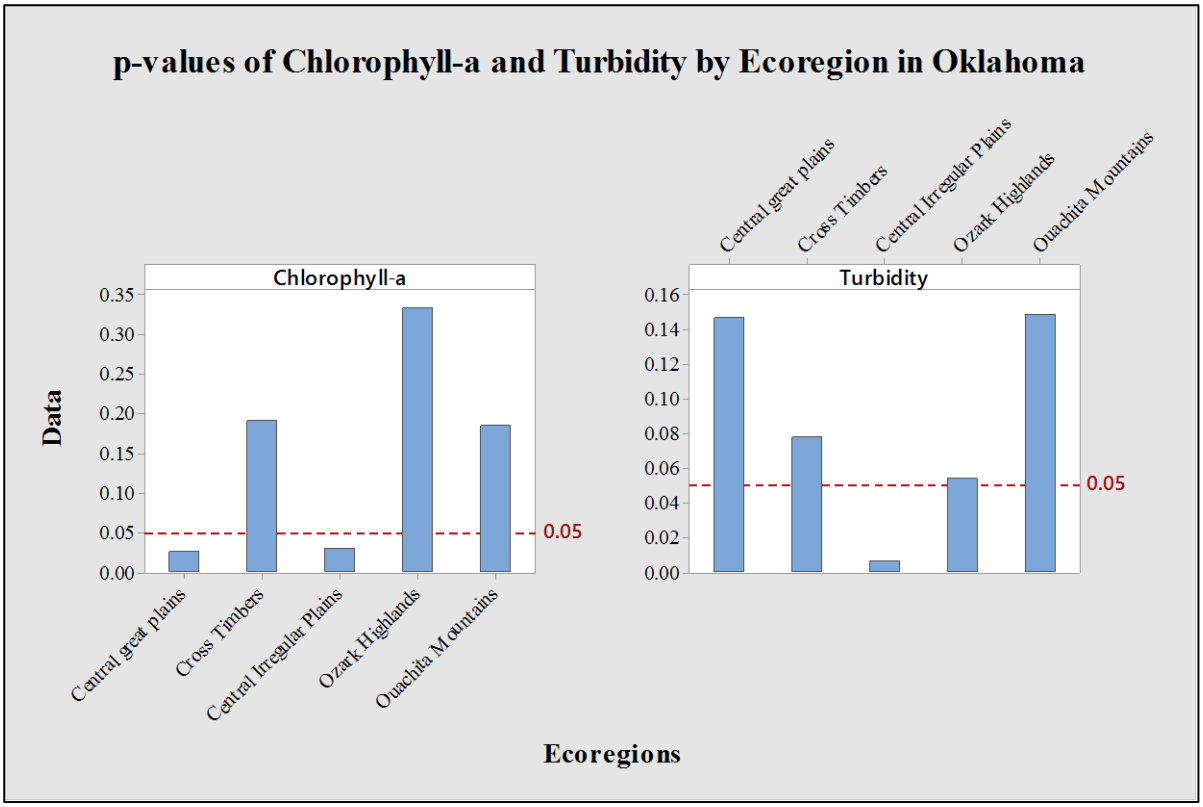

Figure 34. Differences/similarities in water quality between lakes in Oklahoma's ecoregions

In the Central Irregular Plains, both CHLa and turbidity concentrations are different between lakes. This may be because the Chariton, Des Moines, Grand, Missouri, and Thompson Rivers and their tributaries go through an irregular landscape in this region (Karstensen, 2009). These may have led to irregular conditions that cause differences in CHLa and turbidity in the lakes. There is need to further divide the region into hydrologic units, which may help achieve the statistical insignificance in lakes and enhance selection of a representative lake for routine ground-based sampling.

Apart from the Central Irregular Plains, all the ecoregions with two or more lakes have turbidity levels that are not significantly different. We expect this because of the predominant agricultural activities (Patton & Marston, 2009) that cause erosion by wind

and water in Oklahoma (DEQ, 2016)**.** However, a combined ANOVA for turbidity in all 20 lakes showed significant difference between lakes ($\alpha \leq 0.5$).

4.4.2 Water quality by Hydrologic Unit

Table 14 and Figure 34 show p-values that compare average concentrations of parameters within lakes in each hydrologic unit. If the p-value for average concentrations in lakes within one level of a hydrologic unit is significant (i.e. if concentrations of parameters within those lakes are significantly different from each other based on a 95% confidence level), we divide the constituent lakes into a second level hydrologic unit with an area having smaller number of lakes. This continues until we attain a p-value for insignificance in difference between concentrations of parameters in lakes. If a hydrologic unit has an area that have one lake, there is no need for a test of significance.

Table 13. Differences/similarities in water quality between lakes in Oklahoma's HUCs

Hydrologic Unit Code	Lakes	p-value	
		CHLa	Turbidity
1105	Lake McMertury, Lake Hefner, Keystone Lake, Boomer Lake, Lake Carl Blackwell	0.0033*	0.1991
1106	Kaw Lake, Keystone Lake	0.0705	0.1986
1107	Grand Lake O' The Cherokees, Oologah Lake, Lake Eucha, Ft Gibson Lake	0.2069	0.0027
110702	Grand Lake O' The Cherokees, Lake Eucha, Fort Gibson Lake	-	0.0542
1109	Lake Thunderbird, Robert S Kerr Reservoir	0.3223	0.3651
1110	Canton Lake, Robert S Kerr Reservoir	0.5885	0.2283
1111	Robert S Kerr Reservoir, Keystone Lake	0.1679	0.4656
1113	Foss Lake, Waurinka Reservoir, Lake Taxoma	0.0942	0.0213
111303	Foss Lake, Lake Taxoma	-	0.0769
1114	McGee Creek Reservoir, Broken Bow Lake, Hugo Lake	0.0010*	$1.2*10^{-5}$

*Concentrations are significantly different at all HUC levels

The two HUCs where lakes show significantly different water quality are HUC 1105 and HUC 1114. For HUC 1114, dividing lakes into different levels of hydrologic units (4-digit, 6-digit, and even 8-digit HUCs) did not make any difference in statistical

significance for both CHLa and turbidity. This hydrologic unit (HUC 1114) is a forested area with more than one ecoregion. Each lake in this unit have source waters from different river systems. Hence, each of these lakes should be in the representative list for ground-based sampling. A similar situation was observed for CHLa in lakes of hydrologic unit with code 1105. This hydrologic unit lies in both the central Great Plains and the Cross Timbers Ecoregion. Since these two ecoregions have different ecological susceptibilities, we do not expect them to show statistical insignificance.

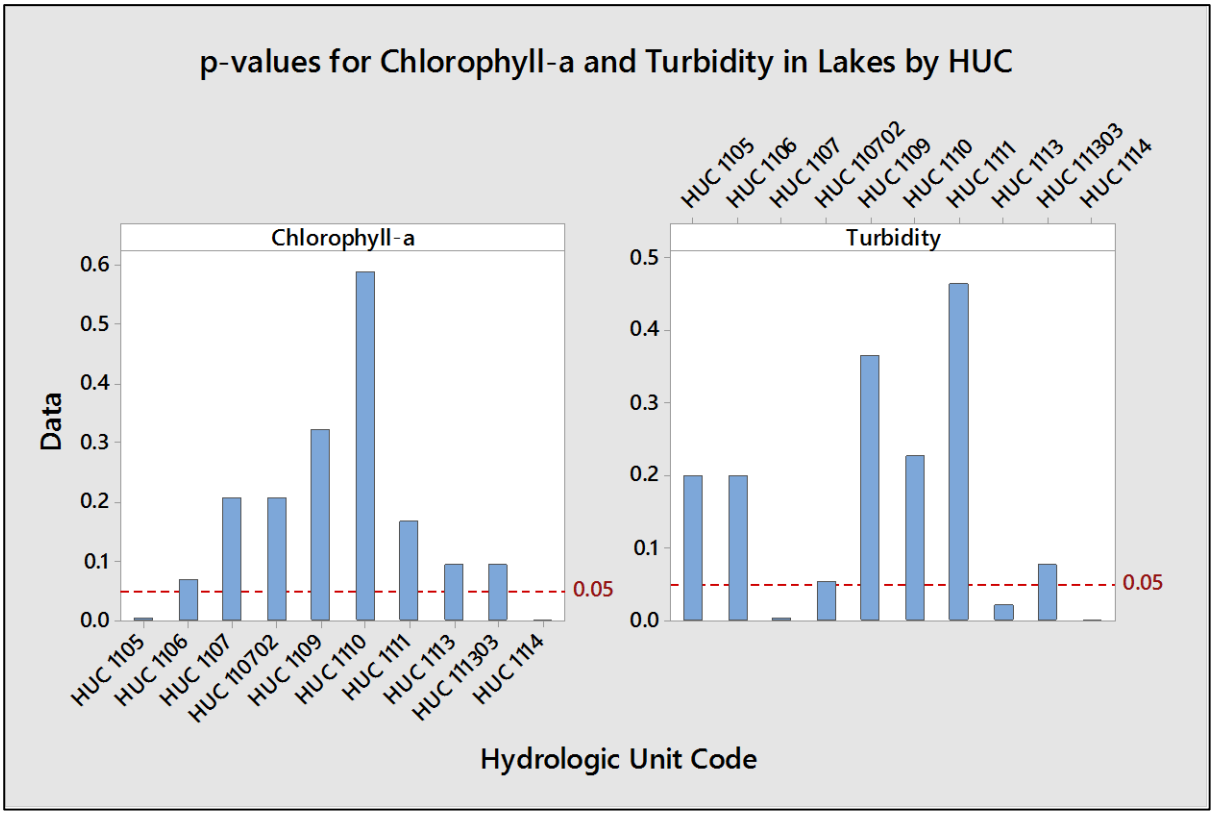

Figure 35. Differences/similarities in water quality between lakes in Oklahoma's HUCs

4.4.3 Landsat 8 fly-over path/rows

Each flyover path and row of Landsat 8 make up an area that coincides with areas having a number of ecoregions and hydrologic units. This makes it possible to have all 20 lakes within at least one path/row of Landsat 8. Therefore, a future Landsat based

automated monitoring at regional level will have satellite data that are spatially coincident and comparable to ground-based water quality data from those lakes.

Table 14 shows four flyover path/rows that spatially coincide with a number of lakes having statistically insignificant differences in concentrations ($\alpha>0.05$) of parameters within those lakes. In path/row 26/35, average CHLa concentrations were statistically insignificant in differences between lakes in the area. Similarly, average concentrations of CHLa and turbidity were statistically insignificant in difference between lakes within path/row 28/35, 28/36, and 29/35. Within those path/rows, the monitoring team could select representative lakes for a sampling routine that is temporally coincident with Landsat schedule. These sets of data could be used for routine calibration of the Landsat based automated monitoring tool for the region. In those path/rows where average concentrations in lakes were significantly different from each other ($\alpha\leq0.5$), the monitoring team could use ecoregions or hydrologic units for further grouping of the lakes by similarity.

Table 14. p-values for path/row combinations

Path	Row	Reservoirs	p-value	
			CHLa	Turbidity
26	35	Grand Lake O' The Cherokees, Lake Eucha; Fort Gibson lake; Oologah Lake; Robert S Kerr Reservoir	0.2753	$2.39*10^{-5}$
26	36	Broken Bow Lake, Hugo Lake; Robert S Kerr Reservoir, McGee Creek Reservoir	0.0010	$4.95*10^{-6}$
27	35	Lake Arcadia, Boomer Lake, Kaw Lake, Keystone Lake, Lake Carl Blackwell, Fort Gibson lake, Lake McMertury, Oologah Lake	0.0016	0.0373
27	36	Lake Arcadia, Lake Thunderbird, Lake Taxoma, McGee Creek Reservoir	0.0207	0.0404
28	35	Lake Arcadia, Boomer Lake, Canton Lake, Kaw Lake, Lake Carl Blackwell, Lake Hefner, Lake McMertury,	0.0673	0.4639
28	36	Lake Thunderbird, Waurika Lake	0.8011	0.2581
29	35	Canton Lake, Foss Reservoir	0.2676	0.1930

4.5 Conclusions

The objective of this study was to determine if representative lakes could be selected based on ecoregions and/or hydrologic units for ground based monitoring in Oklahoma lakes. The goal is to combine this monitoring plan with satellite data and machine learning for an automated monitoring tool for inland water bodies in the state.

Twenty lakes in the OWRB's BUMP were selected for the study. The OWRB provided the turbidity and CHLa data that were used in the analysis. The study used one-factor ANOVA and two-sampled t-test in the study.

For most of the ecoregions, the p-values with an error tolerance limit of 5% ($\alpha \leq 0.05$) showed that a representative lake could be selected per region, except for the Central Great Plains and the Central Irregular Plains. These two regions required further subdivision of lakes by water quality.

For hydrologic units, the p-values showed acceptable representation of a lake per unit. The exceptions were different in HUC 1105 and HUC 1114. Water quality data were statistically different at all sublevels in these HUCs. In these regions, it would be wise to include all the lakes in the representative list of lakes for ground-based sampling.

The study results show that monitoring teams can select representative lakes based on their classification into ecoregions and hydrologic units in Oklahoma. These representative lakes have areas that lie in Landsat flyover path/rows. This makes it possible for combination of ground-based and satellite data for input into an automated monitoring tool for Oklahoma. This tool will increase sampling frequency and expand the spatial extent of lakes covered in OWRB's BUMP for CHLa and turbidity.

CHAPTER V

CONCLUSIONS

The objective of this dissertation was to use Landsat 8 and *in situ* water quality data to develop an automated monitoring tool for HABs detection in the Grand Lake Watershed. The ultimate goal is to have this tool detect HABs in the entire southcentral USA. This need came about because of repeated cases of HABs especially during the summer in Grand Lake O' The Cherokees. The Grand River Dam Authority became concerned over these repeated and erratic HAB events. In 2015, we started monitoring for development of this monitoring tool, which led to this dissertation as an outcome.

This dissertation has five chapters. Chapter 1 introduces the problem, its context, and reviews literature in the subject area. Chapters II, III, and IV are in the form of publishable papers in peer-reviewed journals. Chapter II presents a novel index for photosynthetic algae in the study area. There is also a mineral turbidity index to account for interference from other optically active objects. Chapter III presents a description of an automated monitoring tool developed in this study. The tool downloads processed Landsat images from the USGS Earth Explorer website and extract spectral values for input into the indices. Following this step is an interpretation protocol that determines if PAI is high, medium, or low.

Chapter IV compares lakes by region in Oklahoma in terms of water quality and potential application of the automated monitoring tool at regional level.

This research was limited to activities discussed in the chapters presented. We recommend that further study will complete the development of the automated monitoring tool for the Grand Lake watershed. The following recommendations are opportunities for continuation in improving this tool.

Sampling was limited to one point within a pixel of 900 m^2. It is unclear whether this single point had CHLa concentrations that represented the spatial extent of such pixel. If the situation of mixed pixel is pronounced, relationships between CHLa concentrations and spectral values representing that pixel may be misleading. The recommendation is a future monitoring routine that ensures as many samples within a pixel as possible.

With the Landsat return schedule of 16 days, it becomes challenging to have early detection of HABs when it happens before or after the return period. In this case, ground-based data before or after the flyover schedule may not be useful for input into the automated monitoring tool. Additionally, if cloud cover is high on the day of Landsat flyover the return period becomes even longer. This is particularly challenging because weather conditions are erratic during the summer in Oklahoma. It is recommended that Landsat's European counterpart, Sentinel (2&3) become part of the ground based monitoring protocol. Sentinel has a return period as early as 5 days. This will help increase the number of sample results and make statistical analysis more representative of the reality.

In addition to monitoring frequency, Sentinel has a better spatial resolution with minimum pixel size of 10 m (100 m^2). This will help minimize the problem of mixed pixel and improve validation of results obtained. The existence of image processing protocols that can fuse images of different resolutions makes this recommendation plausible.

This research developed caveats for interpretation of the algal index. The index indicates high, medium, or low based on the following proposed scale: high = 0.5-1, medium = -0.5-0.49 and low is less than -0.5. This determination was based on statistical confidence intervals and literature review; but that may or may not be the case. A future empirical analysis would determine a scale that is based on proven experimental results.

The automated tool is capable of determining the qualitative and spatial extent of HABs in lakes in the study area. However, this tool has not been tested for lakes across the region. This dissertation delineated selection of representative lakes for empirical testing of the software. A future study will consider this as an objective. Additionally, an integration of this software into mapping tools such as ArcGIS and QGIS will make it more powerful.

This research did not involve a social and economic survey of the monitoring tool. The recommendation is for a future social and economic study that will highlight the impact of the tool on the lake management projects, the communities benefiting from such lakes, and the state economy. These will provide the basis for future investment in the tool. A future study that considers the impact of HABs frequency on the value of lakes to amenities is also a good research idea in the future.

REFERENCES

Ahmad, S., Kalra, A., & Stephen, H. (2010). Estimating soil moisture using remote sensing data: A machine learning approach. *Advances in Water Resources, 33*(1), 69-80. doi:10.1016/j.advwatres.2009.10.008

Alikas, K., & Kratzer, S. (2017). Improved retrieval of Secchi depth for optically-complex waters using remote sensing data. *Ecological Indicators, 77*, 218-227. doi:10.1016/j.ecolind.2017.02.007

Allee, R. J., & Johnson, J. E. (1999). Use of satellite imagery to estimate surface chlorophyll-a and Secchi disc depth of Bull Shoals Reservoir, Arkansas, USA. *International Journal of Remote Sensing, 20*(6), 1057-1072. doi:10.1080/014311699212849

Allee, R. J., & Johnson, J. E. (1999). Use of satellite imagery to estimate surface chlorophyll-a and Secchi disc depth of Bull Shoals Reservoir, Arkansas, USA. *International Journal of Remote Sensing, 20*(6), 1057-1072. doi:10.1080/014311699212849

Alpaydın, E. (2010). *Introduction to machine learning* (2nd ed.). Cambridge, Massachusetts: The MIT Press.

Bachmann, R., Hoyer, M., Croteau, A., & Canfield Jr., D. (2017). Factors related to Secchi depths and their stability over time as determined from a probability sample of US lakes. *Environmental Monitoring and Assessment*. doi:https://doi.org/10.1007/s10661-017- 5911-9

Barnes, B. B., Blonski, S., Hua, C., Holekamp, K. L., & Spiering, B. A. (2014). Use of Landsat data to track historical water quality changes in Florida Keys marine environments. *Remote Sensing of Environment, 140*, 485-496. doi:10.1016/j.rse.2013.09.020

Barnes, B. B., Hua, C., Holekamp, K. L., Blonski, S., & Spiering, B. A. (2014). Use of Landsat data to track historical water quality changes in Florida Keys marine environments. *Remote Sensing of Environment, 140*, 485-496. doi:10.1016/j.rse.2013.09.020

Barrett, C. D., & Frazier, A. E. (2016). Automated method for monitoring water quality using Landsat imagery. *Water, 8*(6), 257. doi:10.3390/w8060257

Birth, G. S., & McVey, G. R. (1968). Measuring the color of growing turf with a reflectance spectrophotometer. *American Society of Agronomy, 60*(6), 640-643. doi:10.2134/agronj1968.00021962006000060016x

Bormans, M., Maršálek, B., & Jančula, D. (2016). Controlling internal phosphorus loading in lakes by physical methods to reduce cyanobacterial blooms: a review. *Aquatic Ecology, 50*(3), 407-422. doi:10.1007/s10452-015-9564-x

Boyer, T., Daniels, B., & Melstrom, R. (2017, March). Algal Blooms in Oklahoma: Economic Impacts. *Oklahoma Cooperative Extension Fact Sheets*. Retrieved from http://factsheets.okstate.edu/documents/agec-1063-algal-blooms-in-oklahoma-economic-impacts/

Brassel, K., & Weibel, R. (2007). A review and conceptual framework of automated map generalization. *International Journal of Geographical Information Systems, 2*(3), 229-244. doi:10.1080/02693798808927898

Brooks, B. W., Lazorchak, J. M., Howard, M. D., Johnson, M.-V. V., Morton, S. L., Perkins, D. A., . . . Steevens, J. A. (2016). Are harmful algal blooms becoming the greatest inland water quality threat to public health and aquatic ecosystems? *Environmental Toxicology nad Chemistry, 35*(1), 6-13. doi:10.1002/etc.3220

Campbell, J. (2015). *Free data proves its worth for Observing Earth.* Department of the Interior, U.S. Geological Survey, Office of Communications and Publishing. Reston, VA: Department of the Interior, U.S. Geological Survey. Retrieved from https://www.usgs.gov/news/free-data-proves-its-worth-observing-earth

Campbell, J. B., & Wynne, R. H. (2011). *Introduction to Remote Sensing* (5th ed.). New York, USA: The Guilford Press.

Carpenter, D. J., & Carpenter, S. M. (1983). Modeling Inland Water Quality using Landsat Data. *Remote Sensing of Environment, 13*, 345-352. doi:10.1016/0034-4257(83)90035-4

Chen, M., Schliep, M., Willows, R., Cai, Z.-L., Neilan, B., & Scheer, H. (2010, August 23). A Red-Shifted Chlorophyll. *Science, 329*(5997), 1318-1319. doi:10.1126/science.1191127

Choodarathnakara, A. L., Kumar, T. A., Koliwad, S., & Patil, C. G. (2012). Mixed Pixels: a challenge in remote sensing data classification for improving performance. *International Journal of Advanced Research in Computer Engineering & Technology, 1*(9), 261-271. Retrieved from https://pdfs.semanticscholar.org/63b9/7ce83281e012da96d7be39d84a1739fae67c.pdf

Cord, A., Brauman, K., Chaplin-Kramer, R., Huth, A., Ziv, G., & Seppelt, R. (2017). Priorities to advance monitoring of ecosystem services using earth observation. *Trends in Ecology and Evolution, 32*(6), 416-428. doi:10.1016/j.tree.2017.03.003

Cracknell, M., & Reading, A. (2014). Geological mapping using remote sensing data: A comparison of five machine learning algorithms, their response to variations in the spatial distribution of training data and the use of explicit spatial information. *Computers & Geosciences, 63*, 22-33. doi:10.1016/j.cageo.2013.10.008

Cunningham, K., Little, J., & Montgomery, M. (2013). Satellite eemote sensing & carbon market transparency. *Advances in Forestry Letters, 2*(3), 43-47. Retrieved from https://www.snap.uaf.edu/sites/default/files/files/Satellite%20Remote%20Sensing%20and%20Carbon%20Market%20Transparency.pdf

DEQ. (2016). *Water quality in Oklahoma - 2016 integrated report.* Oklahoma Department of Environmental Quality. Retrieved from Natural Resources Conservaion Service Oklahoma: http://www.deq.state.ok.us/WQDnew/305b_303d/index.html

Deutsch, E., Alameddine, I., & El-Fadel, M. (2014). Developing Landsat based Algorithms to Augment in situ Monitoring of Freshwater Lakes and Reservoirs. *International Conference on Hydroinformatics.* New York: City University of New York. Retrieved July 24, 2016, from http://academicworks.cuny.edu/cc_conf_hic/425

Dormann, C. F., Elith, J., Bacher, S., Buchmann, C., Carl, G., Carré, G., . . . Lautenbach, S. (2013). Collinearity: a review of methods to deal with it and a simulation study evaluating their performance. *Ecography, 36*, 027–046. doi:10.1111/j.1600-0587.2012.07348.x

Downing, D. M. (2011). Scope of "The Watres of the United States" protected by the Clean Water Act. In M. A. Ryan (Ed.), *The Clean Water Act Handbook* (3rd ed., pp. 11-25). Chicago, Illinois, USA: American Bar Association.

EXO. (2017). *EXO user manual.* Retrieved from https://www.ysi.com/File%20Library/Documents/Manuals/EXO-User-Manual-Web.pdf

Filstrup, C., & Downing, J. (2017). Relationship of chlorophyll to phosphorus and nitrogen in nutrient-rich lakes. *Inland Waters, 7*(4), 385-400. doi:10.1080/20442041.2017.1375176

Findlay, S., Pace, M., Lints, D., & Howe, K. (1992). Bacterial metabolism of organic carbon in the tidal freshwater Hudson Estuary. *Marine Ecology Progress Series, 89*(2-3), 147-153. doi:10.3354/meps089147

Frost, J. (2013, May 30). Regression Analysis: How Do I Interpret R-squared and Assess the Goodness-of-Fit? *The Minitab blog*. Retrieved from http://blog.minitab.com/blog/adventures-in-statistics-2/regression-analysis-how-do-i-interpret-r-squared-and-assess-the-goodness-of-fit

Ghimire, M., Boyer, T., Shideler, D., Melstrom, M., & Stoecker, A. (2017). *Estimating lake amenity values on Grand Lake o' the Cherokees* . Grand River Dam Authority and Department of Agricultural Economics, Oklahoma State University.

Gilbert, P. M., & Burford, M. A. (2017). Globally changing nutrient loads and harmful algal blooms: recent advances, new paradigms, and continuing challenges. *Oceanography, 30*(1), 58–69. doi:10.5670/oceanog.2017.110

Han, L., & Rundquist, D. C. (1997). Comparison of NIR/RED ratio and first derivative of reflectance in estimating algal-chlorophyll concentration: A case study in a turbid reservoir. *Remote Sensing of Environment, 62*(3), 253-261. doi:10.1016/S0034-4257(97)00106-5

Harvey, E. T., Kratzer, S., & Anderson, A. (2015). Relationships between colored dissolved organic matter and dissolved organic carbon in different coastal gradients of the Baltic Sea. *Ambio, 44*, 392–401. doi: 10.1007/s13280-015-0658-4

Harvey, E., Kratzer, S., & Philipson, P. (2015). Satellite-based water quality monitoring for improved spatial and temporal retrieval of chlorophyll-a in coastal waters. *Remote Sensing of Environment, 158*, 417-430. doi:10.1016/j.rse.2014.11.017

Hellegers, P., Soppe, R., Perry, C., & Bastiaanssen, W. (2010). Remote sensing and economic indicators for supporting water resources management decisions. *Water Resource Management, 24*(11), 2419–2436. doi:10.1007/s11269-009-9559-2

Holt, D., Corbridge, J., Crowl, L., Gillette, J., Gustavson, K., Grasso, S., . . . Younger, C. (2008). *Grand Lake Watershed Plan.* Grove, Oklahoa: Grand Lake O' the Cherokees Watershed Alliance Foundation, Inc. .

Howarth, R., Marino, R., Lane, J., & Cole, J. (1988). Nitrogen fixation in freshwater, estuarine, and marine ecosystems. Rates and importance. *Limnology and Oceanography, 33*(4, part 2), 669-687. doi:10.4319/lo.1988.33.4part2.0669

Huang, X., & Jensen, J. (1997). A machine-learning approach to automated knowledge-base building for remote sensing image analysis with GIS data. *Photogrammetric Engineering & Remote Sensin, 63*(10), 1185-1194.

Istvánovics, V. (2013). Eutrophication of Lakes and Reservoirs. *Reference Module in Earth Systems and Environmental Sciences*, 157–165. doi:10.1016/B978-012370626-3.00141-1

Jensen, J. R. (2015). *Introductory digital image processing - a remote sensing perspective* (4th ed.). (C. Botting, Ed.) Columbia. SC: Pearson Education Inc. Retrieved February 20, 2017

Johnson, K. S., & Luza, K. V. (2008). *Rivers, streams, and lakes of Oklahoma.* Oklahoma Geological Survey. Oklahoma Geological Survey. Retrieved April 12, 2016, from http://www.ogs.ou.edu/pubsscanned/EP9p12_14water.pdf

Johnson, K., & Luza, K. (2008). *Rivers, streams, and lakes of Oklahoma.* Oklahoma Geological Survey. Retrieved from http://www.ogs.ou.edu/pubsscanned/EP9p12_14water.pdf

Jones, H. G., & Sirault, X. R. (2014). Scaling of thermal images at different spatial resolution: the mixed pixel problem. *Agronomy*, *4*(3), 380-396. doi:10.3390/agronomy4030380

Kallio, K., Attila, J., Härmä, P., Koponen, S., Pulliainen, J., Hyytiäinen, U., & Pyhälahti, T. (2008). Landsat ETM+ images in the estimation of seasonal lake water quality in Boreal River basins. *Environmental Management, 42*(3), 511-522. doi:10.1007/s00267-008-9146-y

Karpatne, A., Khandelwal, A., Chen, X., Mithal, V., Faghmous, J., & Kumar, V. (2016). Global monitoring of inland water dynamics: state-of-the-art, challenges, and opportunities. *Computational Sustainability, 645*, 121-147. doi:10.1007/978-3-319-31858-5_7

Karssenberg, D., de Jong, K., & van der Kwast, J. (2007). Modelling landscape dynamics with Python. *International Journal of Geographical Information Science, 21*(5), 483-495. doi:10.1080/13658810601063936

Karstensen, K. (2009). *Land-Cover Change in the Central Irregular Plains, 1973–2000* . Unted States Geological Surveys. doi:https://landcovertrends.usgs.gov/gp/eco40Report.html

Kim, S. (2017, April 24). How to calculate circular error of probability. *SCIENCING*. Retrieved from https://sciencing.com/calculate-circular-error-probability-8701777.html

Kirk, J. T. (2011). *Light and photosynthesis in aquatic ecosystems* (3rd ed.). New york: Cambridge University Press.

LakeHub LLC. (2018). *Grand Lake OK Information*. Retrieved from Grand Lake OK : http://www.grandlake.com/information

Lary, D., Alavi, A., Gandomi, A., & Walker, A. (2016). Machine learning in geosciences and remote sensing. *Geoscience Frontiers, 7*, 3-10. doi:10.1016/j.gsf.2015.07.003

Machmuller, M., Kramer, M., Cyle, T., Hill, N., Hancock, D., & Thompson, A. (2015). Emerging land use practices rapidly increase soil organic matter. *Nature Communications*. doi:10.1038/ncomms7995

McCullough, I. M., Loftin, C. S., & Sader, S. A. (2012). Combining lake and watershed characteristics with Landsat TM data for remote estimation of regional lake clarity. *Remote Sensing of Environment, 123*, 109-115. doi:10.1016/j.rse.2012.03.006

McCullough, I. M., Loftin, C. S., & Sader, S. S. (2012). Combining lake and watershed characteristics with Landsat TM data for remote estimation of regional lake clarity. *Remote Sensing of Environment, 123*, 109–115. doi:10.1016/j.rse.2012.03.006

Melgani, F., & Bruzzone, L. (2004). Classification of hyperspectral remote sensing images with support vector machines. *IEEE Transactions on Geoscience and Remote Sensing, 42*(8), 1778-1790. doi: 10.1109/TGRS.2004.831865

Mishra, S., & Mishra, D. (2012). Normalized difference chlorophyll index: A novel model for remote estimation of chlorophyll-a concentration in turbid productive waters. *Remote Sensing of Environment, 117*, 394–406. doi:10.1016/j.rse.2011.10.016

Mosley, L. (2015). Drought impacts on the water quality of freshwater systems; review and integration. *Earth Science Reviews, 140*, 203-214. doi:10.1016/j.earscirev.2014.11.010

NRCS-USDA. (2007, June 18). *Watersheds, Hydrologic Units, Hydrologic Unit Codes, Watershed Approach, and Rapid Watershed Assessments.* Retrieved May 8, 2018, from https://www.nrcs.usda.gov/Internet/FSE_DOCUMENTS/stelprdb1042207.pdf

OCC. (2014). *Oklahoma's nonpoint source management program plan 2014-2018.* Water Quality Programs. Oklahoma City: Oklahoma Conservation Commission. Retrieved from https://www.ok.gov/conservation/documents/2014%20NPS%20Mgmt%20Plan.pdf

Oliphant, T. (2007). *Python for ccientific computing.* IEEE CS and the AIP. Retrieved from https://pdfs.semanticscholar.org/35ce/eedd93e2b42f5e2412b1f6e88dd6d5d4679d.pdf

Olmanson, L. G., Brezonik, P. L., Finlay, J. C., & Bauer, M. E. (2016). Comparison of Landsat 8 and Landsat 7 for regional measurements of CDOM and water clarity in lakes. *Remote Sensing of Environment*. doi:10.1016/j.rse.2016.01.007

Orban, V. (2015). Space economy trends in the United States and Europe. *Space Safety Magazine*. Retrieved from http://www.spacesafetymagazine.com/space-on-earth/space-economy/space-economy-trends-in-the-united-states-and-europe/

OWRB. (2001). *Standard operating peocedures (SOP) for field sampling efforts of the Oklahoma Water Resources Board's Beneficial Use Monitoring Program (BUMP).* Water Quality Programs Division. Oklahoma City: Oklahoma Water Resources Board. Retrieved from https://www.owrb.ok.gov/studies/reports/reports_pdf/bump_sopfy01.pdf

OWRB. (2013). *Standard operating procedures for the collection of chlorophyll-a samples in lakes.* Oklahoma City: Oklahoma Water Resoources Board. Retrieved from http://www.owrb.ok.gov/quality/monitoring/bump/pdf_bump/Lakes/SOPs/Collection_of_Water_Quality_Samples.pdf

OWRB. (2017). *Oklahoma Lakes report - Benificial Use Monitoring Program.* Oklahoma City: Oklahoma Water Resource Board (OWRB).

OWRB. (2018, May 17). *Monitoring and Assessment*. (Oklahoma Water Resources Board) Retrieved from http://www.owrb.ok.gov/quality/monitoring/monitoring.php

OWRB. (2018, March 14). *Water Facts*. Retrieved from The Oklahoma Water Resources Board: https://www.owrb.ok.gov/util/waterfact.php

Paerl, H., Gardner, W., Havens, K., Joyner, A., McCarthy, M., Newell, S., . . . ThadScott, J. (2016). Mitigating cyanobacterial harmful algal blooms in aquatic ecosystems impacted by climate change and anthropogenic nutrients. *Harmful Algae, 54,* 213-222. doi:10.1016/j.hal.2015.09.009

Patton, J., & Marston, R. (2009). *Great Plains, The Encyclopedia of Oklahoma History and Culture.* Oklahoma Historical Society. Retrieved from http://www.okhistory.org/publications/enc/entry.php?entry=GR015

Pettersson, K. (19989). Mechanisms for internal loading of phosphorus in lakes. *Hydrobiologia, 373*(0), 21-25. doi:10.1023/A:1017011420035

Pettorelli, N., Laurance, W. F., O'Brien, T. G., Wegmann, M., Nagendra, H., & Turner, W. (2014). Satellite remote sensing for applied ecologists: opportunities and challenges. *Applied Ecology, 51*, 839–848. doi:10.1111/1365-2664.12261

Piñeiro, G., Perelman, S., Juan P. Guerschman, J., & Paruelo, J. (2008). How to evaluate models: Observed vs. predicted or predicted vs. observed? *Ecological Modeling, 216*(3-4), 316-322. doi:10.1016/j.ecolmodel.2008.05.006

Raunikar, R. P., Forney, W. M., & Benjamin, S. P. (2013). What is the Economic Value of Satellite Imagery? *usgs Fact Sheet 2013–3003*.

Roberts, D., Boyer, T., & Lusk, J. (2008). Preferences for environmental quality under uncertainty. *Ecological Economics, 66*, 584-593. doi:10.1016/j.ecolecon.2008.05.010

Rodríguez, J., Beard Jr., T., Bennett, E., Cumming, G., Cork, S., Agard, J., . . . Peterson, G. (2006). Trade-offs across space, time, and ecosystem services. *Ecology and Society, 11*(1). Retrieved from http://www.jstor.org/stable/26267786

Rouse, J., Haas, R., Schell, J., & Deering, D. (1973). Monitoring vegetation systems in the Great Plains with ERTS. *Earth Resources Technology Satellite-1 Symposium. 3*, pp. 309–317. Goddard Space Flight Center Washington DC: NASA.

Ruddick, K. G., Gons, H. J., Rijkeboer, M., & Tilstone, G. (2001). Optical remote sensing of chlorophyll a in case 2 waters by use of an adaptive two-band algorithm with optimal error properties. *APPLIED OPTICS, 40*(21), 3575-3585. Retrieved from https://www.osapublishing.org/ao/abstract.cfm?uri=AO-40-21-3575

Sano, E. E., Ferreira, L. G., Asner, G. P., & Steinke, E. T. (2007). Spatial and temporal probabilities of obtaining cloud-free Landsat images over the Brazilian tropical savanna. *International Journal of Remote Sensing, 28*(12), 2739-2752. doi:10.1080/01431160600981517

Schaeffer, B. A., Schaeffer, K. G., Keith, D., Lunetta, R. S., Conmy, R., & Gould, R. W. (2013). Barriers to adopting satellite remote sensing for water quality management. *International Journal of Remote Sensing, 34*(21), 7534-7544. doi:10.1080/01431161.2013.823524

Sharpley, A. (2016). Managing agricultural phosphorus to minimize water quality impacts. *Scientia Agricola, 73*(1), 1-8. doi:10.1590/0103-9016-2015-0107

Shi, T., Chen, Y., Liu, Y., & Wu, G. (2014). Visible and near-infrared reflectance spectroscopy—An alternative for monitoring soil contamination by heavy metals. *Harzadous Materials, 265*, 166–176. doi:10.1016/j.jhazmat.2013.11.059

Tamburic, B., Szabó, M., Tran, N.-A., Larkum, A., Suggett, D., & Ralph, P. (2014). Action spectra of oxygen production and chlorophyll a fluorescence in the green microalga Nannochloropsis oculata. *Bioresource Technology, 169*, 320-327. doi:10.1016/j.biortech.2014.07.008

Tebbs, E. J., Harper, D. M., & Remedios, J. J. (2013). Remote sensing of chlorophyll-a as a measure of cyanobacterial biomass in Lake Bogoria, a hypertrophic, saline–alkaline, flamingo lake, using Landsat ETM +. *Remote Sensing of Environment, 135*, 92–106. doi:10.1016/j.rse.2013.03.024

Thenkabail, P. S., Mariotto, I., Gumma, M. K., Middleton, l. M., Landis, D. R., & Huemmrich, K. F. (2013). Selection of hyperspectral narrow bands (HNBs) and composition of hyperspectral two-band vegetation indices (HVIs) for biophysical characterization and discrimination of crop types using field... *IEEE Journal od Selecte Topics in Applied Earth Observations and Remote Sensing, 6*(2). doi:10.1109/JSTARS.2013.2252601

Theologou, I., Patelaki, M., & Karantzalos, K. (2015). Can single emperical algorithms accurately predict inland shallow water quality status from high resolution, multi-sensor, multi-temporal satellite data? *36th International Symposium on Remote Sensing of Environment. XL-7/W3*, pp. 1511-1516. Berlin: The International Archives of the Photogrammetry, Remote Sensing and Spatial Information Sciences. doi:10.5194/isprsarchives-XL-7-W3-1511-2015

Thu Ha, N. T., Koike, K., Nhuan, M. T., Parsons, M., & Thao, N. T. (2017). Landsat 8/OLI Two Bands Ratio Algorithm for Chlorophyll-A Concentration Mapping in Hypertrophic Waters: An Application to West Lake in Hanoi (Vietnam). *IEEE Journal of Selected Topics in Applied Earth Oservations and Remote Sensing, 10*(11), 4919-4929. doi:10.1109/JSTARS.2017.2739184

Torbick, N., Hessionb, S., Hagena, S., Wiangwangb, N., Beckerc, B., & Qib, J. (2013). Mapping inland lake water quality across the Lower Peninsula of Michigan using Landsat TM imagery. *International Journal of Remote Sensing*, *34*(21), 7607–7624. doi: 10.1080/01431161.2013.822602

Torbick, N., Hu, F., Zhang, J., Qi, J., Zhang, H., & Becker, B. (2008). Mapping Chlorophyll-a Concentrations in West Lake, China using Landsat 7 ETM+. *Great Lakes Research, 34*(3), 559-565. doi:http://dx.doi.org/10.3394/0380-1330(2008)34[559:MCCIWL]2.0.CO;2

Turner Designs. (2016). *Trilogy Laboratory Fluorometer - User's manual.* Retrieved from http://www.turnerdesigns.com/t2/doc/manuals/998-7210.pdf

U.S. Army Corps of Engineers. (2011). *Council Grove Lake.* Retrieved from U.S. Army Corps of Engineers: http://www.swt.usace.army.mil/Portals/41/docs/missions/recreation/hunting/kansas/cg_hunt2011.pdf

Urquhart, N., Paulsen, S., & Larsen, D. (1998). Monitoring for policy-relevant regional trends over time. *Ecological Applications*. Retrieved from https://doi.org/10.1890/1051-0761(1998)008[0246:MFPRRO]2.0.CO;2

US Army Corps of Engineers. (2018). *Pertinent Data*. Retrieved from Marion Reservoir Links: http://www.swt.usace.army.mil/Locations/Tulsa-District-Lakes/Kansas/Marion-Reservoir/Pertinent-Data/

US Army corpse of Engineers. (2018). *John Redmond Lake - Cuurrent Readings.* Tulsa District Water Control. Retrieved from http://www.swt-wc.usace.army.mil/JOHN.lakepage.html

USEPA. (2010). *Sampling and consideration of variability (temporal and spatial) for monitoring of recreational waters.* Office of Water. U.S. Environmental Protection Agency. Retrieved from

https://www.epa.gov/sites/production/files/2015-11/documents/sampling-consideration-recreational-waters.pdf

USEPA. (2014). *Sampling and analysis plan guidance and template.* Methods. Retrieved from https://www.epa.gov/sites/production/files/2015-06/documents/sap-general.pdf

USEPA. (2017, January 19). *Ecoregion Download Files by State - Region 6*. (United States Environmenal Protection Agency) Retrieved from https://www.epa.gov/eco-research/ecoregion-download-files-state-region-6

USGS. (2015, December 1). *Landsat Missions*. Retrieved from Science for a changing world: http://landsat.usgs.gov

USGS. (2016). *Nitrogen in Lakes Connected to Groundwater.* United States Geological Survey. doi:https://www.usgs.gov/news/nitrogen-lakes-connected-groundwater

USGS. (2016, November 29). *What is the World Reference System?* Retrieved April 12, 2017, from USGS - Landsat Missions: https://landsat.usgs.gov/what-worldwide-reference-system-wrs

USGS. (2017). *Landsat data gap studies.* US Department of Interior, USGS. The USGS Remote Sensing Technologies Project. Retrieved from https://calval.cr.usgs.gov/LDGST.php

USGS. (2018, January 12). *EarthExplorer*. Retrieved from EarthExplorer: https://earthexplorer.usgs.gov/

Vanhellemont, Q., & Ruddick, K. (2015). Advantages of high quality SWIR bands for ocean colour processing: Examples from Landsat-8. *Remote Sensing of Environment, 161*, 89-106. doi:10.1016/j.rse.2015.02.007

Wang, M., & Shi, W. (2006). Cloud masking for ocean color data processing in the coastal regions . *IEEE: Transactions on Geoscience and Remote Sensing, 11*, 44.

Watkins, T. (1978). The economics of remote sensing. *Symposium on Remote Sensing for Vegetation Damage Assessment* (pp. 1167-1172). Seattle: Photogrammetric Engineering and Remote Sensing. Retrieved from https://www.asprs.org/wp-content/uploads/pers/1978journal/sep/1978_sep_1167-1172.pdf

Weber, R., & O'Connell, K. (2011). *Alternative futures: United States commercial satellite imagery in 2020.* Washington, DC: Innovative Analytics and Training, LLC. Retrieved from https://nsarchive2.gwu.edu/NSAEBB/NSAEBB404/docs/37.pdf

Wichmann, M. (2017, September 5). *The Python Wiki.* Retrieved from https://wiki.python.org/moin/FrontPage

Yacobi, Y. Z., Giltelson, A., & Mayo, M. (1995). Remote sensing of chlorophyll in Lake Kinneret using highspectral-resolution radiometer and Landsat TM: spectral features of reflectance and algorithm development. *P1ankton Research, 17*(11), 2155-2173. Retrieved from http://digitalcommons.unl.edu/natrespapers/288

Yong Hoon, K., Ho Kyung, H., Jong-Kuk, C., Jungho, I., & Sunghyun, H. (2014). Machine learning approaches to coastal water quality monitoring using GOCI satellite data. *GIScience & Remote Sensing, 51*(2), 158-174. doi:10.1080/15481603.2014.900983

Zorogastúa C, P., Quiroz, R., Potts, M., & Schulz, S. (2014, January 7). *Agricultural statistics of roots and tubers.* Retrieved from Slide Share: https://www.slideshare.net/CIMMYT/b-5-rt-taller14mx

APPENDICES

Appendix I. Coefficient of determination of studies found in the literature

Author and year	Study	Result of model
Allee and Johnson (1999)	Estimated surface CHLa and SD of Bull Shoals Reservoir in Arkansas, USA	Models for CHLa from July 1994 ($R^2 = 0.80$) and December 1994 ($R^2 = 0.84$) data and for SD ($R^2 = 0.96$)
Carpenter and Carpenter (1983)	Built multiple linear predictors for turbidity and chlorophyll pigment in freshwaters in southeastern Australia	R^2 in the range 0.59-0.95 for turbidity and 0.50-0.85 for chlorophyll pigment
Deutsch et al (2014)	Landsat 7 and Landsat 8 compared for CHLa	Better predictive tendencies of Landsat 8 ($R^2 = 0.70$) than either Landsat 7 ($R^2 = 0.11$) or Landsat 7+8 ($R^2 = 0.46$).
Han and Rundquist (1997)	Ratio of NIR to Red region in relatively turbid Midwestern reservoirs in the US	only on one occasion did they find the NIR/Red ratio to be a good predictor of chlorophyll content
Olmanson et al (2016)	Compared sensors on Landsat 7 ETM+ and Landsat 8 OLI to for SD in Minnesota	Best water clarity model for Landsat 8 used the OLI 2/4 band ratio plus OLI band 1 ($R^2 = 0.82$)
Tebbs et al (2013)	NIR/Red ratio for CHLa as indicator for cyanobacterial biomass.	R^2 as high as 0.85 against high CHLa. Strong R^2 (0.81) for the band ratio. Strong predictive tendency with TOA reflectance ($R^2 = 0.80$)
Torbick et al (2008)	Combinations of Landsat 7 ETM+1 and ETM+3 to develop equations for CHLa in West Lake, China	For single bands, ETM+3 was a better predictor ($R^2 = 0.78$) compared to ETM+1 ($R^2 = 0.45$). A ratio of ETM+3/ETM+1 gave the best predictive equation ($R^2 = 0.81$).
Torbick et al (2013)	Mapping inland lake water quality across the Lower Peninsula of Michigan	For SD, R^2 values for the routines = 0.56 for DN, 0.77 for LEDAPS, 0.58 for DOS, 0.82 for subsurface volumetric modeling, and 0.81 for radiance.
Yacobi et al (1995)	Estimating the concentration of chlorophyll using Landsat data	The correlation between predicted and measured sets was $R^2 = 0.96$

Deliberately left blank. Please go to next page

Appendix II. Landsat overpass schedules

	Sampling dates with coincidental satellite over passes in 2016																													
	1	2	3	4	5	6	7	8	9	10	11	12	13	14	15	16	17	18	19	20	21	22	23	24	25	26	27	28	29	30	31
M																															
J																															
J																															
A																															
S																															
O																															
N																															
D																															
	Sampling dates with coincidental satellite over passes in 2017																														
J																															
F																															
M																															
A																															
M																															
J																															
J																															
A																															
S																															
O																															
N																															
D																															

Grand Lake (Path/Row: 26/35). Council Grove and John Redmond Reservoirs (Path/Row: 27/33). Marion Reservoir (Path/Row: 28/33).

	1	2	3	4	5	6	7	8	9	10	11	12	13	14	15	16	17	18	19	20	21	22	23	24	25	26	27	28	29	30	31
M													S	S								M							M	T	
J							W							W	R									F						F	
J	S								S							S	M								T						
A	T	W								R							R	F								S					
S		S	S								M							M	R								W				
O				W	R								F							F	S							S		
N					S	M								T							T	W							R	

D							R	F								S							S	S							

Marion Lake: Path/Row A: 124/211; Path/Row B: 28/33. Council Grove Lake: Path/Row C: 27/33; Path/Row A: 124/211; Path/Row B: 28/33.

Appendix III: *In situ* concentrations at Grand Lake

Site Name	Lat.	Long.	Date	CHLa-RFU (OSU Probe)	CHLa- µg/L (OSU Probe)	Secchi Disk (m)	CHLa-µg/L (GRDA Probe)	CHLa-RFU (GRDA Probe)
Dream	36.50879	-94.9559	2014-07-25				-0.6	-0.2
Drip	36.49967	-94.95615	2014-07-25				-0.6	-0.2
Drown	36.49768	-94.91853	2014-07-25				-0.6	-0.2
Duck	36.53628	-94.97203	2014-07-25				-0.6	-0.2
Elk	36.64998	-94.70839	2014-07-25					
Grand	36.68269	-94.77281	2014-07-25					
Honey	36.57511	-94.78775	2014-07-25				-0.6	-0.2
Horse	36.62247	-94.9092	2014-07-25				-0.6	-0.2
P Dam	36.49254	-95.0448	2014-07-25				6.6	2.1
Sail	36.64176	-94.81493	2014-07-25				8.5	2.8
Shang	36.55447	-94.8449	2014-07-25					
Tree	36.56396	-94.91276	2014-07-25				-0.6	-0.2
Wood	36.53666	-94.82251	2014-07-25				-0.6	-0.2
Dream	36.50879	-94.9559	2014-08-26				4.6	1.5
Drip	36.49967	-94.95615	2014-08-26				-0.1	0
Drown	36.49768	-94.91853	2014-08-26				-0.1	0
Duck	36.53628	-94.97203	2014-08-26				-0.1	0
Elk	36.64998	-94.70839	2014-08-26				-0.1	0
Grand	36.68269	-94.77281	2014-08-26				-0.1	0
Honey	36.57511	-94.78775	2014-08-26				-0.1	0
Horse	36.62247	-94.9092	2014-08-26				-0.1	0
P Dam	36.49254	-95.0448	2014-08-26				3.4	1.1

Site Name	Lat.	Long.	Date	CHLa-RFU (OSU Probe)	CHLa- µg/L (OSU Probe)	Secchi Disk (m)	CHLa-µg/L (GRDA Probe)	CHLa-RFU (GRDA Probe)
Sail	36.64176	-94.81493	2014-08-26				-0.1	0
Shang	36.55447	-94.8449	2014-08-26				-0.1	0
Tree	36.56396	-94.91276	2014-08-26				-0.1	0
Wood	36.53666	-94.82251	2014-08-26				-0.1	0
Dream	36.50879	-94.9559	2014-10-15				1.5	0.5
Drip	36.49967	-94.95615	2014-10-15				1.3	0.4
Drown	36.49768	-94.91853	2014-10-15				2.1	0.7
Duck	36.53628	-94.97203	2014-10-15				-0.2	-0.1
Elk	36.64998	-94.70839	2014-10-15				-	-
Grand	36.68269	-94.77281	2014-10-15				6	2
Honey	36.57511	-94.78775	2014-10-15				1.4	0.5
Horse	36.62247	-94.9092	2014-10-15				-0.2	-0.1
P Dam	36.49254	-95.0448	2014-10-15				1	0.3
Sail	36.64176	-94.81493	2014-10-15				-0.2	-0.1
Shang	36.55447	-94.8449	2014-10-15				2.6	0.9
Tree	36.56396	-94.91276	2014-10-15				-0.2	-0.1
Wood	36.53666	-94.82251	2014-10-15				-0.2	-0.1
Dream	36.50879	-94.9559	2015-06-11				46.4	6.5
Drip	36.49967	-94.95615	2015-06-11				34.7	4.4
Drown	36.49768	-94.91853	2015-06-11				51.8	7.4
Duck	36.53628	-94.97203	2015-06-11				60.3	8.9
Elk	36.64998	-94.70839	2015-06-11					
Grand	36.68269	-94.77281	2015-06-11					
Honey	36.57511	-94.78775	2015-06-11					
Horse	36.62247	-94.9092	2015-06-11					
P Dam	36.49254	-95.0448	2015-06-11				34.4	4.3

Site Name	Lat.	Long.	Date	CHLa-RFU (OSU Probe)	CHLa- µg/L (OSU Probe)	Secchi Disk (m)	CHLa-µg/L (GRDA Probe)	CHLa-RFU (GRDA Probe)
Sail	36.64176	-94.81493	2015-06-11					
Shang	36.55447	-94.8449	2015-06-11					
Tree	36.56396	-94.91276	2015-06-11				44.6	6.2
Wood	36.53666	-94.82251	2015-06-11				61.4	9.2
Dream	36.50879	-94.9559	2015-07-13	3.25	28.15	1.01	28.15	3.25
Drip	36.49967	-94.95615	2015-07-13	2.9	26.4	1.04	26.4	2.9
Drown	36.49768	-94.91853	2015-07-13	6.7	47.5	0.80	47.5	6.7
Duck	36.53628	-94.97203	2015-07-13	3.7	30.9	1.30	30.9	3.7
Elk	36.64998	-94.70839	2015-07-13	0.29	0.09	0.30		
Grand	36.68269	-94.77281	2015-07-13	0.92	2.66	0.46		
Honey	36.57511	-94.78775	2015-07-13	7.45	28.73	0.78		
Horse	36.62247	-94.9092	2015-07-13	4.7	36.5	0.38	36.5	4.7
P Dam	36.49254	-95.0448	2015-07-13	1.7	15.9	1.40	15.9	1.7
Sail	36.64176	-94.81493	2015-07-13	4.62	17.59	0.57		
Shang	36.55447	-94.8449	2015-07-13	2.63	9.45	1.13		
Tree	36.56396	-94.91276	2015-07-13			0.97		
Wood	36.53666	-94.82251	2015-07-13	6.46	24.76	0.85		
Dream	36.50879	-94.9559	2015-07-29	2.25	21.35	1.40	21.35	2.25
Drip	36.49967	-94.95615	2015-07-29	3.3	28.4	1.31	28.4	3.3
Drown	36.49768	-94.91853	2015-07-29	3.2	27.9	1.38	27.9	3.2
Duck	36.53628	-94.97203	2015-07-29	2.5	23.3	1.50	23.3	2.5
Elk	36.64998	-94.70839	2015-07-29	1.69	6.13	0.99		
Grand	36.68269	-94.77281	2015-07-29	1.41	4.57	1.02		
Honey	36.57511	-94.78775	2015-07-29	2.97	10.72	1.30		
Horse	36.62247	-94.9092	2015-07-29	2.1	19.5	1.52	19.5	2.1
P Dam	36.49254	-95.0448	2015-07-29	2.7	25.4	1.28	25.4	2.7

Site Name	Lat.	Long.	Date	CHLa-RFU (OSU Probe)	CHLa- µg/L (OSU Probe)	Secchi Disk (m)	CHLa-µg/L (GRDA Probe)	CHLa-RFU (GRDA Probe)
Sail	36.64176	-94.81493	2015-07-29	2.20	7.60	1.08		
Shang	36.55447	-94.8449	2015-07-29	2.05	7.14	1.42		
Tree	36.56396	-94.91276	2015-07-29			1.42		
Wood	36.53666	-94.82251	2015-07-29	2.30	8.10	1.37		
Dream	36.50879	-94.9559	2015-08-14	1.90	18.10	1.25	18.10	1.90
Drip	36.49967	-94.95615	2015-08-14	2.50	23.20	1.57	23.20	2.50
Drown	36.49768	-94.91853	2015-08-14	2.30	21.60	1.10	21.60	2.30
Duck	36.53628	-94.97203	2015-08-14	2.40	22.30	1.32	22.30	2.40
Elk	36.64998	-94.70839	2015-08-14	5.90	43.10	0.54	43.10	5.90
Grand	36.68269	-94.77281	2015-08-14	4.20	33.80	0.71	33.80	4.20
Honey	36.57511	-94.78775	2015-08-14	6.40	46.50	1.20	46.50	6.40
Horse	36.62247	-94.9092	2015-08-14	3.30	28.80	0.94	28.80	3.30
P Dam	36.49254	-95.0448	2015-08-14	1.60	15.60	0.76	15.60	1.60
Sail	36.64176	-94.81493	2015-08-14	3.60	29.90	0.77	29.90	3.60
Shang	36.55447	-94.8449	2015-08-14	2.80	25.40	1.12	25.40	2.80
Tree	36.56396	-94.91276	2015-08-14	3.60	30.40	0.76	30.40	3.60
Wood	36.53666	-94.82251	2015-08-14	3.10	27.30	1.20	27.30	3.10
Dream	36.50879	-94.9559	2015-09-15	0.87	2.24	1.85		
Drip	36.49967	-94.95615	2015-09-15	0.77	2.13	1.90		
Drown	36.49768	-94.91853	2015-09-15	0.97	2.81	1.75		
Duck	36.53628	-94.97203	2015-09-15	1.10	3.32	1.50		
Elk	36.64998	-94.70839	2015-09-15	2.43	8.67	0.64		
Grand	36.68269	-94.77281	2015-09-15	1.92	6.63	0.60		
Honey	36.57511	-94.78775	2015-09-15	2.09	7.19	1.15		
Horse	36.62247	-94.9092	2015-09-15	1.66	5.56	0.78		
P Dam	36.49254	-95.0448	2015-09-15	0.85	2.40	1.80		

Site Name	Lat.	Long.	Date	CHLa-RFU (OSU Probe)	CHLa- µg/L (OSU Probe)	Secchi Disk (m)	CHLa-µg/L (GRDA Probe)	CHLa-RFU (GRDA Probe)
Sail	36.64176	-94.81493	2015-09-15	1.17	3.60	0.97		
Shang	36.55447	-94.8449	2015-09-15	0.58	1.28	1.20		
Tree	36.56396	-94.91276	2015-09-15	0.84	2.43	1.38		
Wood	36.53666	-94.82251	2015-09-15	0.27	2.04	1.15		
Dream	36.50879	-94.9559	2016-05-12	1.21	3.90	1.37	6.1	1.4
Drip	36.49967	-94.95615	2016-05-12	1.38	4.64	1.35	8.4	2
Drown	36.49768	-94.91853	2016-05-12	2.34	8.49	1.48	9.5	2.2
Duck	36.53628	-94.97203	2016-05-12	2.00	6.63	1.35	10	2.4
Elk	36.64998	-94.70839	2016-05-12			0.88	17.6	4.2
Grand	36.68269	-94.77281	2016-05-12	1.84	6.21	0.23	11.1	2.6
Honey	36.57511	-94.78775	2016-05-12	3.29	8.32	1.01	5	1.2
Horse	36.62247	-94.9092	2016-05-12	2.68	8.14	1.14	10.4	2.5
P Dam	36.49254	-95.0448	2016-05-12	2.57	8.13	1.16	12.7	3
Sail	36.64176	-94.81493	2016-05-12	1.58	5.56	0.33	9.8	2.3
Shang	36.55447	-94.8449	2016-05-12	0.60	1.42	1.09	5	1.2
Tree	36.56396	-94.91276	2016-05-12	0.63	1.39	1.43	4.4	1.1
Wood	36.53666	-94.82251	2016-05-12	1.00	3.00	1.2	5.8	1.4
Dream	36.50879	-94.9559	2016-06-28	3.01	11.05	1.33	17	4.5
Drip	36.49967	-94.95615	2016-06-28	5.17	19.54	0.95	18.4	4.8
Drown	36.49768	-94.91853	2016-06-28	4.46	16.77	0.87	20.6	5.4
Duck	36.53628	-94.97203	2016-06-28	2.73	9.87	0.94	14.7	3.8
Elk	36.64998	-94.70839	2016-06-28	3.02	10.98	1	16.1	4.2
Grand	36.68269	-94.77281	2016-06-28	11.03	43.13	0.86	46.2	12.1
Honey	36.57511	-94.78775	2016-06-28	4.83	18.04	0.84	23.3	6.1
Horse	36.62247	-94.9092	2016-06-28	2.03	7.06	0.93	11.5	3
P Dam	36.49254	-95.0448	2016-06-28	3.87	14.43	0.93	18.1	4.8

Site Name	Lat.	Long.	Date	CHLa-RFU (OSU Probe)	CHLa- µg/L (OSU Probe)	Secchi Disk (m)	CHLa-µg/L (GRDA Probe)	CHLa-RFU (GRDA Probe)
Sail	36.64176	-94.81493	2016-06-28	4.23	15.56	0.93	23.8	6.2
Shang	36.55447	-94.8449	2016-06-28	4.65	18.10	0.83	28.1	7.4
Tree	36.56396	-94.91276	2016-06-28	2.86	10.36	1.8	14	3.7
Wood	36.53666	-94.82251	2016-06-28	3.37	12.55	1.3	16.4	4.3

Appendix IV. *In situ* data at Council Grove Lake

Site ID	Lat.	Long	Date	CHLa-RFU	CHLa-µg/L	Secchi Depth-m
CG1	38.713066	-96.542366	2017-08-02	1.47	4.79	0.35
CG1	38.713066	-96.542366	2017-08-02	0.98	2.86	
CG2	38.705002	-96.543983	2017-08-02	1.69	5.71	0.35
CG2	38.705002	-96.543983	2017-08-02	1.38	4.46	
CG3	38.700901	-96.534302	2017-08-02	1.24	3.88	0.45
CG3	38.700901	-96.534302	2017-08-02	-	-	
CG4	38.688381	-96.527367	2017-08-02	1.09	3.31	0.35
CG4	38.688381	-96.527367	2017-08-02	0.96	2.79	
CG5	38.689781	-96.513481	2017-08-02	0.73	1.84	0.45
CG5	38.689781	-96.513481	2017-08-02	0.79	2.10	
CG6	38.713783	-96.507782	2017-08-02	1.54	5.11	0.35
CG6	38.713783	-96.507782	2017-08-02	1.50	4.94	
CG7	38.705883	-96.508286	2017-08-02	1.11	3.37	0.35
CG7	38.705833	-96.508286	2017-08-02	1.17	3.63	
CG8	38.693867	-96.502869	2017-08-02	0.78	2.04	0.50
CG8	38.693867	-96.502869	2017-08-02	0.88	2.47	
CG9	38.686684	-96.500748	2017-08-02	0.61	1.38	0.50
CG9	38.686684	-96.500748	2017-08-02	0.59	1.30	
CG10	38.683067	-96.507317	2017-08-02	0.86	2.36	0.65
CG10	38.683067	-96.507317	2017-08-02	0.78	2.05	

Site ID	Lat.	Long	Date	CHLa-RFU	CHLa-µg/L	Secchi Depth-m
CG1	38.713066	-96.542366	2017-08-10	1.37	4.41	0.49
CG1	38.713066	-96.542366	2017-08-10	1.01	2.97	
CG2	38.705002	-96.543983	2017-08-10	0.98	2.87	0.45
CG2	38.705002	-96.543983	2017-08-10	0.62	1.42	
CG3	38.700901	-96.534302	2017-08-10	0.49	0.88	0.49
CG3	38.700901	-96.534302	2017-08-10	0.34	0.31	
CG4	38.688381	-96.527367	2017-08-10	0.85	2.31	0.49
CG4	38.688381	-96.527367	2017-08-10	0.52	1.03	
CG5	38.689781	-96.513481	2017-08-10	0.41	0.56	0.45
CG5	38.689781	-96.513481	2017-08-10	0.34	0.28	
CG6	38.713783	-96.507782	2017-08-10	1.44	4.68	0.52
CG6	38.713783	-96.507782	2017-08-10	0.61	1.37	
CG7	38.705883	-96.508286	2017-08-10	0.78	2.05	0.45
CG7	38.705833	-96.508286	2017-08-10	0.50	0.93	
CG8	38.693867	-96.502869	2017-08-10	0.44	0.70	0.49
CG8	38.693867	-96.502869	2017-08-10	0.30	0.13	
CG9	38.686684	-96.500748	2017-08-10	0.44	0.71	0.44
CG9	38.686684	-96.500748	2017-08-10	-	-	
CG10	38.683067	-96.507317	2017-08-10	0.37	0.42	0.49
CG10	38.683067	-96.507317	2017-08-10	0.34	0.29	
CG1	38.713066	-96.542366	2017-08-17	1.52	5.03	0.35
CG1	38.713066	-96.542366	2017-08-17	-	-	
CG2	38.705002	-96.543983	2017-08-17	1.61	5.38	0.31
CG2	38.705002	-96.543983	2017-08-17	1.18	3.63	
CG3	38.700901	-96.534302	2017-08-17	1.15	3.53	0.48
CG3	38.700901	-96.534302	2017-08-17	1.02	3.02	

Site ID	Lat.	Long	Date	CHLa-RFU	CHLa-µg/L	Secchi Depth-m
CG4	38.688381	-96.527367	2017-08-17	1.07	3.19	0.46
CG4	38.688381	-96.527367	2017-08-17	0.86	2.38	
CG5	38.689781	-96.513481	2017-08-17	0.70	1.72	0.60
CG5	38.689781	-96.513481	2017-08-17	0.64	1.50	
CG6	38.713783	-96.507782	2017-08-17	0.95	2.74	0.40
CG6	38.713783	-96.507782	2017-08-17	0.92	2.62	
CG7	38.705883	-96.508286	2017-08-17	0.95	2.72	0.54
CG7	38.705833	-96.508286	2017-08-17	0.88	2.46	
CG8	38.693867	-96.502869	2017-08-17	0.88	2.44	0.57
CG8	38.693867	-96.502869	2017-08-17	0.83	2.25	
CG9	38.686684	-96.500748	2017-08-17	0.78	2.05	0.70
CG9	38.686684	-96.500748	2017-08-17	0.79	2.09	
CG10	38.683067	-96.507317	2017-08-17	0.78	2.07	0.59
CG10	38.683067	-96.507317	2017-08-17	0.73	1.85	
CG1	38.713066	-96.542366	2017-08-26			0.40
CG2	38.705002	-96.543983	2017-08-26			0.45
CG3	38.700901	-96.534302	2017-08-26			0.45
CG4	38.688381	-96.527367	2017-08-26			0.35
CG5	38.689781	-96.513481	2017-08-26			0.45
CG5 D	38.689781	-96.513481	2017-08-26			-
CG6	38.713783	-96.507782	2017-08-26			0.45
CG7	38.705883	-96.508286	2017-08-26			0.55
CG8	38.693867	-96.502869	2017-08-26			0.60
CG9	38.686684	-96.500748	2017-08-26			0.55
CG10	38.683067	-96.507317	2017-08-26			0.55

Appendix V. *In situ* data at John Redmond Lake

Site ID	Lat.	Long	Date	CHLa-RFU	CHLa-µg/L	Secchi Depth-m
John Red 1	38.247581	95.768265	2017-08-10	3.69	13.70	0.33
John Red 1			2017-08-10	3.69	13.70	
John Red 2	38.266399	95.78743	2017-08-10	4.95	18.72	0.32
John Red 2			2017-08-10			
John Red 3	38.265518	95.807869	2017-08-10	4.75	17.92	0.33
John Red 3			2017-08-10	5.29	20.10	
John Red 4	38.251068	95.822418	2017-08-10	4.38	16.44	0.27
John Red 4			2017-08-10	4.71	17.76	
John Red 5	38.247417	95.80677	2017-08-10	4.13	15.46	0.36
John Red 5			2017-08-10	4.45	16.72	
John Red 6	38.238419	95.808601	2017-08-10	5.17	19.61	0.35
John Red 6			2017-08-10	4.99	18.89	
John Red 7	38.228619	95.802254	2017-08-10	3.62	13.40	0.28
John Red 7			2017-08-10	3.89	14.48	
John Red 8	38.236282	95.788948	2017-08-10	4.47	16.82	0.35
John Red 8			2017-08-10	4.15	15.52	
John Red 1	38.247581	95.768265	2017-08-26	2.11	7.39	0.40
John Red 2	38.266399	95.78743	2017-08-26	2.77	10.02	0.35
John Red 3	38.265518	95.807869	2017-08-26	3.11	11.38	0.30
John Red 4	38.251068	95.822418	2017-08-26	3.99	14.89	0.25
John Red 5	38.247417	95.80677	2017-08-26	3.43	12.64	0.30
John Red 6	38.238419	95.808601	2017-08-26			0.25
John Red 7	38.228619	95.802254	2017-08-26			0.25
John Red 8	38.236282	95.788948	2017-08-26			0.25

Appendix VI. *In situ* data at Marion Lake

Site ID	Lat.	Long	Date	CHLa-RFU	CHLa-µg/L	Secchi Depth-m
M1	38.403099	-97.112579	2017-08-02	2.11	7.38	0.25
M1	38.403099	-97.112579	2017-08-02	1.79	6.10	
M2	38.408066	-97.128136	2017-08-02	2.11	7.38	0.30
M2	38.408066	-97.128136	2017-08-02	1.60	5.32	
M3	38.418282	-97.138733	2017-08-02	2.52	9.02	0.45
M3	38.418282	-97.138733	2017-08-02	2.17	7.61	
M3	38.418282	-97.138733	2017-08-02	2.26	7.98	
M4	38.431683	-97.147919	2017-08-02	2.15	7.54	0.35
M4	38.431683	-97.147919	2017-08-02	3.48	12.86	
M5	38.440617	-97.153603	2017-08-02	3.75	13.94	0.45
M5	38.440617	-97.153603	2017-08-02	3.29	12.09	
M6	38.393482	-97.129715	2017-08-02	1.78	6.06	0.45
M6	38.393482	-97.129715	2017-08-02	2.52	9.03	
M7	38.383385	-97.104836	2017-08-02	1.57	5.19	0.53
M7	38.383385	-97.104836	2017-08-02	1.23	3.83	
M8	38.374119	-97.101402	2017-08-02	0.97	2.82	0.55
M8	38.374119	-97.101402	2017-08-02			
M9	38.372635	-97.089584	2017-08-02			
M9	38.372635	-97.089584	2017-08-02	0.70	1.74	
M1	38.403099	-97.112579	2017-08-17	2.08	7.27	0.50
M1	38.403099	-97.112579	2017-08-17	1.97	6.82	
M2	38.408066	-97.128136	2017-08-17	2.67	9.62	0.43
M2	38.408066	-97.128136	2017-08-17	2.59	9.30	
M3	38.418282	-97.138733	2017-08-17	3.36	12.39	0.32
M3	38.418282	-97.138733	2017-08-17	3.00	10.95	

Site ID	Lat.	Long	Date	CHLa-RFU	CHLa-µg/L	Secchi Depth-m
M4	38.431683	-97.147919	2017-08-17	3.60	13.35	0.28
M4	38.431683	-97.147919	2017-08-17	3.64	13.47	
M5	38.440617	-97.153603	2017-08-17	5.53	21.04	0.20
M5	38.440617	-97.153603		-	-	
M6	38.393482	-97.129715	2017-08-17	2.77	9.99	0.38
M6	38.393482	-97.129715	2017-08-17	3.22	11.80	
M7	38.383385	-97.104836	2017-08-17	2.00	6.92	0.43
M7	38.383385	-97.104836	2017-08-17	1.89	6.50	
M8	38.374119	-97.101402	2017-08-17	2.40	8.51	0.44
M8	38.374119	-97.101402	2017-08-17	2.16	7.56	
M9	38.372635	-97.089584	2017-08-17	2.00	6.94	0.48
M9	38.372635	-97.089584	2017-08-17	1.82	6.22	

Appendix VII. Landsat 8 spectral data for Grand Lake

Site ID	Lat.	Long	Date	Coastal Aerosol (B1)	Blue (B2)	Green (B3)	Red (B4)	NIR (B5)	SWIR1 (B6)	SWIR2 (B7)
Dream	36.50879	-94.9559	2014-08-26	134	48	114	42	44	36	21
Drip	36.49967	-94.95615	2014-08-26	195	87	148	84	11	99	78
Drown	36.49768	-94.91853	2014-08-26	253	146	227	146	100	99	70
Duck	36.53628	-94.97203	2014-08-26	161	62	134	54	32	64	50
Elk	36.64998	-94.70839	2014-08-26	215	125	293	185	73	42	27
Grand	36.68269	-94.77281	2014-08-26	226	145	276	182	81	44	24
Honey	36.57511	-94.78775	2014-08-26	259	134	320	150	42	60	33
Horse	36.62247	-94.9092	2014-08-26	303	224	400	231	132	110	77
P Dam	36.49254	-95.0448	2014-08-26	218	121	172	93	104	73	42
Sail	36.64176	-94.81493	2014-08-26	220	61	252	138	83	53	40

Site ID	Lat.	Long	Date	Coastal Aerosol (B1)	Blue (B2)	Green (B3)	Red (B4)	NIR (B5)	SWIR1 (B6)	SWIR2 (B7)
Shang	36.55447	-94.8449	2014-08-26	206	118	225	102	71	32	19
Tree	36.56396	-94.91276	2014-08-26	210	118	207	105	58	44	28
Wood	36.53666	-94.82251	2014-08-26	217	100	204	96	-9	58	43
Dream	36.50879	-94.9559	2015-06-11	466	377	486	425	339	269	214
Drip	36.49967	-94.95615	2015-06-11	623	531	653	599	468	456	350
Drown	36.49768	-94.91853	2015-06-11	329	225	289	206	135	106	84
Duck	36.53628	-94.97203	2015-06-11	407	308	375	328	244	250	197
Elk	36.64998	-94.70839	2015-06-11	377	286	364	314	279	209	157
Grand	36.68269	-94.77281	2015-06-11	517	454	658	605	291	191	146
Honey	36.57511	-94.78775	2015-06-11	475	373	421	377	231	291	227
Horse	36.62247	-94.9092	2015-06-11	505	389	479	415	370	318	250
P Dam	36.49254	-95.0448	2015-06-11	561	467	570	509	364	305	237
Sail	36.64176	-94.81493	2015-06-11	481	400	532	466	340	265	211
Shang	36.55447	-94.8449	2015-06-11	547	459	632	592	325	223	171
Tree	36.56396	-94.91276	2015-06-11	486	383	501	443	321	238	187
Wood	36.53666	-94.82251	2015-06-11	500	407	472	429	194	217	171
Dream	36.50879	-94.9559	2015-07-13	259	178	256	223	143	161	132
Drip	36.49967	-94.95615	2015-07-13	328	238	280	261	184	233	183
Drown	36.49768	-94.91853	2015-07-13	134	65	123	94	27	66	48
Duck	36.53628	-94.97203	2015-07-13	194	101	148	131	71	127	103
Elk	36.64998	-94.70839	2015-07-13	572	619	1113	1189	232	139	111
Grand	36.68269	-94.77281	2015-07-13	287	253	465	585	117	47	34
Honey	36.57511	-94.78775	2015-07-13	259	165	219	193	143	179	136
Horse	36.62247	-94.9092	2015-07-13	250	169	229	193	133	146	119
P Dam	36.49254	-95.0448	2015-07-13	280	191	244	221	114	177	141
Sail	36.64176	-94.81493	2015-07-13	255	204	351	306	120	91	79

Site ID	Lat.	Long	Date	Coastal Aerosol (B1)	Blue (B2)	Green (B3)	Red (B4)	NIR (B5)	SWIR1 (B6)	SWIR2 (B7)
Shang	36.55447	-94.8449	2015-07-13	268	192	282	241	171	143	116
Tree	36.56396	-94.91276	2015-07-13	249	177	276	233	110	107	86
Wood	36.53666	-94.82251	2015-07-13	162	81	144	117	-25	93	71
Dream	36.50879	-94.9559	2015-07-29	113	35	107	70	11	50	31
Drip	36.49967	-94.95615	2015-07-29	211	133	194	164	118	178	122
Drown	36.49768	-94.91853	2015-07-29	198	119	195	148	89	114	85
Duck	36.53628	-94.97203	2015-07-29	114	30	90	69	35	87	62
Elk	36.64998	-94.70839	2015-07-29	129	71	201	149	37	61	45
Grand	36.68269	-94.77281	2015-07-29	200	146	324	248	73	52	33
Honey	36.57511	-94.78775	2015-07-29	165	45	136	89	32	89	60
Horse	36.62247	-94.9092	2015-07-29	181	109	219	141	61	86	55
P Dam	36.49254	-95.0448	2015-07-29	257	155	220	194	116	182	124
Sail	36.64176	-94.81493	2015-07-29	180	96	215	148	107	78	63
Shang	36.55447	-94.8449	2015-07-29	167	80	176	113	79	59	38
Tree	36.56396	-94.91276	2015-07-29	149	73	154	102	60	59	37
Wood	36.53666	-94.82251	2015-07-29	109	22	104	59	-57	78	51
Dream	36.50879	-94.9559	2015-08-14	189	91	131	76	26	20	12
Drip	36.49967	-94.95615	2015-08-14	200	91	127	72	-21	29	34
Drown	36.49768	-94.91853	2015-08-14	232	130	166	111	27	41	39
Duck	36.53628	-94.97203	2015-08-14	202	96	144	85	4	43	37
Elk	36.64998	-94.70839	2015-08-14	252	179	376	274	20	10	19
Grand	36.68269	-94.77281	2015-08-14	232	139	260	163	53	18	19
Honey	36.57511	-94.78775	2015-08-14	195	96	141	73	-32	24	22
Horse	36.62247	-94.9092	2015-08-14	263	167	261	149	43	39	37
P Dam	36.49254	-95.0448	2015-08-14	238	112	136	74	-8	10	13
Sail	36.64176	-94.81493	2015-08-14	259	163	270	194	69	26	31

Site ID	Lat.	Long	Date	Coastal Aerosol (B1)	Blue (B2)	Green (B3)	Red (B4)	NIR (B5)	SWIR1 (B6)	SWIR2 (B7)
Shang	36.55447	-94.8449	2015-08-14	254	155	238	141	46	7	8
Tree	36.56396	-94.91276	2015-08-14	268	166	239	151	75	50	44
Wood	36.53666	-94.82251	2015-08-14	251	144	210	127	-36	28	31
Dream	36.50879	-94.9559	2015-09-15	177	91	147	89	85	41	27
Drip	36.49967	-94.95615	2015-09-15	195	98	135	81	-2	55	48
Drown	36.49768	-94.91853	2015-09-15	200	118	171	114	73	62	50
Duck	36.53628	-94.97203	2015-09-15	219	132	202	134	60	55	48
Elk	36.64998	-94.70839	2015-09-15	270	194	393	278	112	48	43
Grand	36.68269	-94.77281	2015-09-15	326	255	426	367	134	40	28
Honey	36.57511	-94.78775	2015-09-15	242	142	191	139	37	54	41
Horse	36.62247	-94.9092	2015-09-15	296	212	323	223	163	93	72
P Dam	36.49254	-95.0448	2015-09-15	235	132	158	115	111	85	62
Sail	36.64176	-94.81493	2015-09-15	294	205	357	290	131	61	53
Shang	36.55447	-94.8449	2015-09-15	236	155	243	176	119	58	40
Tree	36.56396	-94.91276	2015-09-15	268	186	273	201	144	83	63
Wood	36.53666	-94.82251	2015-09-15	183	94	170	108	-41	32	27
Dream	36.50879	-94.9559	2016-05-12							
Drip	36.49967	-94.95615	2016-05-12	527	456	619	447	164	210	175
Drown	36.49768	-94.91853	2016-05-12							
Duck	36.53628	-94.97203	2016-05-12							
Elk	36.64998	-94.70839	2016-05-12	508	453	696	495	313	267	229
Grand	36.68269	-94.77281	2016-05-12	539	560	871	997	405	189	168
Honey	36.57511	-94.78775	2016-05-12	474	390	558	413	151	164	135
Horse	36.62247	-94.9092	2016-05-12							
P Dam	36.49254	-95.0448	2016-05-12	196	118	169	95	-7	30	25
Sail	36.64176	-94.81493	2016-05-12	618	613	893	938	387	227	189

Site ID	Lat.	Long	Date	Coastal Aerosol (B1)	Blue (B2)	Green (B3)	Red (B4)	NIR (B5)	SWIR1 (B6)	SWIR2 (B7)
Shang	36.55447	-94.8449	2016-05-12	527	515	754	660	270	209	184
Tree	36.56396	-94.91276	2016-05-12							
Wood	36.53666	-94.82251	2016-05-12	478	417	618	492	61	89	77

Appendix VIII. Landsat 8 spectral data for Council Grove Lake

Site ID	Lat.	Long	Date	Coastal Aerosol (B1)	Blue (B2)	Green (B3)	Red (B4)	NIR (B5)	SWIR1 (B6)	SWIR2 (B7)
CG1	38.713066	-96.542366	2017/08/01	410	493	686	649	366	208	174
CG2	38.705002	-96.543983	2017/08/01	406	500	710	687	345	181	152
CG3	38.700901	-96.534302	2017/08/01	415	498	704	640	337	207	170
CG4	38.688381	-96.527367	2017/08/01	297	369	573	492	173	54	38
CG5	38.689781	-96.513481	2017/08/01	380	474	694	603	289	182	145
CG6	38.713783	-96.507782	2017/08/01	389	472	699	656	292	157	128
CG7	38.705883	-96.508286	2017/08/01	374	462	686	603	277	157	124
CG8	38.693867	-96.502869	2017/08/01	443	532	751	665	389	282	239
CG9	38.686684	-96.500748	2017/08/01	366	449	666	573	288	179	142
CG10	38.683067	-96.507317	2017/08/01	363	440	650	556	280	168	136
CG1	38.713066	-96.542366	2017/08/17	410	493	686	649	366	208	174
CG2	38.705002	-96.543983	2017/08/17	406	500	710	687	345	181	152
CG3	38.700901	-96.534302	2017/08/17	415	498	704	640	337	207	170
CG4	38.688381	-96.527367	2017/08/17	297	369	573	492	173	54	38
CG5	38.689781	-96.513481	2017/08/17	380	474	694	603	289	182	145
CG6	38.713783	-96.507782	2017/08/17	389	472	699	656	292	157	128
CG7	38.705883	-96.508286	2017/08/17	374	462	686	603	277	157	124
CG8	38.693867	-96.502869	2017/08/17	443	532	751	665	389	282	239
CG9	38.686684	-96.500748	2017/08/17	366	449	666	573	288	179	142

Site ID	Lat.	Long	Date	Coastal Aerosol (B1)	Blue (B2)	Green (B3)	Red (B4)	NIR (B5)	SWIR1 (B6)	SWIR2 (B7)
CG10	38.683067	-96.507317	2017/08/17	363	440	650	556	280	168	136
CG1	38.713066	-96.542366	2017/08/26	465	511	643	536	323	85	47
CG2	38.705002	-96.543983	2017/08/26	455	498	625	502	279	77	45
CG3	38.700901	-96.534302	2017/08/26	487	537	672	560	300	88	53
CG4	38.688381	-96.527367	2017/08/26	517	581	729	640	315	90	52
CG5	38.689781	-96.513481	2017/08/26	501	571	726	629	260	70	38
CG6	38.713783	-96.507782	2017/08/26	459	519	660	560	274	72	42
CG7	38.705883	-96.508286	2017/08/26	495	537	660	527	319	106	62
CG8	38.693867	-96.502869	2017/08/26	480	544	693	595	244	56	36
CG9	38.686684	-96.500748	2017/08/26	482	548	705	615	243	60	35
CG10	38.683067	-96.507317	2017/08/26	482	555	707	615	243	59	33

Appendix IX. Landsat 8 spectral data for John Redmond Lake

Site ID	Lat.	Long	Date	Coastal Aerosol (B1)	Blue (B2)	Green (B3)	Red (B4)	NIR (B5)	SWIR1 (B6)	SWIR2 (B7)
John Red 1	38.247581	95.768265	2017/08/10	159	246	484	379	105	6	11
John Red 2	38.266399	95.78743	2017/08/10	172	268	517	400	120	10	12
John Red 3	38.265518	95.807869	2017/08/10	206	294	518	395	102	10	11
John Red 4	38.251068	95.822418	2017/08/10	278	359	579	460	147	12	14
John Red 5	38.247417	95.80677	2017/08/10	211	290	497	374	80	6	12
John Red 6	38.238419	95.808601	2017/08/10	214	296	521	390	91	10	12
John Red 7	38.228619	95.802254	2017/08/10	240	325	567	444	120	5	14
John Red 8	38.236282	95.788948	2017/08/10	204	296	526	416	98	9	9
John Red 1	38.247581	95.768265	2017/08/26	293	366	569	508	189	49	38
John Red 2	38.266399	95.78743	2017/08/26	349	433	641	586	232	65	47
John Red 3	38.265518	95.807869	2017/08/26	326	403	606	552	217	65	48

Site ID	Lat.	Long	Date	Coastal Aerosol (B1)	Blue (B2)	Green (B3)	Red (B4)	NIR (B5)	SWIR1 (B6)	SWIR2 (B7)
John Red 4	38.251068	95.822418	2017/08/26	341	425	639	581	219	51	39
John Red 5	38.247417	95.80677	2017/08/26	300	374	559	484	181	46	36
John Red 6	38.238419	95.808601	2017/08/26	287	363	557	482	166	35	23
John Red 7	38.228619	95.802254	2017/08/26	325	414	625	581	236	49	34
John Red 8	38.236282	95.788948	2017/08/26	302	375	570	501	189	48	34

Appendix X. Land sat 8 spectral data for Marion Lake

Site ID	Lat.	Long.	Date	Coastal Aerosol (B1)	Blue (B2)	Green (B3)	Red (B4)	NIR (B5)	SWIR1 (B6)	SWIR2 (B7)
M1	38.403099	-97.112579	2017/08/01	329	384	526	452	252	143	109
M2	38.408066	-97.128136	2017/08/01	376	428	595	513	303	190	152
M3	38.418282	-97.138733	2017/08/01	366	420	598	530	287	148	117
M4	38.431683	-97.147919	2017/08/01	380	436	621	558	328	155	119
M5	38.440617	-97.153603	2017/08/01	401	477	678	653	432	163	131
M6	38.393482	-97.129715	2017/08/01	303	351	507	421	236	110	87
M7	38.383385	-97.104836	2017/08/01	340	392	525	444	253	148	124
M8	38.374119	-97.101402	2017/08/01	340	385	529	456	271	159	130
M9	38.372635	-97.089584	2017/08/01	362	415	557	481	284	164	134
M1	38.403099	-97.112579	2017/08/17	329	384	526	452	252	143	109
M2	38.408066	-97.128136	2017/08/17	376	428	595	513	303	190	152
M3	38.418282	-97.138733	2017/08/17	366	420	598	530	287	148	117
M4	38.431683	-97.147919	2017/08/17	380	436	621	558	328	155	119
M5	38.440617	-97.153603	2017/08/17	401	477	678	653	432	163	131
M6	38.393482	-97.129715	2017/08/17	303	351	507	421	236	110	87
M7	38.383385	-97.104836	2017/08/17	340	392	525	444	253	148	124
M8	38.374119	-97.101402	2017/08/17	340	385	529	456	271	159	130

Site ID	Lat.	Long.	Date	Coastal Aerosol (B1)	Blue (B2)	Green (B3)	Red (B4)	NIR (B5)	SWIR1 (B6)	SWIR2 (B7)
M9	38.372635	-97.089584	2017/08/17	362	415	557	481	284	164	134

Appendix XI. Water Quality data for selected lakes in Oklahoma (Data were collected by OWRB)

Date	Site	Lake/Reservoir	CHLa (µg/L)	Turbidity (NTU)	Secchi Depth (cm)
10/01/2012	1	Arcadia Lake	18.2	16	40
10/01/2012	2	Arcadia Lake	20	24	30
10/01/2012	3	Arcadia Lake	25.1	19	40
10/01/2012	4	Arcadia Lake	36.9	22	25
10/01/2012	5	Arcadia Lake	43.7	75	7
01/02/2013	1	Arcadia Lake	4.99	18	65
01/02/2013	2	Arcadia Lake	8.87	15	55
01/02/2013	3	Arcadia Lake	7	14	55
01/02/2013	4	Arcadia Lake	13.9	15	57
01/02/2013	5	Arcadia Lake	25	15	55
03/06/2013	2	Arcadia Lake	7.02	29	40
03/06/2013	3	Arcadia Lake	5.87	34	35
03/06/2013	4	Arcadia Lake	11.8	63	27
03/06/2013	5	Arcadia Lake	15.5	52	25
03/06/2013	1	Arcadia Lake	5.47	25	40
08/12/2013	1	Arcadia Lake	20.1	9	66
08/12/2013	2	Arcadia Lake	26.7	11	62
08/12/2013	3	Arcadia Lake	22.9	12	60
08/12/2013	4	Arcadia Lake	17.5	11	52
08/12/2013	5	Arcadia Lake	15.3	20	43

Date	Site	Lake/Reservoir	CHLa (µg/L)	Turbidity (NTU)	Secchi Depth (cm)
12/03/2014	1	Arcadia Lake	16.4	5	150
12/03/2014	2	Arcadia Lake	16.6	7	150
12/03/2014	3	Arcadia Lake	17.1	6	130
12/03/2014	4	Arcadia Lake	21.8	5	153
12/03/2014	5	Arcadia Lake	31.9	6	200
02/25/2015	1	Arcadia Lake	10	13	61
02/25/2015	2	Arcadia Lake	10.6	11	53
02/25/2015	3	Arcadia Lake	11.7	11	70
02/25/2015	4	Arcadia Lake	14.2	13	42
02/25/2015	5	Arcadia Lake	16.3	15	45
06/09/2015	1	Arcadia Lake	15.9	5	155
06/09/2015	2	Arcadia Lake	25.5	7	117
06/09/2015	3	Arcadia Lake	35.6	5	113
06/09/2015	4	Arcadia Lake	21.1	4	140
06/09/2015	5	Arcadia Lake	9.87	5	152
08/24/2015	1	Arcadia Lake	31.2	3	182
08/24/2015	2	Arcadia Lake	41.2	4	107
08/24/2015	3	Arcadia Lake	48.4	4	122
08/24/2015	4	Arcadia Lake	45.3	3	109
08/24/2015	5	Arcadia Lake	59.9	3	134
10/14/2014	1	Boomer Lake	49.7	14	39
10/14/2014	2	Boomer Lake	56.1	16	39
10/14/2014	3	Boomer Lake	57.6	24	36
01/21/2015	1	Boomer Lake	17.8	7	52

Date	Site	Lake/Reservoir	CHLa (µg/L)	Turbidity (NTU)	Secchi Depth (cm)
01/21/2015	2	Boomer Lake	21.1	15	35
01/21/2015	3	Boomer Lake	22.6	19	25
03/31/2015	1	Boomer Lake	21.3	10	30
03/31/2015	2	Boomer Lake	23	13	23
03/31/2015	3	Boomer Lake	24.5	17	19
07/07/2015	1	Boomer Lake	28.3	11	54
07/07/2015	2	Boomer Lake	27.5	15	50
07/07/2015	3	Boomer Lake	26.4	20	38
11/07/2012	1	Broken Bow	2.92	2	250
11/07/2012	2	Broken Bow	3	2	250
11/07/2012	3	Broken Bow	4.33	2	246
11/07/2012	4	Broken Bow	3.65	1	250
11/07/2012	5	Broken Bow	5.65	2	250
11/07/2012	6	Broken Bow	5.34	1	250
11/07/2012	7	Broken Bow	6.91	2	230
11/07/2012	8	Broken Bow	9.15	2	232
03/12/2013	1	Broken Bow	0.72	2	320
03/12/2013	2	Broken Bow	0.62	2	320
03/12/2013	3	Broken Bow	0.71	2	320
03/12/2013	4	Broken Bow	0.7	2	320
03/12/2013	5	Broken Bow	1.25	3	320
03/12/2013	6	Broken Bow	2.54	4	220
03/12/2013	7	Broken Bow	6.17	12	77
03/12/2013	8	Broken Bow	5.39	33	43

Date	Site	Lake/Reservoir	CHLa (µg/L)	Turbidity (NTU)	Secchi Depth (cm)
04/29/2013	1	Broken Bow	2.05	2	320
04/29/2013	2	Broken Bow	1.98	2	305
04/29/2013	3	Broken Bow	3.37	2	305
04/29/2013	4	Broken Bow	2.42	2	287
04/29/2013	5	Broken Bow	2.51	2	300
04/29/2013	6	Broken Bow	4.7	3	198
04/29/2013	7	Broken Bow	8.79	3	152
04/29/2013	8	Broken Bow	7.12	3	155
07/30/2013	1	Broken Bow	8.32	1	225
07/30/2013	2	Broken Bow	2.81	2	200
07/30/2013	3	Broken Bow	6.53	2	230
07/30/2013	4	Broken Bow	5.58	2	200
07/30/2013	5	Broken Bow	4.82	2	200
07/30/2013	6	Broken Bow	5.57	2	210
07/30/2013	7	Broken Bow	7.26	2	200
07/30/2013	8	Broken Bow	9.06	2	210
10/20/2015	1	Broken Bow	3.21	4	300
10/20/2015	2	Broken Bow	2.96	2	300
10/20/2015	3	Broken Bow	2.98	1	238
10/20/2015	4	Broken Bow	2.48	2	218
10/20/2015	5	Broken Bow	2.84	2	234
10/20/2015	6	Broken Bow	3.02	1	210
10/20/2015	7	Broken Bow	3.8	2	150
10/20/2015	8	Broken Bow	4.59	2	144
08/15/2016	1	Broken Bow	4.5	1	253

Date	Site	Lake/Reservoir	CHLa (µg/L)	Turbidity (NTU)	Secchi Depth (cm)
08/15/2016	2	Broken Bow	4.75	1	248
08/15/2016	3	Broken Bow	7.88	2	222
08/15/2016	4	Broken Bow	4.94	2	267
08/15/2016	5	Broken Bow	6.41	2	209
08/15/2016	6	Broken Bow	5.97	2	254
08/15/2016	7	Broken Bow	7.82	2	216
08/15/2016	8	Broken Bow	9.61	2	190
10/07/2013	1	Canton Lake	136	36	13
10/07/2013	2	Canton Lake	105	34	14
10/07/2013	3	Canton Lake	96.2	31	22
04/09/2014	1	Canton Lake	14.9	24	36
04/09/2014	2	Canton Lake	16.7	19	23
04/09/2014	3	Canton Lake	38.7	133	8
07/07/2014	1	Canton Lake	15.4	17	40
07/07/2014	2	Canton Lake	14	22	42
07/07/2014	3	Canton Lake	13.2	34	25
11/30/2016	1	Canton Lake	5.4	15	65
11/30/2016	2	Canton Lake	8.39	12	60
11/30/2016	3	Canton Lake	6.03	12	45
04/03/2017	1	Canton Lake	5.6	8	96
04/03/2017	2	Canton Lake	5.97	8	84
04/03/2017	3	Canton Lake	5.79	9	69
05/31/2017	1	Canton Lake	7.56	7	82
05/31/2017	2	Canton Lake	14.6	7	93

Date	Site	Lake/Reservoir	CHLa (µg/L)	Turbidity (NTU)	Secchi Depth (cm)
05/31/2017	3	Canton Lake	13.3	11	79
08/30/2017	1	Canton Lake	28.9	15	45
08/30/2017	2	Canton Lake	31.00	15	48
08/30/2017	3	Canton Lake	27.7	20	35
10/23/2012	1	Foss Lake	10.1	11	66
10/23/2012	2	Foss Lake	10.8	14	57
10/23/2012	3	Foss Lake	10.7	21	40
10/23/2012	4	Foss Lake	10.5	30	37
10/23/2012	5	Foss Lake	12.2	46	21
03/05/2013	1	Foss Lake	1.49	16	80
03/05/2013	2	Foss Lake	1.53	13	84
03/05/2013	3	Foss Lake	1.67	19	68
03/05/2013	4	Foss Lake	3.72	26	42
03/05/2013	5	Foss Lake	2.7	38	29
04/15/2013	1	Foss Lake	8.48	9	60
04/15/2013	2	Foss Lake	7.61	14	52
04/15/2013	3	Foss Lake	6.83	18	33
04/15/2013	4	Foss Lake	6.82	37	25
04/15/2013	5	Foss Lake	no data	no data	no data
08/28/2013	1	Foss Lake	16.8	8	79
08/28/2013	2	Foss Lake	16.6	6	68
08/28/2013	3	Foss Lake	13.3	18	45
08/28/2013	4	Foss Lake	21.9	39	25
08/28/2013	5	Foss Lake	33.1	91	15

Date	Site	Lake/Reservoir	CHLa (µg/L)	Turbidity (NTU)	Secchi Depth (cm)
10/13/2015	1	Foss Lake	11.1	7	82
10/13/2015	2	Foss Lake	10.2	8	77
10/13/2015	3	Foss Lake	17.6	16	50
10/13/2015	4	Foss Lake	17	16	45
10/13/2015	5	Foss Lake	19.8	11	35
08/10/2016	1	Foss Lake	3.04	5	170
08/10/2016	2	Foss Lake	3.02	4	190
08/10/2016	3	Foss Lake	5.73	6	117
08/10/2016	4	Foss Lake	9.2	14	70
08/10/2016	5	Foss Lake	21.7	22	40
11/27/2012	1	Grand Lake	1.31	10	80
11/27/2012	2	Grand Lake	1.59	10	105
11/27/2012	3	Grand Lake	2.11	11	95
11/27/2012	4	Grand Lake	5.76	10	100
11/27/2012	5	Grand Lake	2.84	12	93
11/27/2012	6	Grand Lake	7.11	10	90
11/27/2012	7	Grand Lake	3.09	9	100
11/27/2012	8	Grand Lake	5.68	12	77
11/27/2012	9	Grand Lake	5.63	14	78
11/27/2012	10	Grand Lake	6.55	15	85
11/27/2012	11	Grand Lake	13.1	13	87
11/27/2012	12	Grand Lake	12.9	13	54
11/27/2012	13	Grand Lake	29.5	14	47
02/05/2013	1	Grand Lake	1.56	4	150

Date	Site	Lake/Reservoir	CHLa (µg/L)	Turbidity (NTU)	Secchi Depth (cm)
02/05/2013	2	Grand Lake	2.63	4	150
02/05/2013	3	Grand Lake	4.04	4	150
02/05/2013	4	Grand Lake	10.6	7	85
02/05/2013	5	Grand Lake	5.54	6	90
02/05/2013	6	Grand Lake	4.82	7	100
02/05/2013	7	Grand Lake	4.33	10	75
02/05/2013	8	Grand Lake	5.67	10	65
02/05/2013	9	Grand Lake	7.31	11	65
02/05/2013	10	Grand Lake	9.09	10	65
02/05/2013	11	Grand Lake	5.98	9	75
02/05/2013	12	Grand Lake	14.5	16	45
02/05/2013	13	Grand Lake	10.7	20	40
04/02/2013	1	Grand Lake	9.85	6	115
04/02/2013	2	Grand Lake	10.7	6	120
04/02/2013	3	Grand Lake	13.1	10	95
04/02/2013	4	Grand Lake	20.5	10	85
04/02/2013	5	Grand Lake	21	13	101
04/02/2013	6	Grand Lake	16.5	7	116
04/02/2013	7	Grand Lake	15.8	20	67
04/02/2013	8	Grand Lake	11.7	18	45
04/02/2013	9	Grand Lake	7.54	49	30
04/02/2013	10	Grand Lake	22.7	12	47
04/02/2013	11	Grand Lake	24	11	64
04/02/2013	12	Grand Lake	17.4	94	13
04/02/2013	13	Grand Lake	8.68	206	12

Date	Site	Lake/Reservoir	CHLa (µg/L)	Turbidity (NTU)	Secchi Depth (cm)
08/13/2013	1	Grand Lake	27.7	4	73
08/13/2013	2	Grand Lake	39.7	6	89
08/13/2013	3	Grand Lake	48.9	6	86
08/13/2013	4	Grand Lake	43.6	5	82
08/13/2013	5	Grand Lake	27.3	11	78
08/13/2013	6	Grand Lake	x	9	
08/14/2013	7	Grand Lake	8.86	17	58
08/14/2013	8	Grand Lake	8.97	28	49
08/14/2013	9	Grand Lake	7.82	27	45
08/14/2013	10	Grand Lake	6.18	48	29
08/14/2013	11	Grand Lake	20.1	38	34
08/14/2013	12	Grand Lake	6.97	45	26
08/14/2013	13	Grand Lake	7.21	41	30
10/28/2014	1	Grand Lake	1.71	5	119
10/28/2014	2	Grand Lake	4.37	5	112
10/28/2014	3	Grand Lake	4.86	4	122
10/28/2014	4	Grand Lake	16.5	5	98
10/28/2014	5	Grand Lake	6.25	3	119
10/28/2014	6	Grand Lake	64.7	9	89
10/28/2014	7	Grand Lake	9.09	5	110
10/28/2014	8	Grand Lake	13.8	7	72
10/28/2014	9	Grand Lake	21.4	8	61
10/28/2014	10	Grand Lake	13.9	12	47
10/28/2014	11	Grand Lake	33	7	64
10/28/2014	12	Grand Lake	x	x	

Date	Site	Lake/Reservoir	CHLa (µg/L)	Turbidity (NTU)	Secchi Depth (cm)
10/28/2014	13	Grand Lake	x	x	
01/27/2015	1	Grand Lake	1.32	2	315
01/27/2015	2	Grand Lake	1.54	2	337
01/27/2015	3	Grand Lake	1.06	2	279
01/27/2015	4	Grand Lake	7.93	2	153
01/27/2015	5	Grand Lake	2.13	3	202
01/27/2015	6	Grand Lake	19.1	3	94
01/27/2015	7	Grand Lake	7.24	3	108
01/27/2015	8	Grand Lake	x	x	
01/27/2015	9	Grand Lake	x	x	
01/27/2015	10	Grand Lake	x	x	
01/27/2015	11	Grand Lake	x	x	
01/27/2015	12	Grand Lake	x	x	
01/27/2015	13	Grand Lake	x	x	
04/28/2015	1	Grand Lake	2.05	2	270
04/28/2015	2	Grand Lake	2.18	2	204
04/28/2015	3	Grand Lake	2.63	4	153
04/28/2015	4	Grand Lake	x	2	165
04/28/2015	5	Grand Lake	4.91	3	107
04/28/2015	6	Grand Lake	49.1	3	71
04/28/2015	7	Grand Lake	5.55	3	47
04/28/2015	8	Grand Lake	2.08	2	45
04/28/2015	9	Grand Lake	3.2	2	30
04/28/2015	10	Grand Lake	4.85	40	27
04/28/2015	11	Grand Lake	14.6	13	53

Date	Site	Lake/Reservoir	CHLa (µg/L)	Turbidity (NTU)	Secchi Depth (cm)
04/28/2015	12	Grand Lake	11.7	55	20
04/28/2015	13	Grand Lake	9.62	54	19
07/22/2015	1	Grand Lake	17.2	3	130
07/22/2015	2	Grand Lake	14.1	3	125
07/22/2015	3	Grand Lake	15.6	4	120
07/22/2015	4	Grand Lake	13.3	4	127
07/22/2015	5	Grand Lake	18.7	4	110
07/22/2015	6	Grand Lake	19.1	6	90
07/22/2015	7	Grand Lake	18.5	5	95
07/22/2015	8	Grand Lake	25.5	11	60
07/22/2015	9	Grand Lake	21.7	9	82
07/22/2015	10	Grand Lake	19.5	6	89
07/22/2015	11	Grand Lake	39.9	7	53
07/22/2015	12	Grand Lake	15.1	21	47
07/22/2015	13	Grand Lake	26.8	23	38
12/02/2014	1	Hugo Lake	27.7	53	23
12/02/2014	2	Hugo Lake	29.4	53	27
12/02/2014	3	Hugo Lake	24.7	54	25
12/02/2014	4	Hugo Lake	26.9	53	28
12/02/2014	5	Hugo Lake	26.9	54	24
03/03/2015	1	Hugo Lake	20.3	36	25
03/03/2015	2	Hugo Lake	30.2	37	29
03/03/2015	3	Hugo Lake	25.6	34	27
03/03/2015	4	Hugo Lake	19.6	34	34

Date	Site	Lake/Reservoir	CHLa (µg/L)	Turbidity (NTU)	Secchi Depth (cm)
03/03/2015	5	Hugo Lake	9.38	22	43
11/28/2016	1	Hugo Lake	13.2	18	35
11/28/2016	2	Hugo Lake	10.9	18	36
11/28/2016	3	Hugo Lake	14.4	45	21
11/28/2016	Canceled	Hugo Lake	Canceled	Canceled	Canceled
11/28/2016	5	Hugo Lake	15.3	50	10
02/28/2017	1	Hugo Lake	6.93	34	32
02/28/2017	2	Hugo Lake	8.68	34	31
02/28/2017	3	Hugo Lake	9.88	45	32
02/28/2017	Canceled	Hugo Lake	Canceled	Canceled	Canceled
02/28/2017	Canceled	Hugo Lake	Canceled	Canceled	Canceled
10/09/2012	1	Kaw Lake	5.42	9	58
10/09/2012	2	Kaw Lake	4.7	11	50
10/09/2012	3	Kaw Lake	12.1	13	30
10/09/2012	4	Kaw Lake	16.4	36	20
10/09/2012	5	Kaw Lake	52.6	57	20
02/11/2013	1	Kaw Lake	no data	5	93
02/11/2013	2	Kaw Lake	no data	4	130
02/11/2013	3	Kaw Lake	4.98	12	60
02/11/2013	4	Kaw Lake	6.88	18	50
02/11/2013	5	Kaw Lake	9.98	18	29
04/22/2013	1	Kaw Lake	3.62	10	65
04/22/2013	2	Kaw Lake	6.26	12	60
04/22/2013	3	Kaw Lake	15.3	20	35

Date	Site	Lake/Reservoir	CHLa (µg/L)	Turbidity (NTU)	Secchi Depth (cm)
04/22/2013	4	Kaw Lake	14.2	44	30
04/22/2013	5	Kaw Lake	40.6	32	28
10/15/2014	1	Kaw Lake	2.6	14	49
10/15/2014	2	Kaw Lake	3.53	17	38
10/15/2014	3	Kaw Lake	7	23	31
10/15/2014	4	Kaw Lake	8.67	38	27
10/15/2014	5	Kaw Lake	11.5	308	4
01/13/2015	1	Kaw Lake	2.22	11	92
01/13/2015	2	Kaw Lake	2.1	7	91
01/13/2015	3	Kaw Lake	9.85	9	81
01/13/2015	4	Kaw Lake	3.4	14	64
01/13/2015	5	Kaw Lake	frozen	frozen	frozen
04/21/2015	1	Kaw Lake	0.82	3	201
04/21/2015	2	Kaw Lake	1.02	3	159
04/21/2015	3	Kaw Lake	4.97	12	61
04/21/2015	4	Kaw Lake	1.79	12	52
04/21/2015	5	Kaw Lake	45.2	19	35
07/06/2015	1	Kaw Lake	6.29	7	112
07/06/2015	2	Kaw Lake	16.2	7	103
07/06/2015	3	Kaw Lake	28.8	7	90
07/06/2015	4	Kaw Lake	34.2	9	75
07/06/2015	5	Kaw Lake	26.5	11	63
11/01/2016	1	Keystone Lake	1.6	46	35
11/01/2016	2	Keystone Lake	2.35	48	30

Date	Site	Lake/Reservoir	CHLa (µg/L)	Turbidity (NTU)	Secchi Depth (cm)
11/01/2016	3	Keystone Lake	12.9	67	28
11/01/2016	4	Keystone Lake	7.77	67	20
11/01/2016	5	Keystone Lake	72.2	31	20
11/01/2016	6	Keystone Lake	1.56	45	25
11/01/2016	7	Keystone Lake	18.5	17	45
11/01/2016	8	Keystone Lake	5.77	25	40
11/01/2016	9	Keystone Lake	2.71	34	23
11/01/2016	10	Keystone Lake	9.09	34	25
11/01/2016	11	Keystone Lake	98.6	103	10
11/01/2016	na	Keystone Lake			
01/31/2017	1	Keystone Lake	37.5	5	83
01/31/2017	2	Keystone Lake	24.7	11	60
01/31/2017	3	Keystone Lake	23.7	9	70
01/31/2017	4	Keystone Lake	18.7	17	45
01/31/2017	5	Keystone Lake	25.4	35	25
01/31/2017	6	Keystone Lake	36.3	6	77
01/31/2017	7	Keystone Lake	64	7	70
01/31/2017	8	Keystone Lake	44	5	100
01/31/2017	9	Keystone Lake	34.1	4	80
01/31/2017	10	Keystone Lake	119	7	45
01/31/2017	11	Keystone Lake	39.4	52	18
01/31/2017	na	Keystone Lake			
05/02/2017	1	Keystone Lake	0.96	56.8	21
05/02/2017	2	Keystone Lake	1.36	82	15
05/02/2017	3	Keystone Lake	6.16	97.5	11

Date	Site	Lake/Reservoir	CHLa (µg/L)	Turbidity (NTU)	Secchi Depth (cm)
05/02/2017	4	Keystone Lake	10.3	128	10
05/02/2017	5	Keystone Lake	17.2	196	10
05/02/2017	6	Keystone Lake	1.86	54.4	20
05/02/2017	7	Keystone Lake	17.8	15.4	55
05/02/2017	8	Keystone Lake	5.47	34.7	30
05/02/2017	9	Keystone Lake	1.92	53.6	19
05/02/2017	10	Keystone Lake	8.93	435	6
05/02/2017	11	Keystone Lake	7.61	556	4
05/02/2017	12	Keystone Lake	8.01	599	4
09/18/2017	1	Keystone Lake	6.91	6	107
09/18/2017	2	Keystone Lake	7.91	11	70
09/18/2017	3	Keystone Lake	29.3	16	41
09/18/2017	4	Keystone Lake	64.9	34	23
09/18/2017	5	Keystone Lake	57.6	63	19
09/18/2017	6	Keystone Lake	15.4	9	86
09/18/2017	7	Keystone Lake	20.7	11	65
09/18/2017	8	Keystone Lake	25	6	84
09/18/2017	9	Keystone Lake	23.7	10	74
09/18/2017	10	Keystone Lake	26.4	13	47
09/18/2017	11	Keystone Lake	44.6	90	13
09/18/2017	12	Keystone Lake	na	na	
10/10/2012	1	Lake Carl Blackwell	19.1	27	25
10/10/2012	2	Lake Carl Blackwell	33.4	31	28

Date	Site	Lake/Reservoir	CHLa (µg/L)	Turbidity (NTU)	Secchi Depth (cm)
10/10/2012	3	Lake Carl Blackwell	28	25	20
10/10/2012	4	Lake Carl Blackwell	20.9	61	13
03/06/2013	1	Lake Carl Blackwell	x	20	60
03/06/2013	2	Lake Carl Blackwell	x	22	52
03/06/2013	3	Lake Carl Blackwell	x	17	48
03/06/2013	4	Lake Carl Blackwell	x	x	
04/24/2013	1	Lake Carl Blackwell	33.5	16	54
04/24/2013	2	Lake Carl Blackwell	45.3	23	46
04/24/2013	3	Lake Carl Blackwell	34	20	42
04/24/2013	4	Lake Carl Blackwell	x	x	
07/01/2013	1	Lake Carl Blackwell	10.2	13	43
07/01/2013	2	Lake Carl Blackwell	23.5	32	22
07/01/2013	3	Lake Carl Blackwell	16.9	17	35
07/01/2013	4	Lake Carl Blackwell	25.1	60	14
12/21/2015	1	Lake Carl Blackwell	5.4	27	33
12/21/2015	2	Lake Carl Blackwell	5.1	30	32
12/21/2015	3	Lake Carl Blackwell	6.2	30	30
12/21/2015	4	Lake Carl Blackwell	6.9	39	X
09/27/2016	1	Lake Carl Blackwell	18.5	11	62
09/27/2016	2	Lake Carl Blackwell	27.3	16	50
09/27/2016	3	Lake Carl Blackwell	26.5	12	44
09/27/2016	4	Lake Carl Blackwell	27.0	38	24
12/17/2012	1	Lake Eucha	11.9	7	110
12/17/2012	2	Lake Eucha	15	6	112

Date	Site	Lake/Reservoir	CHLa (µg/L)	Turbidity (NTU)	Secchi Depth (cm)
12/17/2012	3	Lake Eucha	1.2	9	118
02/4/2013	1	Lake Eucha	11.3	5	150
02/4/2013	2	Lake Eucha	0.6	11	95
02/4/2013	3	Lake Eucha	13.3	5	150
03/26/2013	1	Lake Eucha	20.3	4	144
03/26/2013	2	Lake Eucha	14.1	7	90
03/26/2013	3	Lake Eucha	2.38		210
08/19/2013	1	Lake Eucha	16.9	5	70
08/19/2013	2	Lake Eucha	15.4	3	78
08/19/2013	3	Lake Eucha	18.3	4	75
10/27/2014	1	Lake Eucha	17.7	no data	no data
10/27/2014	2	Lake Eucha	15.9	no data	no data
10/27/2014	3	Lake Eucha	23.9	no data	no data
01/26/2015	1	Lake Eucha	8.57	3	140
01/26/2015	2	Lake Eucha	9.41	3	100
01/26/2015	3	Lake Eucha	9.78	6	81
04/27/2015	1	Lake Eucha	14.3	2	132
04/27/2015	2	Lake Eucha	13	2	173
04/27/2015	3	Lake Eucha	19.7	2	85
07/21/2015	1	Lake Eucha	41.9	7	78
07/21/2015	2	Lake Eucha	39.6	5	75
07/21/2015	3	Lake Eucha	38.7	7	71
11/13/2012	1	Fort Gibson Lake	13.4	5	102
11/13/2012	2	Fort Gibson Lake	12.1	5	88

Date	Site	Lake/Reservoir	CHLa (µg/L)	Turbidity (NTU)	Secchi Depth (cm)
11/13/2012	3	Fort Gibson Lake	11.7	8	78
11/13/2012	4	Fort Gibson Lake	10.7	7	78
01/22/2013	1	Fort Gibson Lake	22.1	6	70
01/22/2013	2	Fort Gibson Lake	17	7	70
01/22/2013	3	Fort Gibson Lake	18.7	8	70
01/22/2013	4	Fort Gibson Lake	22.8	8	70
04/01/2013	1	Fort Gibson Lake	24.2	17	54
04/01/2013	2	Fort Gibson Lake	17.1	7	102
04/01/2013	3	Fort Gibson Lake	15.7	6	110
04/01/2013	4	Fort Gibson Lake	13.5	7	98
10/07/2014	1	Fort Gibson Lake	9.51	7	87
10/07/2014	2	Fort Gibson Lake	15.1	6	78
10/07/2014	3	Fort Gibson Lake	31.8	6	71
10/07/2014	4	Fort Gibson Lake	18.1	9	61
10/07/2014	5	Fort Gibson Lake	18.1	6	67
10/07/2014	6	Fort Gibson Lake	36.9	8	62
10/07/2014	7	Fort Gibson Lake	22.2	10	53
10/07/2014	8	Fort Gibson Lake	22.3	10	32
01/13/2015	1	Fort Gibson Lake	14.3	6	72
01/13/2015	2	Fort Gibson Lake	15.3	7	74
01/13/2015	3	Fort Gibson Lake	15.8	6	62
01/13/2015	4	Fort Gibson Lake	15.7	6	67
01/13/2015	5	Fort Gibson Lake	15.2	7	69
01/13/2015	6	Fort Gibson Lake	14.7	6	72
01/13/2015	7	Fort Gibson Lake	11.6	7	69

Date	Site	Lake/Reservoir	CHLa (µg/L)	Turbidity (NTU)	Secchi Depth (cm)
01/13/2015	8	Fort Gibson Lake	7.06	7	77
04/14/2015	1	Fort Gibson Lake	24.8	6	82
04/14/2015	2	Fort Gibson Lake	35	9	62
04/14/2015	3	Fort Gibson Lake	26.5	9	72
04/14/2015	4	Fort Gibson Lake	22.7	10	65
04/14/2015	5	Fort Gibson Lake	38.9	15	5.2
04/14/2015	6	Fort Gibson Lake	19.9	9	11.3
04/14/2015	7	Fort Gibson Lake	17.4	12	11.5
04/14/2015	8	Fort Gibson Lake	6.54	15	6.3
06/23/2015	1	Fort Gibson Lake	25.3	4	98
06/23/2015	2	Fort Gibson Lake	18.4	4	85
06/23/2015	3	Fort Gibson Lake	30.4	5	75
06/23/2015	4	Fort Gibson Lake	30.4	4	89
06/23/2015	5	Fort Gibson Lake	16.5	4	82
06/23/2015	6	Fort Gibson Lake	28.2	7	68
06/23/2015	7	Fort Gibson Lake	6.89	8	59
06/23/2015	8	Fort Gibson Lake	23.7	7	78
03/13/2013	1	Lake Hefner	16.7	12	52
03/13/2013	2	Lake Hefner	19.8	12	52
03/13/2013	3	Lake Hefner	25.1	12	45
08/12/2013	1	Lake Hefner	29.4	6	70
08/12/2013	2	Lake Hefner	36.2	7	60
08/12/2013	3	Lake Hefner	24.8	7	62
09/17/2013	1	Lake Hefner	44.3	x	x

Date	Site	Lake/Reservoir	CHLa (µg/L)	Turbidity (NTU)	Secchi Depth (cm)
09/17/2013	2	Lake Hefner	34.1	x	x
09/17/2013	3	Lake Hefner	44.7	x	x
07/29/2013	1	Lake Hefner	23.3	x	x
07/29/2013	3	Lake Hefner	22.2	x	x
10/21/2015	1	Lake Hefner	43.7	6	50
10/21/2015	2	Lake Hefner	41.2	6	60
10/21/2015	3	Lake Hefner	45	6	58
08/09/2016	1	Lake Hefner	65.9	9	70
08/09/2016	2	Lake Hefner	57.9	13	52
08/09/2016	3	Lake Hefner	61	9	61
10/16/2013	1	Lake McMertury	8.94	X	55
10/16/2013	2	Lake McMertury	10	X	50
10/16/2013	3	Lake McMertury	10	X	38
01/13/2014	1	Lake McMertury	3.3	16	50
01/13/2014	2	Lake McMertury	3.03	17	52
01/13/2014	3	Lake McMertury	2.98	21	42
04/07/2014	1	Lake McMertury	1.89	17	68
04/07/2014	2	Lake McMertury	3.45	17	62
04/07/2014	3	Lake McMertury	6.01	21	47
07/01/2014	1	Lake McMertury	6.94	15	42
07/01/2014	2	Lake McMertury	4.59	18	45
07/01/2014	3	Lake McMertury	7.04	32	30
10/03/2016	1	Lake McMertury	6.97	7	97
10/03/2016	2	Lake McMertury	12.1	10	94

Date	Site	Lake/Reservoir	CHLa (µg/L)	Turbidity (NTU)	Secchi Depth (cm)
10/03/2016	3	Lake McMertury	7.41	9	89
01/04/2017	1	Lake McMertury	5.49	12	70
01/04/2017	2	Lake McMertury	4.96	14	70
01/04/2017	3	Lake McMertury	5.13	10	70
04/04/2017	1	Lake McMertury	9.13	10	X
04/04/2017	2	Lake McMertury	8.39	12	X
04/04/2017	3	Lake McMertury	8.27	19	X
12/12/2012	1	McGee Creek Reservoir	3.02	8	105
12/12/2012	2	McGee Creek Reservoir	5.82	9	78
12/12/2012	3	McGee Creek Reservoir	X	6	105
12/12/2012	4	McGee Creek Reservoir	10.7	7	85
12/12/2012	5	McGee Creek Reservoir	3.7	7	100
03/13/2013	1	McGee Creek Reservoir	3.89	43	130
03/13/2013	2	McGee Creek Reservoir	5.03	72	100
03/13/2013	3	McGee Creek Reservoir	3.87	7	80
03/13/2013	4	McGee Creek Reservoir	6.35	19	70
03/13/2013	5	McGee Creek Reservoir	3.68	22	300
05/14/2013	1	McGee Creek Reservoir	2.81	6	142
05/14/2013	2	McGee Creek Reservoir	5.09	6	116
05/14/2013	3	McGee Creek Reservoir	3.64	5	145
05/14/2013	4	McGee Creek Reservoir	5.29	5	140
05/14/2013	5	McGee Creek Reservoir	3.8	6	122
07/29/2013	1	McGee Creek Reservoir	10.2	4	160
07/29/2013	2	McGee Creek Reservoir	14.7	4	159

Date	Site	Lake/Reservoir	CHLa (µg/L)	Turbidity (NTU)	Secchi Depth (cm)
07/29/2013	3	McGee Creek Reservoir	12.2	3	145
07/29/2013	4	McGee Creek Reservoir	7.5	5	125
07/29/2013	5	McGee Creek Reservoir	10.6	4	155
12/03/2014	1	McGee Creek Reservoir	4.34	7	93
12/03/2014	2	McGee Creek Reservoir	2.52	11	75
12/03/2014	3	McGee Creek Reservoir	6.99	6	104
12/03/2014	4	McGee Creek Reservoir	10.8	8	80
12/03/2014	5	McGee Creek Reservoir	4.35	8	87
03/03/2015	1	McGee Creek Reservoir	1.53	8	103
03/03/2015	2	McGee Creek Reservoir	3.69	12	63
03/03/2015	3	McGee Creek Reservoir	3.19	7	106
03/03/2015	4	McGee Creek Reservoir	2.58	11	67
03/03/2015	5	McGee Creek Reservoir	3.92	8	80
06/29/2015	1	McGee Creek Reservoir	13.2	4	67
06/29/2015	2	McGee Creek Reservoir	11.6	5	70
06/29/2015	3	McGee Creek Reservoir	14	3	83
06/29/2015	4	McGee Creek Reservoir	12.9	3	101
06/29/2015	5	McGee Creek Reservoir	10.5	4	84
09/01/2015	1	McGee Creek Reservoir	4.83	3	140
09/01/2015	2	McGee Creek Reservoir	7.68	3	130
09/01/2015	3	McGee Creek Reservoir	4.75	2	135
09/01/2015	4	McGee Creek Reservoir	10.9	3	110
09/01/2015	5	McGee Creek Reservoir	5.55	3	140
01/22/2013	1	Lake Thunderbird	5.8	21	33

Date	Site	Lake/Reservoir	CHLa (µg/L)	Turbidity (NTU)	Secchi Depth (cm)
01/22/2013	2	Lake Thunderbird	6.95	23	30
01/22/2013	3	Lake Thunderbird	8.11	25	25
01/22/2013	4	Lake Thunderbird	6.11	24	30
01/22/2013	5	Lake Thunderbird	10.3	23	28
01/22/2013	6	Lake Thunderbird	10	28	20
01/22/2013	7	Lake Thunderbird	10	24	29
03/13/2013	1	Lake Thunderbird	7.37	23	40
03/13/2013	2	Lake Thunderbird	5.99	23	35
03/13/2013	3	Lake Thunderbird	8.05	24	30
03/13/2013	4	Lake Thunderbird	5.67	25	40
03/13/2013	5	Lake Thunderbird	10.4	25	30
03/13/2013	6	Lake Thunderbird			
03/13/2013	7	Lake Thunderbird	14.5	28	25
10/20/2014	1	Lake Thunderbird	41.4	10	56
10/20/2014	2	Lake Thunderbird	39.3	11	50
10/20/2014	3	Lake Thunderbird	46.3	11	47
10/20/2014	4	Lake Thunderbird	33.8	11	42
10/20/2014	5	Lake Thunderbird	38.6	14	45
10/20/2014	6	Lake Thunderbird	23.3	23	X
10/20/2014	7	Lake Thunderbird	-	-	X
10/20/2014	8	Lake Thunderbird	-	-	X
10/20/2014	11	Lake Thunderbird	-	-	X
01/14/2015	1	Lake Thunderbird	10.2	7	102
01/14/2015	2	Lake Thunderbird	9.29	8	97
01/14/2015	3	Lake Thunderbird	13.4	7	97
01/14/2015	4	Lake Thunderbird	9.57	8	80

Date	Site	Lake/Reservoir	CHLa (µg/L)	Turbidity (NTU)	Secchi Depth (cm)
01/14/2015	5	Lake Thunderbird	14.2	10	58
01/14/2015	6	Lake Thunderbird	12.3	22	23
01/14/2015	7	Lake Thunderbird	6.51	9	79
01/14/2015	8	Lake Thunderbird	-	-	-
01/14/2015	11	Lake Thunderbird	-	-	-
04/23/2015	1	Lake Thunderbird	5.5	13	70
04/23/2015	2	Lake Thunderbird	8	11	76
04/23/2015	3	Lake Thunderbird	13.9	14	70
04/23/2015	4	Lake Thunderbird	7.17	14	68
04/23/2015	5	Lake Thunderbird	11.7	24	38
04/23/2015	6	Lake Thunderbird	53.8	78	16
04/23/2015	7	Lake Thunderbird	15.7	17	57
04/23/2015	8	Lake Thunderbird	21.8	-	38
04/23/2015	11	Lake Thunderbird	35.6	-	21
05/13/2015	1	Lake Thunderbird	3.96	46	30
05/13/2015	2	Lake Thunderbird	5.29	63	28
05/13/2015	3	Lake Thunderbird	11.8	51	20
05/13/2015	4	Lake Thunderbird	5.56	50	28
05/13/2015	5	Lake Thunderbird	7.5	71	22
05/13/2015	6	Lake Thunderbird	6.4	120	9
05/13/2015	7	Lake Thunderbird	-	-	-
05/13/2015	8	Lake Thunderbird	6.03	99	9
05/13/2015	11	Lake Thunderbird	5.75	104	18
06/03/2015	1	Lake Thunderbird	9.40	21	27
06/03/2015	2	Lake Thunderbird	15	20	12
06/03/2015	3	Lake Thunderbird	17.2	26	24

Date	Site	Lake/Reservoir	CHLa (µg/L)	Turbidity (NTU)	Secchi Depth (cm)
06/03/2015	4	Lake Thunderbird	18.6	9	27
06/03/2015	5	Lake Thunderbird	21.4	23	33
06/03/2015	6	Lake Thunderbird	22.8	27	34
06/03/2015	7	Lake Thunderbird	-	-	-
06/03/2015	8	Lake Thunderbird	26.7	22	25
06/03/2015	11	Lake Thunderbird	17.8	24	33
06/17/2015	1	Lake Thunderbird	13.90	7	98
06/17/2015	2	Lake Thunderbird	24.1	8	88
06/17/2015	3	Lake Thunderbird	30.4	11	69
06/17/2015	4	Lake Thunderbird	18.1	7	96
06/17/2015	5	Lake Thunderbird	22.2	12	73
06/17/2015	6	Lake Thunderbird	14.3	52	31
06/17/2015	7	Lake Thunderbird	-	-	-
06/17/2015	8	Lake Thunderbird	20.9	16	59
06/17/2015	11	Lake Thunderbird	26.5	17	62
07/01/2015	1	Lake Thunderbird	22.73	6	62
07/01/2015	2	Lake Thunderbird	19.5	7	38
07/01/2015	3	Lake Thunderbird	23.2	9	58
07/01/2015	4	Lake Thunderbird	21.3	7	68
07/01/2015	5	Lake Thunderbird	18.1	7	64
07/01/2015	6	Lake Thunderbird	32.7	13	33
07/01/2015	7	Lake Thunderbird	17.9	11	-
07/01/2015	8	Lake Thunderbird	0.13	10	33
07/01/2015	11	Lake Thunderbird	15.2	10	39
07/15/2015	1	Lake Thunderbird	22.03	6	52
07/15/2015	2	Lake Thunderbird	20.9	9	56

Date	Site	Lake/Reservoir	CHLa (µg/L)	Turbidity (NTU)	Secchi Depth (cm)
07/15/2015	3	Lake Thunderbird	22.7	10	34
07/15/2015	4	Lake Thunderbird	20.5	6	53
07/15/2015	5	Lake Thunderbird	19.4	11	41
07/15/2015	6	Lake Thunderbird	20.3	20	25
07/15/2015	7	Lake Thunderbird	-	-	-
07/15/2015	8	Lake Thunderbird	20.2	12	36
07/15/2015	11	Lake Thunderbird	16.7	19	31
07/29/2015	1	Lake Thunderbird	23.63	7	54
07/29/2015	2	Lake Thunderbird	31	8	63
07/29/2015	3	Lake Thunderbird	27.3	9	57
07/29/2015	4	Lake Thunderbird	25.6	6	67
07/29/2015	5	Lake Thunderbird	34.3	17	29
07/29/2015	6	Lake Thunderbird	14.4	43	24
07/29/2015	7	Lake Thunderbird	-	-	-
07/29/2015	8	Lake Thunderbird	29.6	25	35
07/29/2015	11	Lake Thunderbird	37.7	48	30
08/12/2015	1	Lake Thunderbird	29.45	9	40
08/12/2015	2	Lake Thunderbird	29.3	8	57
08/12/2015	3	Lake Thunderbird	38	9	6
08/12/2015	4	Lake Thunderbird	31.3	9	68
08/12/2015	5	Lake Thunderbird	26.6	9	59
08/12/2015	6	Lake Thunderbird	23.8	45	48
08/12/2015	7	Lake Thunderbird	-	-	-
08/12/2015	8	Lake Thunderbird	22.7	21	39
08/12/2015	11	Lake Thunderbird	34.2	16	45
08/26/2015	1	Lake Thunderbird	31.57	6	72

Date	Site	Lake/Reservoir	CHLa (µg/L)	Turbidity (NTU)	Secchi Depth (cm)
08/26/2015	2	Lake Thunderbird	32.7	7	66
08/26/2015	3	Lake Thunderbird	38.1	9	62
08/26/2015	4	Lake Thunderbird	29.2	8	64
08/26/2015	5	Lake Thunderbird	48.1	15	47
08/26/2015	6	Lake Thunderbird	41.5	40	21
08/26/2015	7	Lake Thunderbird	-	-	-
08/26/2015	8	Lake Thunderbird	35.8	23	35
08/26/2015	11	Lake Thunderbird	35	56	21
09/09/2015	1	Lake Thunderbird	30.37	5	75
09/09/2015	2	Lake Thunderbird	38.6	6	53
09/09/2015	3	Lake Thunderbird	45.2	12	39
09/09/2015	4	Lake Thunderbird	38.6	5	63
09/09/2015	5	Lake Thunderbird	34.3	11	40
09/09/2015	6	Lake Thunderbird	57.5	73	9
09/09/2015	7	Lake Thunderbird	-	-	-
09/09/2015	8	Lake Thunderbird	24.3	27	19
09/09/2015	11	Lake Thunderbird	66.2	41	13
09/23/2015	1	Lake Thunderbird	24.60	8	68
09/23/2015	2	Lake Thunderbird	37.4	7	85
09/23/2015	3	Lake Thunderbird	52	10	54
09/23/2015	4	Lake Thunderbird	39.8	7	68
09/23/2015	5	Lake Thunderbird	44.3	9	48
09/23/2015	6	Lake Thunderbird	45.7	68	13
09/23/2015	7	Lake Thunderbird	-	-	-
09/23/2015	8	Lake Thunderbird	48.3	24	30
09/23/2015	11	Lake Thunderbird	41.1	39	13

Date	Site	Lake/Reservoir	CHLa (µg/L)	Turbidity (NTU)	Secchi Depth (cm)
12/09/2015	1	Lake Thunderbird	6.02	X	X
12/09/2015	2	Lake Thunderbird	3.1	X	X
12/09/2015	3	Lake Thunderbird	13.4	X	X
12/09/2015	4	Lake Thunderbird	4.21	X	X
12/09/2015	5	Lake Thunderbird	5.02	X	X
12/09/2015	6	Lake Thunderbird	13.2	X	X
12/09/2015	7	Lake Thunderbird	-	X	X
12/09/2015	8	Lake Thunderbird	25.4	X	X
12/09/2015	11	Lake Thunderbird	8.52	X	X
12/16/2013	1	Oologah Lake	3.2	17	29
12/16/2013	2	Oologah Lake	3.17	18	30
12/16/2013	3	Oologah Lake	3.52	20	43
12/16/2013	4	Oologah Lake	2.68	17	33
12/16/2013	5	Oologah Lake	2.5	23	24
12/16/2013	6	Oologah Lake	4.73	43	20
12/16/2013	7	Oologah Lake	5.21	34	-
03/10/2014	1	Oologah Lake	27.6	10	54
03/10/2014	2	Oologah Lake	27.7	9	66
03/10/2014	3	Oologah Lake	15.8	8	53
03/10/2014	4	Oologah Lake	22	10	55
03/10/2014	5	Oologah Lake	14.8	11	46
03/10/2014	6	Oologah Lake	10.7	10	47
03/10/2014	7	Oologah Lake	9.15	9	50
05/19/2014	1	Oologah Lake	5.21	19	31
05/19/2014	2	Oologah Lake	4.23	27	-

Date	Site	Lake/Reservoir	CHLa (µg/L)	Turbidity (NTU)	Secchi Depth (cm)
05/19/2014	3	Oologah Lake	9.89	25	25
05/19/2014	4	Oologah Lake	6.46	27	22
05/19/2014	5	Oologah Lake	10.3	36	27
05/19/2014	6	Oologah Lake	5.27	47	23
05/19/2014	7	Oologah Lake	9.57	57	19
08/25/2014	1	Oologah Lake	3.52	6	70
08/25/2014	2	Oologah Lake	6.89	8	51
08/25/2014	3	Oologah Lake	11.8	10	50
08/25/2014	4	Oologah Lake	5.58	7	60
08/25/2014	5	Oologah Lake	7.24	12	43
08/25/2014	6	Oologah Lake	13.8	15	38
08/25/2014	7	Oologah Lake	17	20	35
11/14/2016	1	Oologah Lake	0.92	30	34
11/14/2016	2	Oologah Lake	1.12	32	29
11/14/2016	3	Oologah Lake	3.05	29	35
11/14/2016	4	Oologah Lake	0.87	40	25
11/14/2016	5	Oologah Lake	1.2	45	20
11/14/2016	6	Oologah Lake	5.11	50	17
11/14/2016	7	Oologah Lake	5.29	56	18
02/13/2017	1	Oologah Lake	3.83	17	63
02/13/2017	2	Oologah Lake	4.98	16	65
02/13/2017	3	Oologah Lake	9.86	15	69
02/13/2017	4	Oologah Lake	9.64	13	58
02/13/2017	5	Oologah Lake	11.6	13	58
02/13/2017	6	Oologah Lake	46.1	27	32
02/13/2017	7	Oologah Lake	60.5	35	24

Date	Site	Lake/Reservoir	CHLa (µg/L)	Turbidity (NTU)	Secchi Depth (cm)
12/16/2014	1	Robert S Kerr Reservoir	8.47	26	29
12/16/2014	2	Robert S Kerr Reservoir	12.5	25	32
12/16/2014	3	Robert S Kerr Reservoir	5.34	43	26
12/16/2014	4	Robert S Kerr Reservoir	9.99	25	28
12/16/2014	5	Robert S Kerr Reservoir	15.5	26	27
12/16/2014	6	Robert S Kerr Reservoir	9.12	12	44
03/18/2015	1	Robert S Kerr Reservoir	10.5	36	34
03/18/2015	2	Robert S Kerr Reservoir	15	23	42
03/18/2015	3	Robert S Kerr Reservoir	4.72	79	20
03/18/2015	4	Robert S Kerr Reservoir	22.4	26	34
06/16/2015	1	Robert S Kerr Reservoir	5.93	56	27
06/16/2015	2	Robert S Kerr Reservoir	10.8	48	26
06/16/2015	3	Robert S Kerr Reservoir	22.8	56	29
06/16/2015	4	Robert S Kerr Reservoir	5.47	54	26
06/16/2015	5	Robert S Kerr Reservoir	4.99	46	27
06/16/2015	6	Robert S Kerr Reservoir	5.98	63	-
09/22/2015	1	Robert S Kerr Reservoir	8.75	28	27
09/22/2015	2	Robert S Kerr Reservoir	12.3	28	21
09/22/2015	3	Robert S Kerr Reservoir	43.5	19	22
09/22/2015	4	Robert S Kerr Reservoir	13.2	36	15
09/22/2015	5	Robert S Kerr Reservoir	15.6	28	15
09/22/2015	6	Robert S Kerr Reservoir	26	17	22
12/05/2012	1	Waurika Lake	25.3	18	37

Date	Site	Lake/Reservoir	CHLa (µg/L)	Turbidity (NTU)	Secchi Depth (cm)
12/05/2012	2	Waurika Lake	25.7	17	35
12/05/2012	3	Waurika Lake	30.3	21	31
12/05/2012	4	Waurika Lake	23.5	73	12
02/27/2013	1	Waurika Lake	4.88	20	50
02/27/2013	2	Waurika Lake	6.88	22	45
02/27/2013	3	Waurika Lake	7.32	28	45
02/27/2013	4	Waurika Lake	34.5	169	10
04/30/2013	1	Waurika Lake	8.05	27	45
04/30/2013	2	Waurika Lake	14.4	30	40
04/30/2013	3	Waurika Lake	37.7	42	15
04/30/2013	4	Waurika Lake	41.8	204	10
07/15/2013	1	Waurika Lake	9.85	23	32
07/15/2013	2	Waurika Lake	13.9	20	26
07/15/2013	3	Waurika Lake	23.3	35	42
07/15/2013	4	Waurika Lake	44.5	158	15
12/02/2014	1	Waurika Lake	5.13	23	40
12/02/2014	2	Waurika Lake	5.65	25	32
12/02/2014	3	Waurika Lake	8.53	34	25
12/02/2014	4	Waurika Lake	19.5	-	-
12/02/2014	5	Waurika Lake	-	-	-
03/09/2015	1	Waurika Lake	24.6	12	65
03/09/2015	2	Waurika Lake	20.8	15	58
03/09/2015	3	Waurika Lake	16.8	24	39
03/09/2015	4	Waurika Lake	17.9	-	-
03/09/2015	5	Waurika Lake	-	-	-

Date	Site	Lake/Reservoir	CHLa (µg/L)	Turbidity (NTU)	Secchi Depth (cm)
06/08/2015	1	Waurika Lake	2.79	37	30
06/08/2015	2	Waurika Lake	9.52	37	32
06/08/2015	3	Waurika Lake	7.17	36	32
06/08/2015	4	Waurika Lake	37.2	17	52
06/08/2015	5	Waurika Lake	37.20	12	57
08/31/2015	1	Waurika Lake	10.9	10	82
08/31/2015	2	Waurika Lake	14.6	8	78
08/31/2015	3	Waurika Lake	9.04	9	75
08/31/2015	4	Waurika Lake	14.4	6	88
08/31/2015	5	Waurika Lake	14.4	10	70
01/28/2013	1	Lake Texoma	4.49	3	250
01/28/2013	2	Lake Texoma	4.89	2	180
01/28/2013	3	Lake Texoma	8.38	3	-
01/28/2013	4	Lake Texoma	5.97	5	-
04/15/2013	1	Lake Texoma	1.76	3	105
04/15/2013	2	Lake Texoma	6.37	3	95
04/15/2013	3	Lake Texoma	4	2	105
04/15/2013	4	Lake Texoma	4.44	3	85
08/26/2013	1	Lake Texoma	18.2	2	118
08/26/2013	2	Lake Texoma	24.3	2	108
08/26/2013	3	Lake Texoma	18.9	3	83
08/26/2013	4	Lake Texoma	26.2	4	68
08/26/2013	5	Lake Texoma	20.2	3	83
08/26/2013	6	Lake Texoma	22.7	3	98

Date	Site	Lake/Reservoir	CHLa (µg/L)	Turbidity (NTU)	Secchi Depth (cm)
08/26/2013	7	Lake Texoma	24	4	77
08/26/2013	8	Lake Texoma	23	4	78
08/26/2013	9	Lake Texoma	22.3	7	69
08/26/2013	10	Lake Texoma	31.9	10	58
08/26/2013	11	Lake Texoma	32.8	6	68
08/26/2013	12	Lake Texoma	40.3	11	59
08/26/2013	13	Lake Texoma	35	44	25
12/07/2015	1	Lake Texoma	3.37	5	106
12/07/2015	2	Lake Texoma	3.84	5	112
12/07/2015	3	Lake Texoma	6.77	5	102
12/07/2015	4	Lake Texoma	5.17	8	84
12/07/2015	5	Lake Texoma	6.83	5	101
12/07/2015	6	Lake Texoma	5.25	4	90
12/07/2015	7	Lake Texoma	5.73	7	78
12/07/2015	8	Lake Texoma	9.12	17	40
12/07/2015	9	Lake Texoma	3.91	38	29
12/07/2015	10	Lake Texoma	3.98	53	27
12/07/2015	11	Lake Texoma	7.9	29	25
12/07/2015	12	Lake Texoma	2.52	77	11
12/07/2015	13	Lake Texoma	3.92	88	7
09/19/2016	1	Lake Texoma	11	3	130
09/19/2016	2	Lake Texoma	9.02	3	120
09/19/2016	3	Lake Texoma	11.1	2	102
09/19/2016	4	Lake Texoma	13	6	95
09/19/2016	5	Lake Texoma	11	4	110

Date	Site	Lake/Reservoir	CHLa (µg/L)	Turbidity (NTU)	Secchi Depth (cm)
09/19/2016	6	Lake Texoma	10.5	5	126
09/19/2016	7	Lake Texoma	12.4	4	92
09/19/2016	8	Lake Texoma	17.6	4	78
09/19/2016	9	Lake Texoma	23	9	44
09/19/2016	10	Lake Texoma	20.8	11	40
09/19/2016	11	Lake Texoma	16.6	7	52
09/19/2016	12	Lake Texoma	20	6	58
09/19/2016	13	Lake Texoma	27.8	14	30

VITA

ABUBAKARR SIDIQUE MANSARAY

Candidate for the Degree of

Doctor of Philosophy

Dissertation: SATELLITE REMOTE SENSING OF HARMFUL ALGAL BLOOMS IN THE GRAND LAKE WATERSHED

Major Field: ENVIRONMENAL SCIENCE

Biographical:

Education:

Completed the requirements for the Doctor of Philosophy in Environmental Science at Oklahoma State University, Stillwater, Oklahoma in July, 2018.

Experience: Professor of Environmental Chemistry, Njala University (2005-2015); Water Resource Scientist/Researcher West Africa and USA (2010-2015); Environmental consulting (2005-2015).

Professional Memberships: Oklahoma Clean Lakes and Watersheds Association; National Association of Environmental Professionals Sierra Leone (NEPA-SL), Society for Environmental Scientists, Oklahoma State University (SES-OSU); Njala University Society for the Advancement of Academic Affairs (NUSAA); Rural Water and Sanitation Network (RWSN).